



**POLITECNICO**  
**MILANO 1863**

SCHOOL OF INDUSTRIAL AND INFORMATION  
ENGINEERING

Master of Science – Energy Engineering

**Adapting trailing edge flap control system for HAWT: the  
implementation in the BEM algorithm and an economic feasibility  
study**

Supervisor: Prof. Paolo Silva

Co-supervisor: Ing. Tomas Vronsky

Francesco Corrigan

Matr. 927889

Academic Year 2020/2021



# 1 ACKNOWLEDGEMENTS

---

A Papà, Mamma, Sara e Sabrina,

Ad Alice,

A Pietro,

A Thomas,

A Chicco,

A Carre, Elena, Lollo e Giò,

A Ric, Cit, Bil, David e la Bea,

A Simo,

All'altro Simo,

Alla Fra,

Senza di voi avrei mollato prima.

A Beethoven ed a Chopin,

All'Erasmus,

Al caffè.

## 2 EXTENDED ABSTRACT

---

### 2.1 INTRODUCTION

This Master Thesis starts from a proposal project made by Vestas. Vestas is a world leader company in the field of wind turbines, and continuously have some projects dedicated to students. This opportunity gives students the possibility to complete the technical knowledge learnt at school and apply it in a real practical work. The project studied in this thesis is called "Adaptive trailing edge for wind turbine blade"; it is an very big project, in fact, different students applied to it and different parts were studied by each of them. Literature about smart controls applied to wind turbines is still quite poor, most of it relies on simulations or experiments in wind tunnels. An overview of the existing different type of controls, together with the actuators and sensors needed, has been made in the first chapters. As the name of the project explain, the focus of this Thesis is the Trailing edge flap smart control system. The specific part investigated in this document develops the effect that a possible configuration of this flap, hinged at the 80% of the chord for the outer 50% of the blades, can have on the power output of the turbine itself. The expected results are related to the power coefficient, the power curve and the axial forces experienced by the turbine before and after the installation of the flap. This achievement is accomplished by the development of a program in MATLAB that exploits the Blade Element Moment algorithm. Data about the hypothetical value of lift coefficient and drag coefficient of the profiles with the flap installed are gathered through the program Xflr5, which exploits Xfoil's computations to find them. Results show a weak effect on the power output but a strong difference in the axial forces. Then, the presence of a gust has been implemented and a possible effect of this flap in case of environment with gust has been studied, which represents one of the most probable implementations of this concept. After that, starting from the obtained results, an economic feasibility analysis has been made to verify the effective economic convenience of this application. This analysis finds a result through a Discounted Cash Flow (DCF) model, comparing two different turbines, one existing Vestas V-90 3W and another one which simulates the previous same turbine with the flap installed. The result is a value

of about £180.000,00 per turbine which could be invested at maximum in this flap to make in economically convenient.

## 2.2 DEFINITION OF PROJECT'S PARAMETERS

The chosen primary profile of the turbine has been selected by Vestas, and it is the Nrel S809. Then, the selection of the control system to apply to the turbine has been done. On this field literature is wide, the two main used types of regulation are the stall regulation and the pitch regulation. The former relies on the fact that blades operate close to the stall condition, and naturally reduce the pitch angle and increase the angle of attack in case of rise of the wind speed. On the other hand, the pitch regulation is provided with a motion system at the hub of the blades which rotates them so to increase the pitch angle and to reduce the angle of attack. This last technology has been further developed to achieve even better control with a non-simultaneous motion of the blades. The chosen control strategy for the project is the standard pitch control system since it is the most widely used configuration and provides some benefit compared to the stall control system: more predictable behaviour of the flow close to the profile, less noise, less vibrations. The main disadvantage is its intrinsic slowness, which makes it unsuitable to bear with sudden gusts, but this disadvantage should be overcome by the Trailing edge flap system. Then, a variable rotational speed generator has been selected, to make the turbine able to vary its rotational speed as the wind speed increases, allowing it to reach high values of power efficiency at different conditions.

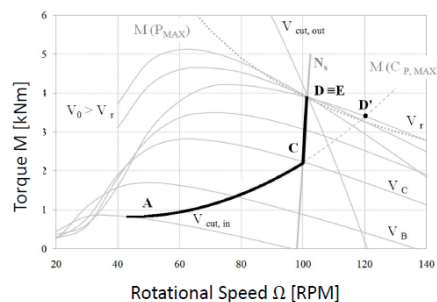


Figure 1: control regulation system

The Trailing edge flap is a smart control system, so a technology which aims to overcome the weaknesses of the HAWT actively changing some properties of the blades, acting

depending on the conditions. The trailing edge flap consists of a system that can modify the camber of the airfoil on a selected portion of the blade, acting on the lift coefficient. The selected type for this study is the discrete flaps, so flaps that are hinged at a selected portion of the airfoil. The other option would have been the continuous deformable flaps, but they are not the selected technology Vestas want to study with this project.

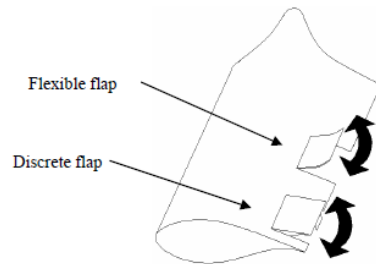


Figure 2: trailing edge flap examples

The Selected configuration for the project is the following: the Nrel family of airfoils S811, S809 and S810, and the configuration for the flap to be hinged at 80% of the airfoil chord on the outer 50% of the blade.

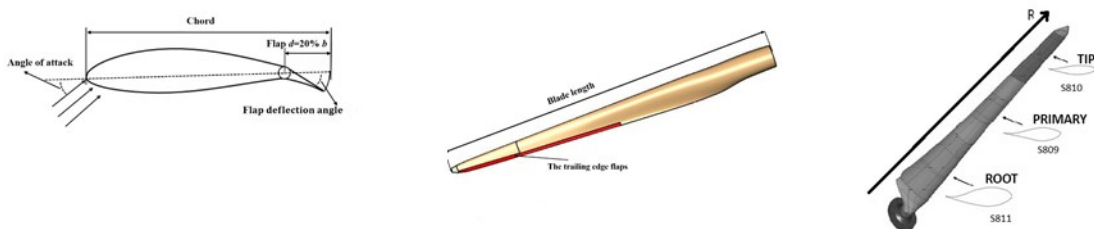


Figure 3: blade configuration for the project

The diameter of the turbine has been selected following the Nrel suggestions for this family of airfoils, choosing the maximum suggested diameter of 30m.

The other fixed parameters have been chosen by Mr. Vronsky and I, based mostly on his experience with HAWT, and are the main speeds used in the following studies:

$$V_{cut\ in\ or\ V_A} = 3.5 \frac{m}{s} \quad V_{rated\ or\ V_D} = 11 \frac{m}{s} \quad V_{cut\ out\ or\ V_E} = 20 \frac{m}{s}$$

$V_C$  , (subscripts A,B,C,D refer to Figure 1) the wind speed at which the maximum rotational speed of the turbine is achieved, is chosen applying as constraint the maximum rotational speed of the blade at the tip at 70 m/s, so its value is:

$$\Omega_C = \frac{70 \frac{m}{s}}{15 m} = 4.6667 \text{ rpm} \quad V_C = 10 \frac{m}{s}$$

After that, a gust has been implemented in the BEM code, simply inserting a vector representing it. The selected configuration for the gust has been a vector having as magnitude 1 m/s and hitting the airfoil with an angle of 45° compared to the main wind speed, adding so a value of 0.7071 m/s to the mean wind speed. Both the conditions studied here below, the first without the gust and the other with the gust, have been studied in a steady state condition. This hypothesis is very strong, overall considering the gust presence, since it is straightforward to understand that a gust is a sudden event, which could bring different kind of unexpected loads on the turbine.

### 2.3 RESULTS

	flap	gust	D [m]	P <sub>rated</sub> [kW]	Max pitch angle [°]	max axial force [N]
A	no	no	30	256	18.5	2.85x10 <sup>5</sup>
B	yes	yes	30	260	18.5	2.95x10 <sup>5</sup>
C	yes	yes	30	256	18.5	2.50x10 <sup>5</sup>
D	no	yes	30		18.5	3.00x10 <sup>5</sup>

Table 1: comparison between turbines with same diameter

	flap	gust	D [m]	P <sub>rated</sub> [kW]	Max pitch angle [°]	max axial force [N]
A	no	no	30	256	18.5	2.85x10 <sup>5</sup>
B	yes	yes	30	260	18.5	2.95x10 <sup>5</sup>
C	yes	yes	30	256	18.5	2.50x10 <sup>5</sup>
D	no	yes	30		18.5	3.00x10 <sup>5</sup>

Table 1 highlights the results of the first analysis made through the BEM algorithm. Case A is the reference case, with a 30m turbine, in an ideal environment with no gusts, and without the trailing edge flap. Case B and C are both cases of turbine having a diameter of 30m, installed in an environment which have gusts and with the flap installed. Both the cases have the pitch regulation stuck at the same value computed in case A, since it is a slow control system, and it moves only in relation with the mean wind speed, computed every 10 minutes and that is not affected by the presence of gusts, and the same maximum rotational speed as the reference turbine, since the electric generator is considered to be the same. The difference between cases B and C is in the algorithm that

control the flap motion. In case B the objective is to try to have the higher power output from the turbine, in fact that the rated power is 4kW higher that case A, increasing of 1.5%. Case C, instead, look for the position of the flap that allow the turbine to release the same power as in case A. It is showed that in this case the maximum axial load experienced by the turbine is reduced of 12.3% with respect to case A, which represents a consistent value, overall considering the presence of the gust only in case C. To evaluate the real potential of the flap case C is therefore compared with cade D, the case which studies a turbine having a 30m diameter, no flap installed, but which experience some gusts that have the same magnitude and direction as the one studied until now. The difference in the maximum value of axial force is higher than before, reaching a reduction of 16.6%. A comparison considering all the speeds from the cut-in to the cut-off wind speed can be seen in the figure below.

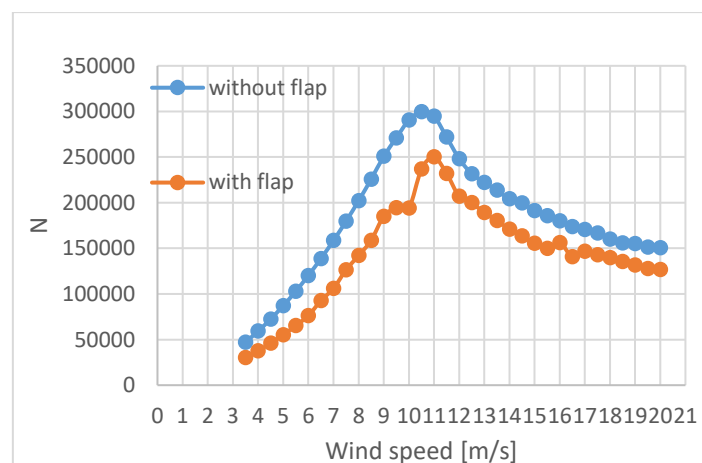


Figure 4: axial load's changes due to trailing edge flap

Then, another MATLAB evaluation has been done. It calculates how much it should be possible to increase the diameter of this turbine until the axial forces acting on the bigger turbine reach the values of the reference turbine's ones. The result shows that the overall closest value is achieved with a turbine having a diameter of 36m, so 20% bigger than the reference one. This new, bigger turbine open the possibility to have a higher production with the turbine affected by the same amount of strain, in particular the bigger turbine has a  $P_{rated}$  25% higher.

After that, these results have been used to perform an economic feasibility analysis on an existing turbine to verify the effective convenience of the trailing edge flap control.



The method used is the Discounted Cash Flow (DCF) method, which allows to evaluate some parameters, like the Net Present Value (NPV), the Internal Rate of Return (IRR), the Payback Time (PT) and the Levelized Cost of Energy (LCOE), starting from an initial condition and then evaluate the performances of an investment based on the found values. The DCF approach has the main advantage to make easy to compute all the values just starting from the investor choices, so, in the field of renewables, the technology to use, the budget and the plant location. The chosen turbine is the Vestas V-90 operating in the wind farm of Barrow (UK).

	mean wind speed [m/s]	shape factor	scale factor	incentive subsidy	$r_{infl}$	$r_{tax}$	$r_{disc}$
Barrow wind farm	9.15	1.5	10.1357	ROC	1.71%	30%-20%	7.25%

Table 2: Barrow economic parameters

In Table 2 are highlighted the economic rates and the wind parameters typical of the Barrow wind farm, considering its inauguration year: 2006. The shape factor has been chosen to make the capacity factor to be as close as possible to the real value of 0.36. The estimated lifespan of the wind farm has been set to 20 years. The results of the economic evaluation of the Barrow's plant have been compared with the results of another, hypothetical plant. The V-90 turbine has been substitute in the same wind farm with a V-108 turbine with trailing edge flap, which has been conceived by applying all the previous results at the V-90 original turbine, so with a diameter 20% higher and a power rated 25% higher than the original V-90.

	Diameter [m]	$P_{rated}$ [kW]	CAPEX [£]	OPEX [£]	$h_{available}$	capacity factor
V-90	90	300	4.101.000	110.618	8200	0.38
V-108	108	375	4.667.034	120.876	8000	0.36

Table 3: data of the two turbines

The Capital expenditure (CAPEX) has changed considering the bigger starting turbine, the Operative expenditure (OPEX) has been kept the same in percentage to consider the increase due to the presence of the flap, the availability hours have been reduced by 200h to consider the reduction in reliability due to the flap.

The results of the economic analysis are showed in Table 4.

	NPV	IRR	PB [y]	LCOE
V-90	1128687,4	10.30%	15	0.773
V-108	1534991,2	10.85%	15	0.744

Table 4: results of the two economic analysis

As depicted the results highlight that the investment considering the turbine with the Trailing edge flap smart control is more convenient, in fact its NPV, IRR are higher while the LCOE is lower. To evaluate the effective convenience of the investment the Weighted Average Cost of Capital (WACC) has been computed, it represents the minimum value of the IRR that an investment should have to be convenient for a specific company. In this case the WACC of Orsted in 2006, the owner company of the wind farm of Barrow, has been done, and the result is of 8.81%, which is lower than both the IRR of the project.

The last computation is done to find the overall price the Trailing edge flap system should have to cope with the economic convenience. To calculate it has been made an equivalence between the two IRR of the two turbines installed in Barrow, the V-90 and the V-108, and then the difference in CAPEX between these results and the previous project with the same turbine is considered. The IRR has been chosen, and not the NPV, since the latter one depends too much on the value of the initial investment, and so a higher NPV is expected also in a case of economic inconvenience.

The result is the following:

	NPV	IRR	PB [y]	LCOE	CAPEX [£]
V-108	1336985,8	10.30%	15	0.772	4847097

Table 5: results

As expected, the IRR is of course the same as the previous one computed in the V90 case, while the NPV still remains higher. The difference in CAPEX and so the maximum allowable price of the overall Trailing Edge Flap smart control is:

$$\Delta_{CAPEX} = 4.847.097 - 4.667.034 = 180.063,00 \text{ £/turbine}$$

## 2.4 CONCLUSION

The results of the work highlight the slight effect that the flap have on the variation of the power output of the turbine while show the great potential it has in the reduction of the axial loads the turbine is subject to. Therefore, it is not expected a variation of the

power curve of a turbine, but the annual production should increase, due to the possibility to operate the turbine more hours per year in an environment with gusts, or an increase of the lifespan of the turbine, subjected to weaker strains thanks to the flap. The MATLAB computations has found the possibility to increase the dimension of a turbine of 20% keeping the same amount of axial strain thanks to the installation of the flap. Moreover, the economic feasibility analysis gives an idea on the maximum cost that this technology could have per turbine. This value is very important in this very first phase of the project: it is related to some strong hypothesis, but it can modify the next choices that will be made in the other phases. For example, it can affect the choice of the actuator to use, this step can significantly modify the final weight of the blade, the effectiveness of the flap and the added consumption. Or maybe the extension of the flap on the blade can be reduced, or the flap installed at a different percentage of the chord, to reduce the needed power and so the dimension of the actuator. All the hypothesis that has been made can be changed to find the optimal solution, this first step represents the starting point of a more complete selection. The economic study can also be extended to find a more precise result. The methodology relates on some hypothesis, typical of the Discounted Cash Flow model, which end up in three main limitations: it does not allow the possibility to make changes of the initial projects ones it has begun, it does not consider the possible fluctuation of the cash flow, it uses an actualisation coefficient which is itself affected by estimation errors. These hypotheses can be overcome adopting the Real Option approach as integration of the DCF method used here. The RO approach considers an investment as a financial option and its value relies in the possibility of choosing whether to exercise the option or not, therefore this approach lets the investor decides to make a decision or postpone it to another moment, for instance. So, as it can be seen, the obtained results open to many different opportunities of modification of the project and selection of the best application for this technology. I hope this first investigation will be useful for Vestas and the pursuit of an effective Trailing Edge Flap control for their wind turbines.

### 3 SUMMARY

---

1	Acknowledgements .....	3
2	Extended Abstract .....	4
2.1	Introduction .....	4
2.2	Definition of project's parameters.....	5
2.3	Results.....	7
2.4	Conclusion.....	10
4	Abstract.....	15
5	Italian abstract.....	16
6	Key words .....	17
7	The company and the project .....	18
8	State of the art .....	20
8.1	Control and regulation .....	20
8.2	Smart controllers .....	24
8.2.1	Smart pitch control.....	24
8.2.2	Part span pitch control.....	25
8.2.3	Trailing edge flaps.....	25
8.2.4	Micro tabs .....	27
8.2.5	Active twist.....	28
8.2.6	Camber control (morphing).....	29
8.2.7	Inflatable structures .....	30
8.2.8	Boundary layer suction.....	30
8.2.9	Synthetic jets.....	31
8.2.10	Non-aerodynamic control concepts.....	31
8.3	Actuators .....	32
8.3.1	Conventional actuators.....	32
8.3.2	Smart material actuators.....	33
8.4	Sensors .....	36
8.4.1	Electrical strain sensors .....	36
8.4.2	Optical type strain sensors .....	37
8.4.3	Accelerometers.....	37

8.4.4	Inflow measurements .....	37
9	Aerodynamics of a Wind Turbine .....	38
9.1	One-dimensional Momentum Theory and the Betz Limit .....	38
9.2	Ideal Horizontal Axis Wind Turbine with Wake Rotation.....	41
9.3	Momentum theory and blade element theory .....	45
9.3.1	BEM theory.....	45
9.3.2	Computational and aerodynamic issues in BEM evaluation.....	51
9.3.3	Non ideal steady State Aerodynamic Issues .....	51
9.3.4	Turbine wakes.....	51
9.3.5	Unsteady aerodynamic effects.....	52
10	BEM evaluation of the study-case turbine.....	53
10.1	Choice of profiles and data processing .....	53
10.1.1	Data Collection .....	55
10.1.2	Design .....	59
10.1.3	Off Design.....	65
10.2	Inclusion of the flap.....	70
10.2.1	Turbine flap orientation but with no pitch regulation.....	70
10.2.2	A turbine which introduces the pitch regulation only after having exploited the flap orientation at its maximum.....	71
10.2.3	A turbine with a combined configuration of the flap orientation and the pitch regulation.....	73
10.3	Implementation of the gust.....	75
10.3.1	Gust with no flap.....	76
10.3.2	Gust with flap control.....	80
11	Economic feasibility analysis.....	86
11.1	Economic parameters.....	86
11.1.1	Net Present Value.....	86
11.1.2	Internal Rate of Return .....	88
11.1.3	Payback Period .....	88
11.1.4	Levelized cost of energy .....	88
11.1.5	Procedure.....	89
11.2	Reference site .....	91
11.2.1	The turbine .....	94

11.2.2	Reference wind distribution .....	97
11.2.3	Incentives.....	99
11.2.4	Computation .....	103
11.3	Turbine with flap.....	106
12	Future developments.....	116
12.1	Ten Points Plan .....	118
13	Conclusions .....	119
14	ANNEX [A] .....	121
15	ANNEX [f1A].....	132
16	ANNEX [f2A].....	133
17	ANNEX [f3A].....	133
18	ANNEX [B].....	134
19	ANNEX [f1B] .....	148
20	ANNEX [C] .....	149
21	Figures.....	160
22	Tables .....	162
23	List of the acronyms.....	163
24	References.....	164

## 4 ABSTRACT

---

The aim of this Master Thesis is to analyse a specific part of a project proposed by Vestas concerning the study of the Trailing Edge Flap smart control system for Horizontal Axis Wind Turbines. It has been particularly interesting working together with Lorenzo Cantoni, since it has allowed the comparison between the projects and their different outcomes, obtained considering the diversity of the studied domains. This analysis will concern the variation of the power output of a turbine which undergoes the application of the flap through an elaboration of data with MATLAB. Then, the effect on the axial strains is studied. After that, an economic feasibility analysis of the introduction of the flap is performed. The first part of the thesis highlights the weak effect the flap has on the power output but shows the consequences that the installation of the flap has on the axial strains undergone by the turbine's blades. The second part of the thesis starts from this result and goes on conceiving a bigger turbine that is subjected to the same axial strains of the first one thanks to the flap. Finally, the economic analysis compares these two configurations, applying the results on a real existing turbine: The Vestas V-90 used in the wind farm of Barrow (UK). The economic analysis ends up with the result that, on that specific turbine, the implemented configuration of the flap is convenient only if it costs less than £180.069,00 per turbine.

## 5 ITALIAN ABSTRACT

---

L'obiettivo di questa Tesi di Laurea Magistrale è quello di studiare una specifica parte di un progetto proposto da Vestas. Lo studio è focalizzato sull'applicazione per pale di turbine eoliche ad asse orizzontale chiamata "smart control Trailing Edge flap". Il progetto è stato iniziato da me e da un altro studente, Lorenzo Cantoni, il quale ha studiato il comportamento a fatica tramite computazione fluidodinamica; ovviamente il confronto tra i risultati trovati da entrambi è stato periodico durante tutta la durata del progetto. L'obiettivo di questa tesi è quello di verificare quale sia l'effetto di un ipotetico flap sulla produzione di potenza della turbina nel range di velocità del vento tra la velocità di cut-in e quella di cut-off. Questo obiettivo è stato raggiunto tramite l'implementazione di un programma su MATLAB che sfrutta l'algoritmo del Blade Element Moment (BEM). Sempre tramite MATLAB è stato poi studiato quale effetto si genera sugli sforzi assiali cui la turbina è sottoposta. Per ultimo ho eseguito un'analisi di fattibilità economica della soluzione in esame applicata ad una turbina reale e operante in un parco eolico esistente. La prima parte della tesi mette in luce il debole effetto che il flap è in grado di produrre sull'erogazione di potenza della turbina ma allo stesso tempo mostra una grande variazione per quanto riguarda gli sforzi assiali: la presenza del flap permette loro di ridursi notevolmente. La seconda parte della tesi si sviluppa dai risultati della prima e opera un confronto tra due turbine. La turbina di riferimento è la turbina operante nel parco eolico di Barrow, in Inghilterra, la Vestas V-90 3MW. La seconda turbina presa in esame è una turbina identica alla precedente, ma alla quale è stato installato il flap e incrementato il diametro, affinché il diagramma degli sforzi assiali delle due turbine risultasse simile. Confrontare queste due turbine, a parità di condizioni, permette di valutare quale possa essere un possibile costo massimo di questa tecnologia poichè risulti economicamente valida in una possibile futura applicazione. Il risultato finale garantisce questa possibilità nel caso in cui la spesa globale in conto capitale per turbina dedicata al flap sia inferiore a £180.069,00. Questo valore fornirà un riferimento per gli sviluppi futuri del progetto e permetterà una più consapevole scelta delle componenti da installare, nonché potrebbe portare alla variazione dei parametri ipotizzati in questa prima fase per variarne i risultati.



## 6 KEY WORDS

---

- Smart control system
- HAWT
- Trailing edge flap
- Wind turbine
- Blade Element Moment

## 7 THE COMPANY AND THE PROJECT

---

Vestas is a world leader company in the wind energy industry. It is a manufacturer company of wind turbines, it performs the design, the manufacturing, the installation and service of wind turbines, making it a reference in this field. Vestas has more than 136 GW of installed capacity around the world with 117GW under service. Vestas strongly believes in development, that is the reason why a continuous work of data harvesting is done, and these actions enhance the ability of the company to interpret, forecast and exploit wind resources around the globe. At present, Vestas has almost 30 thousand employees and it is one of the world leading companies in the green revolution, helping the entire population of the world to achieve a better life in the next years. Two of the leading objectives in Vestas are sustainability and making the interest of the future generations.

Thanks to its vision of the future, I had the possibility to enter this team and give my help to their mission with this Master Thesis, which I hope will bring some useful data in the research of the smart systems that can increase wind turbine's performances.

The project I applied to is named "Adaptive trailing edge for wind turbine blade" and, as it can be understood, it aims for achieving some interesting results in the study of the adaptive trailing edge flap: a smart control system for wind turbines.

Power and load control is critical for achieving safety and reliability of modern wind turbines and for bringing down the levelized cost of energy. Traditional load control requires full span adjustment of the blade pitch angle, however with ever increasing blade size, inertia, and flexibility, this solution may not provide sufficient control authority and the turbine could benefit from more localized load control, with short response time and ability to alleviate local gusts. Various feasibility studies reported reduced fatigue and extreme loads, enabling increased power rating or lighter blades.

The key challenge is to develop robust and reliable system which could provide fast changes of the blade trailing edge shape and operate in hostile environment with minimum maintenance. The system must be simple, low cost and fail safe.

There are several aspects which could be chosen to study in greater detail all aimed at increasing robustness and confidence in achieving cost and reliability targets required for system integration into future products.

The chosen aspect to be studied in this thesis is the effective modification in power production of a turbine set up with the trailing edge flap comparing it with a traditional one. The study then has brought me to the evaluation of the axial strains experienced by the turbine and how the adaptive trailing edge flap can modify them. After that, a preliminary economic feasibility study has been done comparing a turbine of the Barrow wind farm with a modified version of itself: bigger and with the trailing edge flap on its blades. The first part of the thesis exploits the BEM algorithm to forecast the behaviour of the turbine while the second part uses a classic Discount Cash Flow computation to achieve some economic results.

## 8 STATE OF THE ART

### 8.1 CONTROL AND REGULATION

The control of the blade in different kind of conditions is one of the major issues that should be considered to achieve the maximum exploitation of the wind energy in all the operating conditions. Different concepts can be derived to achieve the numerous targets related to those technologies, with the main purpose to mitigate loads in the turbine components to increase their lifetime [1].

For what concern the generator, a variable rpm one is required to obtain a good control system.

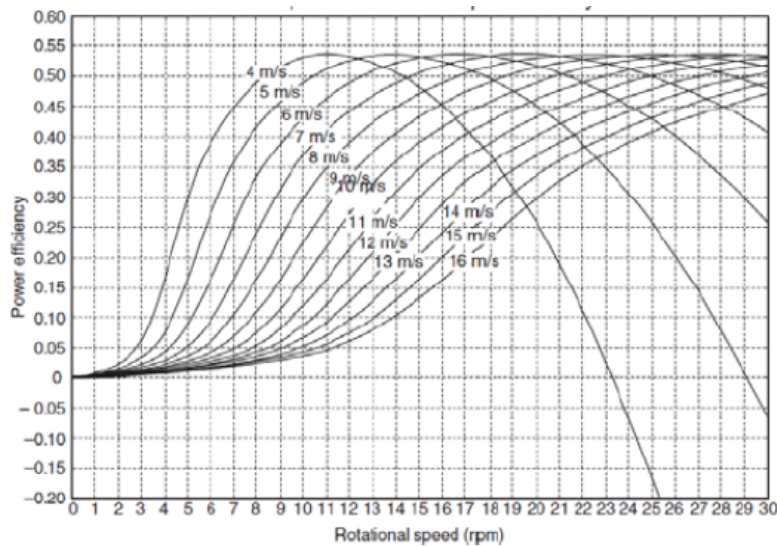


*Figure 5: efficiency at different constant wind speeds*

Displayed in Figure 5 that to achieve a high-power efficiency in a wide range of wind speeds it is imperative to change the rotational speed of the generator, so this kind of generator has been chosen as reference.

Two main ways of controlling a turbine are described here below, the pitch regulation and the stall active control, which are currently used by almost all the commercialized HAWT.

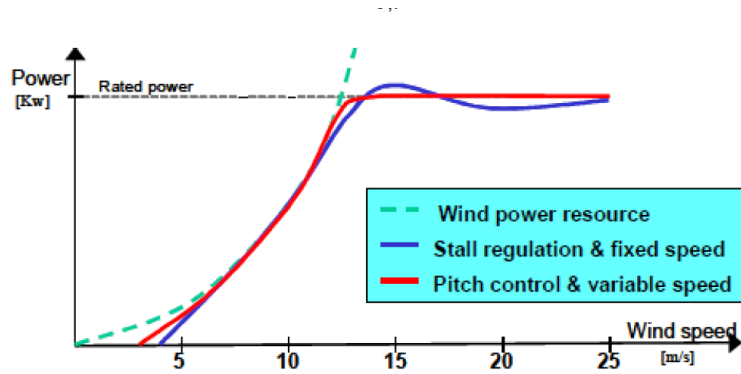


Figure 6: usual power curve for stall and pitch regulation

As showed in Figure 6 the form of the power chart slightly varies for these different concepts, but it is always possible to recognize two different areas: a third-degree polynomial curve up to the rated wind speed, where the nominal power of the turbine is reached, and an almost constant line at the rated power until the cut off wind speed is achieved.

The pitch control consists of the mobilization of the blade so that the pitch angle is increased, and the relative wind attack angle reduced. In this way both the  $C_L$  and the  $C_D$  reduce with the attack angle. Figure 7 explains the physical behavior that is followed by the three parameters  $C_L$ ,  $C_D$  and  $C_m$  moving from point D to point E'.

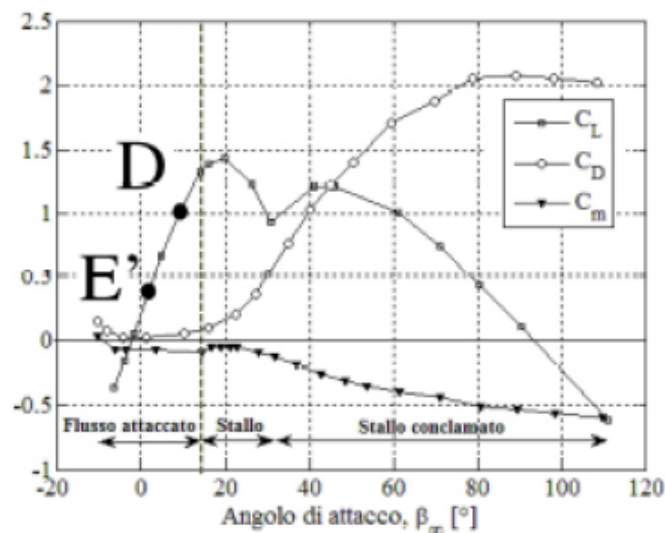


Figure 7: pitch regulation

Pitch regulation is traditionally done through an actuation system located at the hub that pitches simultaneously all the blades that compose the turbine. Two other possibilities

are proposed: pitching the blades independently (individual pitch) or equally but with a time delay among the different blades (cyclic pitch). These improvements of the pitch regulations allow to achieve a 15% and 29% of increased load reduction for the blade flap fatigue loads [2].

The active stall control, on the contrary, acts reducing the pitch and increasing the attack angle. In this way the same level of the parameter  $C_L/C_D$  is attended causing the stall of the blade. As displayed in Figure 8 the working point is now moving towards right in the chart, always from point D toward point E'. To achieve stall regulation, the blades usually work close to the stall region, resulting in an overall lower efficiency.

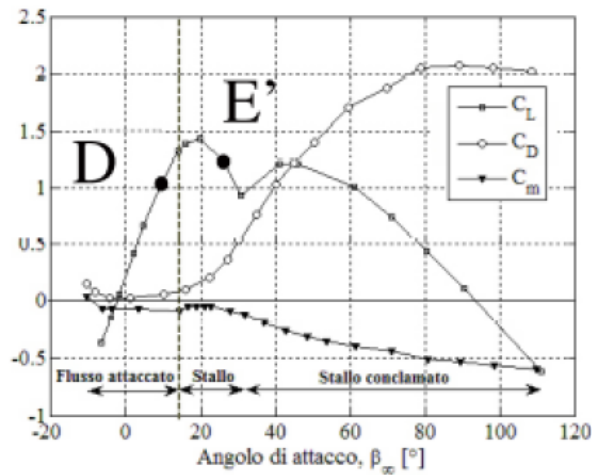


Figure 8: stall regulation

This configuration has several disadvantages compared to the pitch regulation. It causes the detachment of the flow from the profile, which brings difficulties to predict the exact behavior of the flow and unsteadiness of the blade, a higher value of noise and vibrations, a higher value of the loads on the blade. On the other hand, it reaches the same values of  $C_L/C_D$  with smaller adjustment of the blade, as pictured in Figure 10, that makes this control system faster than the previous one, and naturally behaves better in case of gusts.

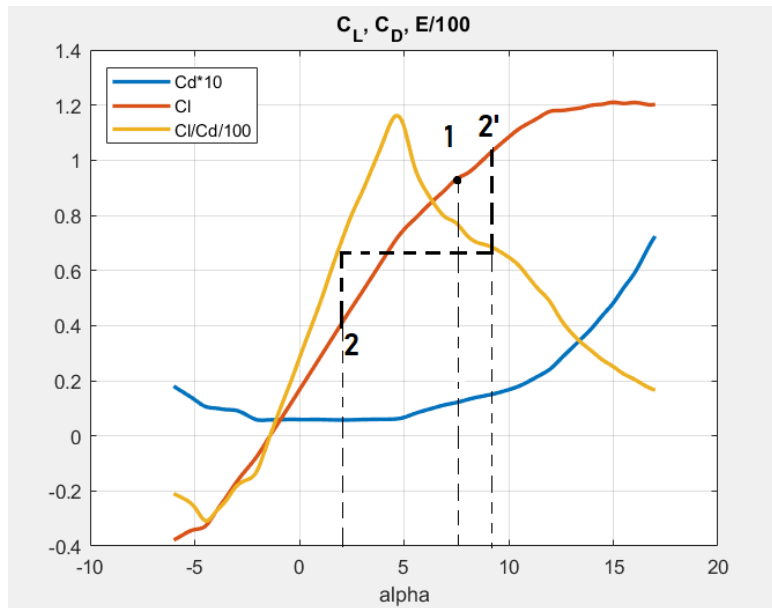


Figure 9: 1=initial condition; 2= adjustment with pitch regulation; 2'=adjustment with stall regulation

Gusts are an effective event especially at high wind speeds, usually in the range of wind speeds between the rated speed and the cut-off wind speed, so in the part of the power curve where the aim is to keep the power production as constant as possible, since it represents the maximum possible power that can be generated by the electric machine. Since a gust produces a natural increase of the attack angle and the pitch regulation is a relative slow control system, it does not have enough time to operate and the turbine can deal with the gust only increasing the power output, damaging the generator, and producing unsteadiness on the grid; or acting on the break, which is the preferred solution, but without reducing the strains the blades are subjected to. Vice versa, the active stall control naturally reacts faster, decreasing the value of  $C_L$  or increasing the value of  $C_D$ , always worsening the  $C_p$ , and keeping the power output of the turbine almost constant.

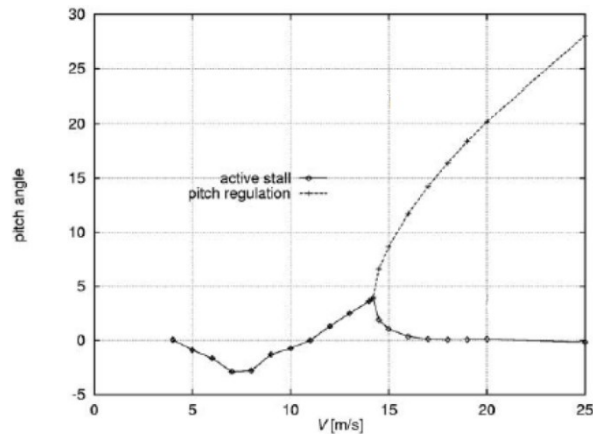


Figure 10: degrees of motion of pitch and stall regulations

Due to the significant growth of wind turbines of the last years and with it the force and energy required to the regulations systems, blade load control has become one of the main challenges for wind turbines [3]. A lot of different technologies have been implemented during the years that focuses on the alleviation of blade loads by applying smart active control. In this part of the thesis different kinds of controllers, actuators and sensors are presented.

## 8.2 SMART CONTROLLERS

This section will focus on the concept of aerodynamic control surfaces used for active control purposes.

### 8.2.1 Smart pitch control

Due to the very high forces that are necessary to move such masses, traditional actuators for pitch regulation can rotate a complete blade at a maximum rate of  $6^\circ$  per second, which is not enough to cope with fast fluctuating loads. This problem can be overcome by applying a smart actuator instead. This concept requires a torsion tube to be used parallel to the blade, which provides all-movable blade control. It theoretically can produce fast enough changes in the pitch, increasing both the weight and the cost of the blade, other than the required maintenance due to the increase of mechanical parts that should be placed on the blade. [4]



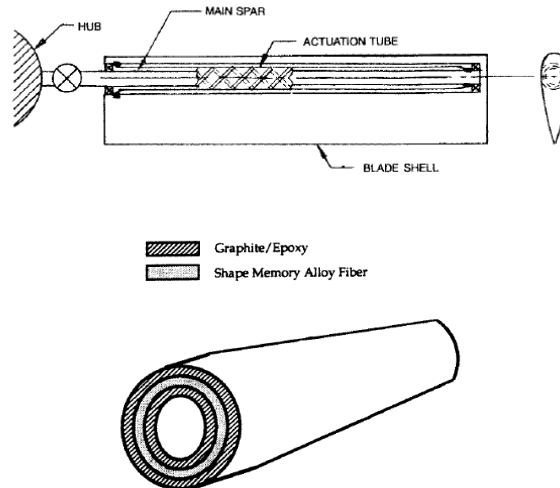


Figure 11: SMA actuation application for the entire blade and section of the actuator

### 8.2.2 Part span pitch control

This concept includes the pitch motion of only the tip of the blade. Even if it seems attractive since rapid control is achieved and large pitch torques are avoided, it brings with it some disadvantages like an increased and more difficult maintenance, multiple parts of the blade and a longer control signal way. Due to these facts, this smart active control is not very attractive. [4]

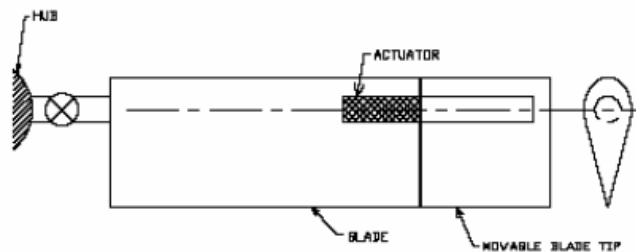


Figure 12: part span pitch control [3]

### 8.2.3 Trailing edge flaps

Increasing or decreasing the camber of the airfoil, trailing edge flaps act on the lift coefficient of the airfoil, making them one of the most promising concepts. Trailing edge flaps have smaller power requirements than the full or part span pitch control and an intrinsic better structural feature. Two kinds of flaps could be installed: discrete flaps or continuous deformable flaps. The formers are hinged to the blade and are traditionally used in aircrafts (where they assume the name of ailerons). This concept is theoretically

promising, but it has some disadvantages: it does not comprise an integrated design and all the additional parts it requires need maintenance and can be affected by wear problems. Furthermore, the sharp edge that it creates on the camber line reduces the aerodynamic performances. On the other hand, continuous deformable trailing edge has a smooth change in shape, it consists of an integrated solution and it is composed of a simple and uniform parts. The main disadvantage of the continuous deformable trailing edge technology is the fact it works directly on the structural rigidity of the trailing edge, bringing severe fatigue loads to it.

Another difference of these two options is the actuation system they can support. Discrete flaps can be actuated with a wide range of different actuators: piezoelectric bender actuators, piezoelectric stack devices, torsion tubes, SMA wires, hydraulic or electro-mechanical ones. An overview of those possibilities will be investigated later in this chapter. Continuous deformable trailing edge provides an integrated actuator in the trailing edge, which can set the requirements in terms of maintenance to the minimum, but usually this approach uses smart material actuators, which bring some advantages but also some disadvantages.

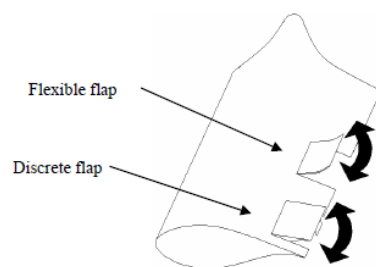


Figure 13: trailing edge flaps [5]

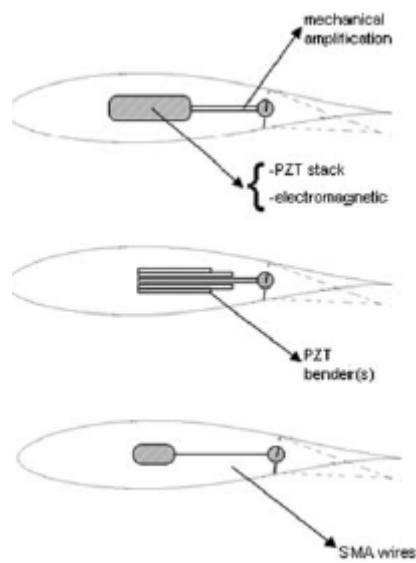


Figure 14: actuations on trailing edge flaps [6]

### 8.2.4 Micro tabs

Micro tabs are small deployable devices placed near the trailing edge of an airfoil. The action is perpendicular to the surface, and their height is likely 1% of the chord length [3], in the order of the boundary layer thickness [7]. They provide the change of the trailing edge flow development that brings to change in the lift coefficient (Figure 16).

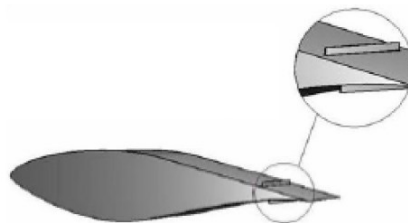


Figure 15: micro tabs [8]

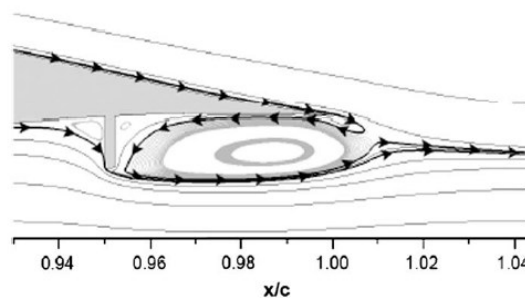
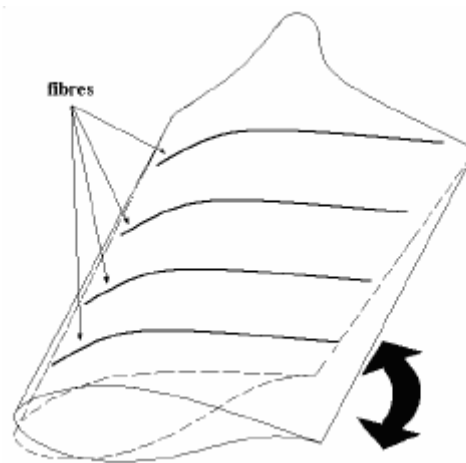


Figure 16: aerodynamic effects of micro tabs [5]

Depending on the position of the micro tab enabled the lift coefficient can be increased or mitigated. These tabs are usually called MEM tabs (Micro Electrical Mechanical Tabs) since the control-actuation system is usually a small integrated electronic circuit. Their small size allows very fast response time, and they are very small, light, and cheap. Their performances allow the lift coefficient to be increased of  $\Delta C_L = 0.3$  if the height-to-chord ratio is in the order of 1%, while it can increase until  $\Delta C_L = 0.4$  for a value of the same ratio up to 2%. The mitigation value can be changed up to  $\Delta C_L = -0.55$  [5].

### 8.2.5 Active twist



*Figure 17: active twist*

This approach focuses on acting twisting the entire blade, or part of it, over its complete span. The local angle of attack will consequently change, with a bigger change on the tip, which is effective for aerodynamic control. The actuator is usually made of smart materials, it is attached under the skin in fiber form and must be integrated with the blade. This large-scale integration of smart material produces a very heavy and expensive blade. Moreover, span-wise distributed control is not possible, and the large inertia of the blades make time responses quite slow. Also, the forces that are needed to twist an entire blade are estimated to be high [5].

### 8.2.6 Camber control (morphing)

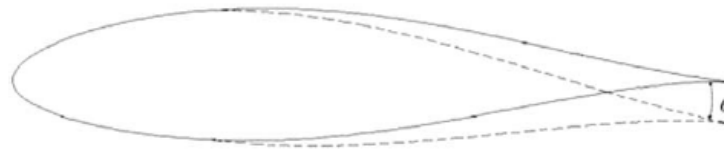


Figure 18: camber control

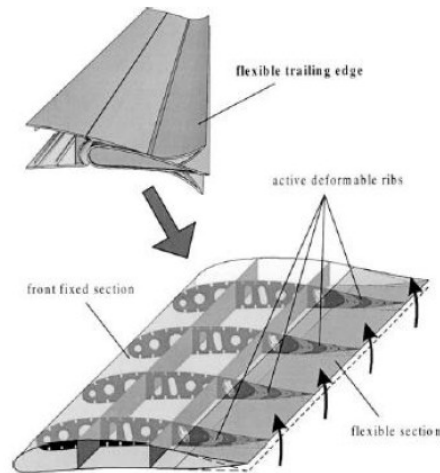


Figure 19: internal structure for camber control

This concept is the application of the direct deformation of the shape of the airfoil, which have direct effects on the force distribution on the blade, and so it can lead to a load alleviation. Two main technologies can be exploited to achieve this purpose: implementation of smart materials inside the blade skin (Figure 18) or the design of an internal deformable structure (Figure 19). These concepts can be actuated as said through smart materials actuators, discrete actuators, or solutions similar to the ones described for the continuous trailing edge flap concept. The main challenge of this technology is that it is associated with very large strains in the skin of the blade, that could lead to weaker skin section, but it is important not to compromise the integrity of the blade structure [5]. A lot of research is done on this field, and a lot of promising results are coming from the application of this concept to wind turbines [9].

### 8.2.7 Inflatable structures

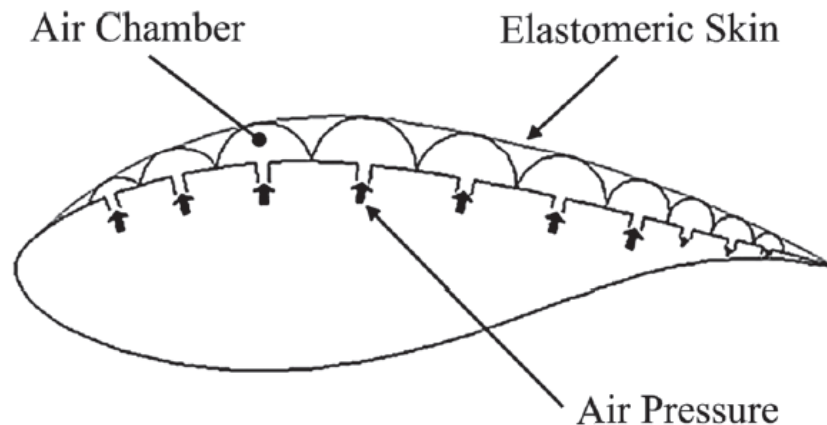


Figure 20: inflatable structures [6]

UAV (Unmanned Aerial Vehicle) and space applications of this concept have been studied until now [10], due to the characteristic of this concept of being stiff when inflated while it occupies a small volume when deflated. We can see in Figure 20 that the camber changes are achieved through the inflation of different chambers located on the upper (or lower) side of the airfoil. Changes in lift coefficient is estimated to be comparable to the one achieved with conventional trailing edge flaps [6]. An advantage of this concept is the smoother surface and consequently a noise reduction. The main disadvantage of this control is the complex system that should be designed to make it operative, which include an air pump and should not have any leakage. Weight penalization of the blade and extra maintenance are other issues that can affect its feasibility in horizontal axes wind turbines [11].

### 8.2.8 Boundary layer suction

This concept consists in operating a powered system to suck boundary layer flow from closely spaced vertical slots. It can prevent laminar and turbulent separation, by removing flow at low momentum, and reduce drag. Also, a lift control can be achieved since using actively control suction the virtual shape of the airfoil changes. Actuation purpose can be achieved by controlled pumps, that can lead to an increase of the complexity of the overall concept, power consumption and maintenance required.

### 8.2.9 Synthetic jets

Synthetic jets are zero-net mass flux jets created thanks to an oscillation created by a surface in a restricted cavity. The creation of an alternating ejection and suction across this cavity performs the jet, which is made of the fluid that is moved, so that no external fluid ducting is necessary. The outcomes are a net momentum addition and a change in direction. The actuation system is usually a piezoelectric diaphragm excited in a periodic way [6].

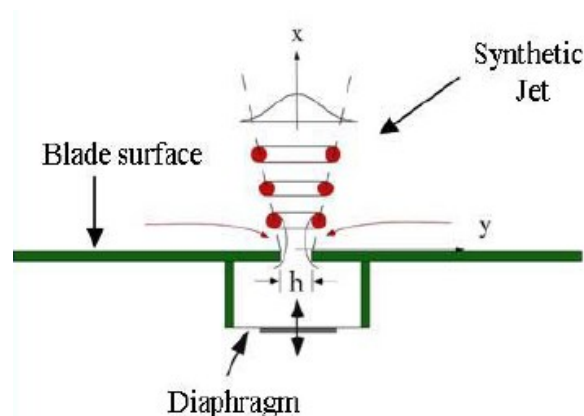


Figure 21: synthetic jets

### 8.2.10 Non-aerodynamic control concepts

If the aim is to reduce vibrations, damping systems and materials are worth a mention in this state of the art. Foams, SMA and piezo layers, that have a high damping coefficient, can be used as active or passive constrained layer. The active variant is usually composed by piezo-electric material and exerts an opposite force against the vibrating structure. The main disadvantage is the brittleness of the piezo-electric layer and its intrinsic small tensile strength. The passive variant is made of a stiff layer of visco-elastic material glued against the load carrying structure. Those techniques have never been applied for the damping of large-scale structures [11].

### 8.3 ACTUATORS

One of the most important part of an active control system is the actuator. It exists mainly two categories of them: embedded ones and discrete. It is important to highlight that the choice of the actuator is mainly dependent on the type of control system chosen, which regulate the requirements that are necessary by the actuator. A set of these requirements are:

- Lightweight
- Broadband response
- Large strains
- Minimum delays
- Minimum sensitivity to temperature
- Minimal effect of system dynamics (frequencies, mode shapes)
- Low maintenance requirement
- Low power requirement
- Stiffness
- Linear behavior, to simplify the control.
- Able to fit.
- Resistance to hard environmental conditions (rain, corrosion, humidity, salt, lightning)

A presentation of different kinds of actuators with the highlights of their main features is done here below.

#### 8.3.1 Conventional actuators

With the term conventional actuators, the reference is to hydraulic, pneumatic, electrical and electro-mechanical actuators. These actuators can provide high forces and are



already widely used in wind turbines for traditional control purposes (pitch regulation) since the frequency range required by this system is in the working range of the actuators. Using them to control active smart concepts is trivial. Hydraulic actuators have got leakage problems, they need regular maintenance, a lot of space and they suffer delays in actuation. Pneumatic actuators are lighter compared to hydraulic ones, but they have a reduced frequency range, and they show certain instabilities [5]. Electro-mechanical actuators are the most widely used for pitch regulation since the maintenance they require is lower than the other types of conventional actuators.

### **8.3.2 Smart material actuators**

Traditional actuators cannot intrinsically meet the requirements imposed by the concept of smart rotor blade control, especially in the case of offshore turbines. Moreover, the concepts described previously require fast actuation times and large energy-to-weight ratio. A promising solution seems to be the one related to smart material actuators systems. A smart material is a material which has got the capability to sense and actuate in a controlled way in response to variable ambient stimulations [11]. This family of materials has the advantage of high energy density, ease of control, variable stiffness, and the ability to tolerate large amounts of strains [12]. The most common smart materials are piezoelectric materials, variable rheology materials (electrorheological, magnetorheological), and shape memory alloy (SMA). Piezoelectric and SMA will be further investigated since they are the most famous ones exploited in actuators.

#### **8.3.2.1 Piezoelectric**

Piezoelectric actuators convert electrical energy into mechanical energy. In actuators, the widely used are the PZT (piezoceramic) and PVDT (piezopolymer). Single crystal piezo materials are promising but not used yet into actuators. PZTs have got a small power requirement and exhibits high deformations, so they are used for actuation purposes, while PVDT do not respond in a way as wide as PZTs, so they are used as sensors. Depending on the size of the electric field they are subjected, piezoelectric materials can have a very linear behavior (for small electric fields) or a very non-linear one. They have a fast response with low saturation strains, they are light and the flexibility of being both sensors and actuators make them very promising. The shapes they are usually proposed

are sheets, uniform benders, bimorph benders, stacks, tubes, and piezoelectric fiber composites. Sheets can be used to perform motion in the thickness, length and width directions, bimorph (two-layer elements) have the same properties as the sheets but can also be used to bend and extend, stacks can deliver and support high forces but providing small motion. Piezoelectric fiber composites are fibers of PZT (not layers) embedded into the polymer, this makes them the most versatile. Three well known actuators layouts concerning the piezoelectric materials are the THUNDER, the RAINBOW and the LiPCA actuators. It's imperative to make the right choice in the voltage range that should be used in order to avoid unpredictable behaviors [13].

The use of piezoelectric actuators obliges to use a mechanical amplifier as well to increase the displacement and they are usually made of rods, arms etc. This makes the complete device quite complex and increase the maintenance requested by it. Piezoelectric materials are still very versatile, and they can be used as discrete actuators (for flaps, micro tabs, synthetic jets) or as embedded actuators (for active twist and camber control systems).

Some problems can affect the efficacy of the piezoelectric potential of being deformed by applying a voltage in the poling direction. The first one is the fact that most of the piezo electrics act as a capacitor: they create an opposite field once they are electrically charged. Then the fact that they can't be used at very low frequencies and, when loaded dynamically, they show a high hysteresis [14]. Some extreme condition can affect the behavior too:

- A high temperature depoles the piezo electric material. The temperature at which it happens is the Curie Temperature.
- Very high compressive pressures reduce or destroy the piezo electric effect.
- High voltages applied against the poling direction can act in the same way as high pressures. [15]

Even the placement of these element brings to some considerations. It strictly depends on the way they are used, if as actuators or as sensors, on the chosen boundary conditions and on the criterion that is chosen. Since usually actuators are more massive that sensors,

the placement of actuators has greater significance than that of sensors. Such criteria are well examined in [16].

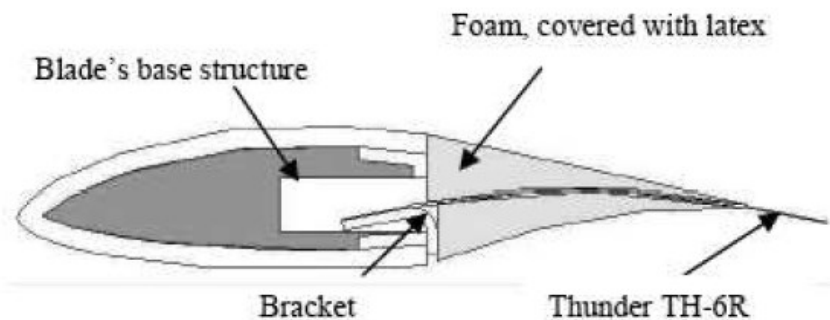


Figure 22: THUNDER piezoelectric actuator [17]

### 8.3.2.2 Shape memory alloy

Shape Memory Alloy (SMA) can sustain and recover relatively large strain without undergoing plastic deformation. The main feature these actuators have got is the so-called shape memory effect: they can be deformed at low temperature but remains still able to recover the original shape once they are heated up over the transition temperature. The process is austenite  $\rightarrow$  cooling  $\rightarrow$  martensite  $\rightarrow$  heat recovery  $\rightarrow$  austenite and it is reversible. Bandwidth is short and response times are long due to the cooling and the heating process. Non-linear effects are one of the biggest disadvantages in the use of this technology. The SMA concept is very versatile, and SMAs can be embedded (used for camber control, flexible flaps, and active twist control), attached or included in tubes, or drawn into bar stock, rod, wire, tubing, sheets, and foils. A promising form is a discrete coil spring used when high forces and small displacements are required. It should always be considered that large layers of smart materials add considerable weight and cost to the blade, also the flexibility of the skin should be taken into consideration. The structural properties of the blade itself should be well investigated before deciding to use such actuators for full blade deformations, this makes their use quite complex. A feasible concept should be in the use of integrated or under-the-skin smart actuators to deform small surfaces of trailing edge flaps, where it is easier to consider the flexibility of the skin.

## 8.4 SENSORS

Sensors are a point of high importance into the concept of smart blade control. Sensors have the duty of determine the aerodynamic loads acting on the blade, which are then sent as input to the controller. Also, gravitational and inertial loads must be sensed and recognized to consider them in the controller. To accomplish this objective a lot of possibilities can be considered, the position of the sensors, the physical state we choose to measure, the type of sensor. These choices are made depending on the control strategy and on practical issues and capabilities of measurement equipment.

Requirements for sensors for wind turbines' blades are the following:

- lightweight
- Immunity to electromagnetic waves (which can affect the measurement)
- minimum sensitivity to temperature
- Ease of integration in the structure
- Robustness on a long term
- minimum calibration requirements
- Precision of measurements (adequate range and time response)
- Long term stability of measurements
- Reliable operation in harsh environment

### 8.4.1 Electrical strain sensors

Different electrical strain gauges exist, Resistance strain gauges, Capacitance ones, Photoelectric and semiconductor and are traditionally used in wind turbines applications to sense the strain in different part of the turbine, especially in the root [5]. The use of strain gauges in smart control applications seems appropriate due to their characteristics (measurement range and time response) and an example has been done in [18]. Their main drawback is that the mounting process is very complex and needs a lot of accuracy, it's than a costly process. Calibration is very important as for all sensors and strain gauges won't last all the lifetime of a wind turbine without a periodical recalibration. Furthermore, none of the strain gauge types can last for the entire lifetime, they are not robust enough to sustain such a high number of stress cycles.

### **8.4.2 Optical type strain sensors**

Optical strain gauges are: Photoelastic strain gauges, Moire interferometry ones, Holographic interferometry, and fiber optic strain gauges. Only the fiber optic ones constitute an option in the domain of wind turbines measurements. They are very promising since they are very light, small in diameter, resistant to corrosion and fatigue, immune to electrical interference, flexible, they have a wide bandwidth operation, an extreme sensitivity and do not generate heat or electromagnetic interference, they need low maintenance while have high reliability. A single strand of optical fiber can substitute a lot of wires needed for strain gauges, so even if it's a more expensive technology, it allows to economize on other ways. The main drawback is the extreme sensibility to temperature. [19]

### **8.4.3 Accelerometers**

Accelerometers are sensors that transform accelerations into electric signals by means of two different transducers: the primary one transform acceleration into displacement (it could be a spring retained seismic mass or a double cantilever beam), the secondary transducer translate the displacement into an electric signal (it could be a piezoelectric, a servo strain gauge etc.). Accelerometers have a lower frequency (around 1 Hz) that is too high to measure blade vibration, so they are usually considered not suitable for this application. In wind turbines accelerometers are usually used to measure bearing, generator, gearbox vibrations, so for a maintenance purpose. The cost is not high.

### **8.4.4 Inflow measurements**

This category comprises all the devices able to measure the incoming wind field, a commonly used one is the Pitot tube, which measure the local dynamic pressure a with it the velocity sensing the total and the static pressure on the tube.

Another method is to use the lidar (laser anemometry), which guarantee a remote wind speed measurement. Remote measurements detect the Doppler shift for light backscattered from natural aerosols in the atmosphere (dust, pollen etc.) [5]. Research for the use of Lidar to measure gusts has been made [20].

## 9 AERODYNAMICS OF A WIND TURBINE

The interaction between the rotor of the turbine and the wind allows the production of energy. The wind can be considered as a combination of the mean wind and turbulent fluctuations. The component that is usually exploited to produce energy is the mean one over 10 minutes, while the other components are source of unwanted loads for the turbine. The next chapter will analyse the aerodynamics in the steady state conditions, which is the considered situation of the following work.

A few methods to study the steady state aerodynamic have been derived during the years, firstly by Betz and Glauert in the 1930s. In this chapter the momentum theory and the blade element theory are developed in simple and simplified methods, operating in ideal conditions, and then their limitations will be discussed. Finally, in the next chapter, a combination of those methods (steady state BEM theory) will be applied on MATLAB to compute the characteristics of a case-study turbine.

### 9.1 ONE-DIMENSIONAL MOMENTUM THEORY AND THE BETZ LIMIT

This method, developed in 1926 by Betz, allows to determine the power from an ideal turbine rotor, the thrust of the wind on the ideal rotor, and the effect of the rotor operation on the local wind field. The base theory used the linear momentum theory used to predict the performances of a ship propeller.

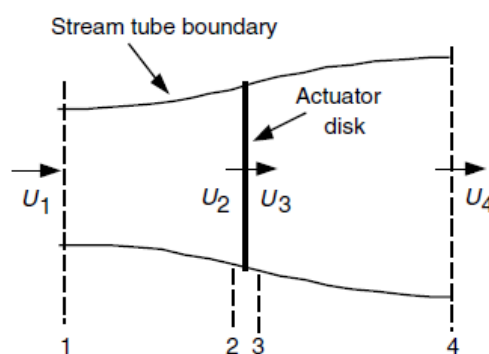


Figure 23: actuator disc model for a wind turbine [21]

Many hypotheses characterise this theory:

- The flow exists only between the ends of the control volume;

- The turbine is assumed as a uniform actuator disc, so it creates a discontinuity on the pressure;
- The fluid flow is homogenous, incompressible and in steady state conditions;
- There is no fictional drag;
- The number of blades is infinite;
- The thrust over the disc rotor area is uniform;
- The wake does not rotate;
- Pressures at section 1 and 4 in Figure 23 is equal to the atmospheric pressure.

The simple conservation of the linear momentum law gives us some quite strong results: considering that the force is equal and opposite to the thrust,  $T$ , the thrust itself is so equal and opposite to the rate of change of momentum of the air system.

$$T = U_1(\rho AU)_1 - U_4(\rho AU)_4$$

$\rho =$  air density

$U =$  air velocity

Applying after the hypothesis of the steady state flow:

$$(\rho AU)_1 = (\rho AU)_4 = \dot{m}$$

$\dot{m} =$  mass flow rate

And so

$$T = \dot{m}(U_1 - U_4)$$

This result tells us that the positive thrust coincides with a lower velocity of the wind in section 4 than in section 1 with no work done by the turbine. Applying then the Bernoulli function: upstream and downstream the disc with the assumption  $p_1 = p_4$  and  $U_2 = U_3$

$$p_1 + \frac{1}{2}\rho U_1^2 = p_2 + \frac{1}{2}\rho U_2^2$$

$$p_3 + \frac{1}{2}\rho U_3^2 = p_4 + \frac{1}{2}\rho U_4^2$$

The thrust is now defined as

$$T = A_2(p_2 - p_3)$$

$$T = \frac{1}{2}\rho A_2(U_1^2 - U_4^2)$$

Recalling that  $\dot{m} = \rho A_2 U_2$ :

$$U_2 = \frac{U_1 + U_4}{2}$$

The wind velocity at the rotor of the turbine is so equal to the average speed of the wind measured upstream and downstream far from the turbine, using all the assumption made above.

We can now define a parameter,  $a$ , called the *axial induction factor*, as

$$a = \frac{U_1 - U_2}{U_1}$$

And have those relations among velocities:

$$U_2 = U_1(1 - a)$$

$$U_4 = U_1(1 - 2a)$$

Note that this law is no longer applicable if the axial induction factor overtakes the value of 0.5, in fact equation (1.11) will result in a wind speed at section 4  $\leq 0$ .

From those results, it is possible to compute the power almost straight forward.

Substituting in the second equation  $A_2 = A$  and  $U_1 = U$  :

$$P = \frac{1}{2} \rho A_2 (U_1^2 - U_4^2) U_2 = \frac{1}{2} \rho A_2 U_2 (U_1 + U_4) (U_1 - U_4)$$

$$P = \frac{1}{2} \rho A U^3 4a(1 - a)^2$$

Then, the definition of another very important coefficient, called the power coefficient,  $C_p$ , which is the ratio between the rotor power and the theoretical power of the wind is done.

$$P_{wind} = \frac{1}{2} \rho A U^3$$

$$C_p = \frac{P}{\frac{1}{2} \rho A U^3}$$

It is a non-dimensional coefficient and represents the fraction of the power of the wind that is extracted by the turbine.

Doing the derivative of the power coefficient over  $a$  equal to zero  $C_p$  is maximised, and a  $a = 1/3$  , the so-called Betz limit, is obtained:

$$C_{p,max} = \frac{16}{27} = 0.5926$$

This result is quite important since it tells us that the maximum power obtainable by a wind turbine is done in the condition where the wind speed at the rotor is 2/3 of the free wind speed.

Turning back to the thrust, it can be computed as



$$T = \frac{1}{2} \rho A U^2 (4a(1-a))$$

In the same way we defined the power coefficient, we can now define the thrust coefficient, just by doing:

$$C_T = \frac{T}{\frac{1}{2} \rho U^2 A}$$

We see that  $C_T = 1$  when  $a = 0.5$  but at the maximum  $C_p$  value, so at  $a = 1/3$ , we obtain  $C_T = 8/9$ .

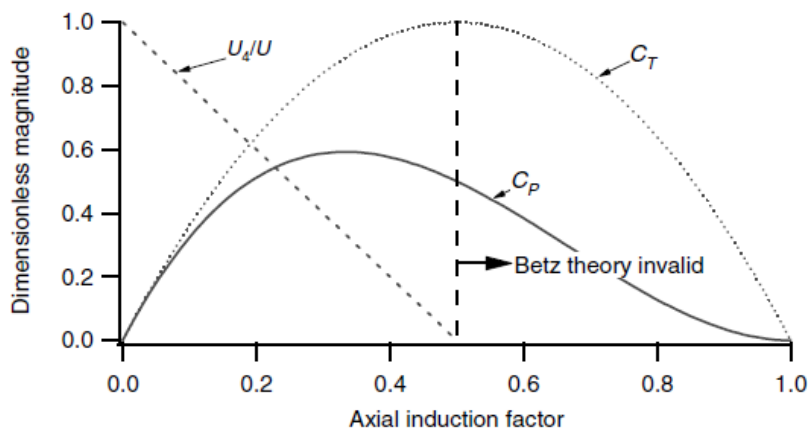


Figure 24: operating parameter for a Betz turbine

As we have seen before, this theory is no longer applicable in the case  $a > 0.5$ , but in practice it can happen and will be studied in the next sections.

It is important to highlight the three parameters that make us work in an ideal environment, enable to reach the power coefficient of  $16/27$ , and that will impede us to reach this value in real applications:

- Rotational wake behind the rotor
- Finite number of blades and their tip losses
- Presence of aerodynamic drag

## 9.2 IDEAL HORIZONTAL AXIS WIND TURBINE WITH WAKE ROTATION

This theory extends the previous one to the case where the rotating rotor generates angular momentum, which can be related to the rotor torque.

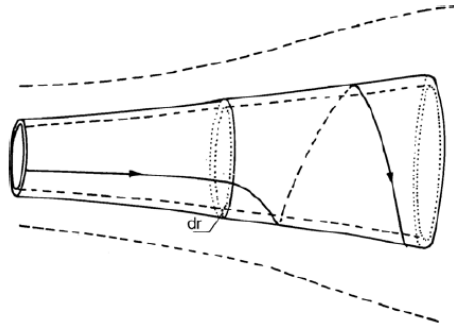


Figure 25: stream tube with wake rotation [22]

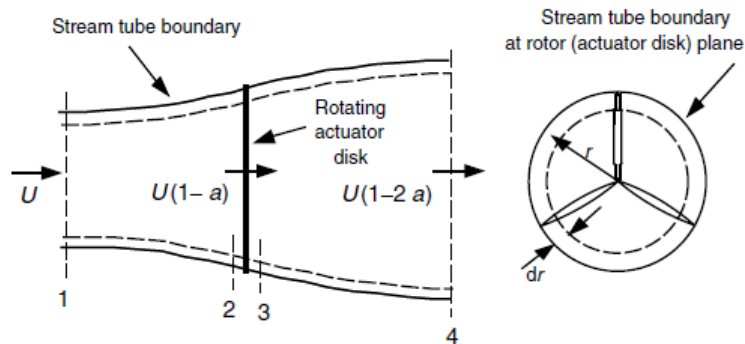


Figure 26: geometry for the rotor analysis: stream tube

The presence of a radial contribution in the wind speed in section 3 results obviously in less energy extraction by the rotor. Also, we can expect a higher extra kinetic energy in the downstream wake with a higher torque, so a slow-running turbine (with a high torque) experiences more wake rotation losses than a high-running one, which nominally has a smaller torque.

In the following, the concept of annular stream tube will be used, with a stream tube with radius  $r$  and thickness  $dr$ , resulting in a cross-sectional area equal to  $2\pi r dr$ .

Glauert, in 1935, derived the difference in pressure between the sections just before and just after the blades, applying the energy equation in a control volume that moves with the angular velocity of the blades. Passing through the disc, the angular velocity of the air relative to the blade increases from the value  $\Omega$  to the value  $\Omega + \omega$ , keeping the axial component constant:

$$P_2 + \frac{1}{2}\rho U_2^2 = P_3 + \frac{1}{2}\rho U_3^2 \rightarrow P_2 - P_3 = \frac{1}{2}\rho(U_3^2 - U_2^2) = \frac{1}{2}\rho((\Omega + \omega)^2 + \Omega^2)r^2$$

$$p_2 - p_3 = \rho \left( \Omega + \frac{1}{2}\omega \right) \omega r^2$$

The thrust on the annular element is then:

$$dT = (p_2 - p_3)dA = \left[ \rho \left( \Omega + \frac{1}{2} \omega \right) \omega r^2 \right] 2\pi r dr$$

We can now define another coefficient, called the *tangential induction factor*:

$$a' = \frac{\omega}{2\Omega}$$

Turning to the airfoil, we can now graphically represent the situation as in Figure 27:

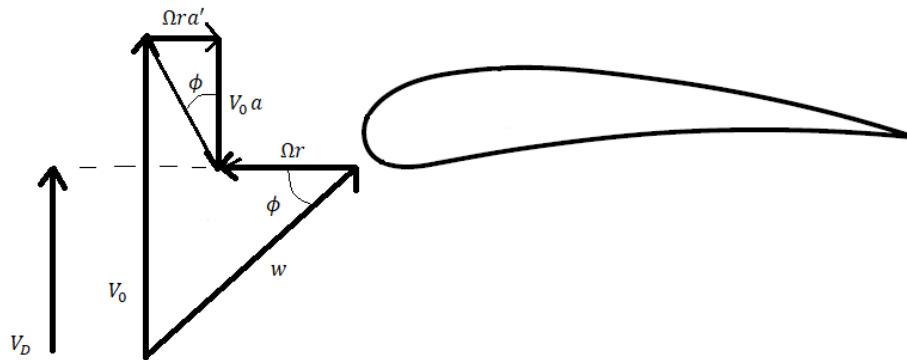


Figure 27: vectors of the considered wind speeds

So now the thrust can be computed as

$$dT = \frac{1}{2} 4a'(1 + a') \rho \Omega^2 r^2 2\pi r dr$$

But we know that the thrust can be computed as well following the previous linear momentum analysis, that uses the axial induction factor  $a$ :

$$dT = \frac{1}{2} 4a(1 - a) \rho U^2 2\pi r dr$$

Equating functions (1.21) and (1.22) we obtain

$$\frac{a(1 - a)}{a'(1 + a')} = \frac{\Omega^2 r^2}{U^2} = \lambda_r^2 = x^2$$

And we defined  $x$  as the local speed ratio.

In the same way, we define the tip speed ratio as the local speed ratio computed at the maximum tip:

$$\lambda = \frac{\Omega R}{U}$$

We can now exploit these values to derive other expressions for the power and the power coefficient as functions of the induction factors and the speed ratio:

$$dP = \frac{1}{2} \rho A U^3 \left[ \frac{8}{\lambda^2} a' (1 - a) x^3 dx \right]$$

$$dC_p = \frac{1}{2 \rho A U^3} dP$$

$$C_p = \frac{8}{\lambda^2} \int_0^\lambda a' (1 - a) x^3 dx$$

$a$  and  $a'$  are related through the triangle that can be seen in Figure 27, this allows us to write this relation:

$$\tan \phi = \frac{a' \Omega r}{a V_0} = \frac{(1 - a) V_0}{(1 + a') \Omega r}$$

Together with the maximisation of the equation of  $C_p$  it is possible to find the relation between  $a$  and  $a'$  that follows, which is known as the Glauert optimal distribution of  $a$  and  $a'$ .

$$a' = \frac{1 - 3a}{4a - 1}$$

It is possible to demonstrate that an axial induction factor  $a = \frac{1}{3}$  gives an infinite tip speed ratio while a value of  $a = \frac{1}{4}$  results in  $x = 0$ .

This imposes a condition on the possible values of  $a$ :

$$\frac{1}{4} < a < \frac{1}{3}$$

All those considerations bring to two strong results: the first regarding the power coefficient, which will always be smaller than  $\frac{16}{32}$ ,

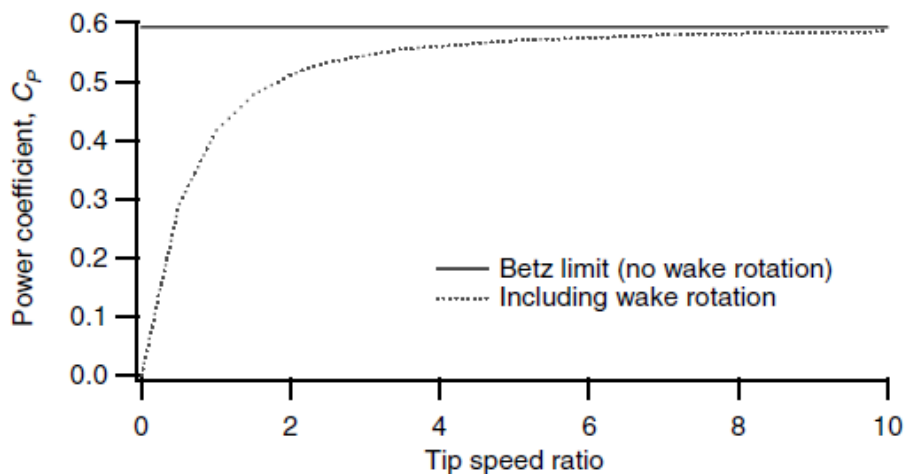


Figure 28: variation of the power coefficient with the tip speed ratio

the second regarding the values of the axial and the tangential induction factors, which behave like that:

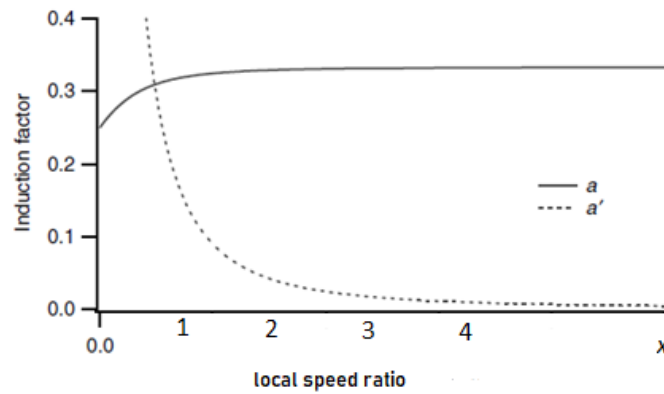


Figure 29: variation of  $a$  and  $a'$  with the local speed ratio  $x$

We can notice some main points in this last graph:

- Between  $x = 0$  and  $x = 1$   $a'$  is very big.
- As  $x$  increases (so towards the tip of the blade),  $a'$  becomes more and more negligible.
- $a$  has an opposite behaviour than  $a'$ .
- The change in  $a$  is small but it is necessary to be considered.
- For high  $x$   $a \rightarrow 1/3$  and  $a' \rightarrow 0$ , so towards the Betz results.

### 9.3 MOMENTUM THEORY AND BLADE ELEMENT THEORY

Based on the results obtained in the previous sections, now will be presented the way to compute a calculation on the aerodynamics and the final shape of a wind turbine's blade. The analysis will use the momentum theory and the blade element theory, which results in the blade element momentum (BEM) theory [23]. In this thesis this computation will cover three main sections:

- BEM theory.
- Performance characteristics for a blade of known chord distribution, including wake rotation, drag, and tip losses due to finite number of blades.
- A simple optimum blade design.

#### 9.3.1 BEM theory

##### *Momentum Theory*

The equations have already been developed in the previous sections, in particular the one including the wake rotation. So, axial and tangential induction factors are a function of  $r$ . (T=thrust, M=torque)

$$dT = \rho U^2 4a(1-a)\pi r dr$$

$$dM = 4a'(1-a)\rho U \pi r^3 \Omega dr$$

Blade element theory

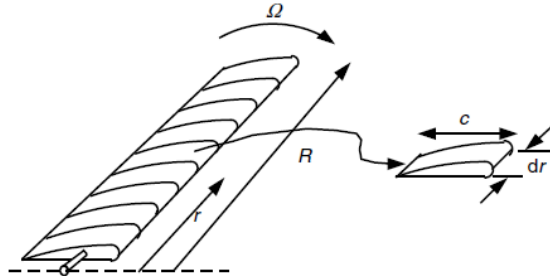


Figure 30: schematics of the blade elements

As shown in Figure 30 the blade is assumed to be divided into N different sections (elements), and, in each of them forces will be expressed through lift and drag coefficients.

These assumptions are made:

- No aerodynamic interaction among the elements.
- Forces on the blade are determined only by the drag and lift coefficient, due to the chosen airfoil.

As the theory of the airfoils shows, lift and drag are perpendicular and parallel to the relative wind speed seen by the blade. [24]

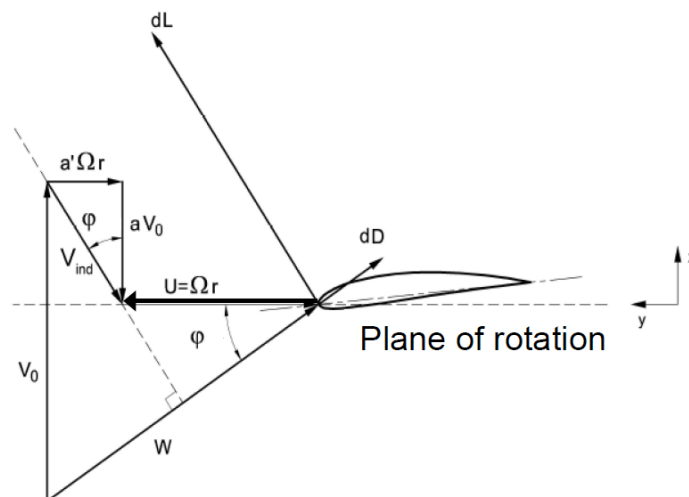


Figure 31: airfoil with Lift and Drag vector representation

The tilt angle  $\gamma_c$  of the blade, which is usually present in turbines to avoid blades to interfere with the column, will be considered zero in this analysis.

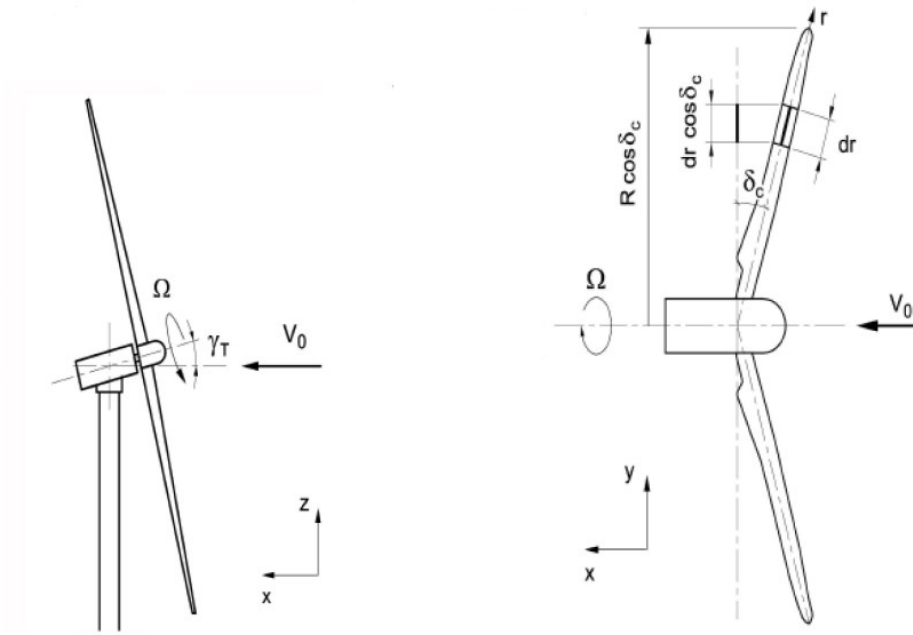


Figure 32: tilt angle and coning angle

The coning angle  $\delta_c$  will be considered in the computations of the formulas but in the analysis will be put equal to zero too. It is usually present to counterbalance deformations of the blades due to strong wind and centrifugal forces and end up with an almost  $90^\circ$  angle between blades and wind during operational time, this is why it is coherent to put it equal to zero in the design computations.

At the end the considered hypothesis are:

- Steady state condition for the wind.
- Tilt angle  $\gamma_c = 0$ .

From the airfoil theory and simple trigonometric we can obtain these relations:

$$C_N = C_L \cos \beta_\infty + C_D \sin \beta_\infty$$

$$C_T = C_L \sin \beta_\infty - C_D \cos \beta_\infty$$

$$dF_N = \frac{1}{2} \rho w^2 c C_N dr$$

$$dF_T = \frac{1}{2} \rho w^2 c C_T dr$$

where subscript  $X_T$  stays for “tangential” and subscript  $X_N$  stays for “normal”. From these equations we can see that  $C_N$  and  $C_T$  are functions of the profile, the number of Reynolds and the value of  $\beta_\infty$ .

It is very easy to derive now the formula of the axial force and, with it, the one of the torque acting on one blade:

$$dF_x = (dF_N \cos \beta_c - dF_T \sin \beta_c) \cos \delta_c$$

$$dM = dF_y r \cos \delta_c = \frac{1}{2} \rho w^2 c (C_N \sin \beta_c + C_T \cos \beta_c) r \cos \delta_c dr$$

To compute the total force acting on the turbine we just need to multiply the obtained value times the number of the blades:

$$dF_x^{tot} = N_b \cdot dF_x$$

$$dM^{tot} = N_b \cdot dM$$

Now we define a new non-dimensional parameter, *solidity*:

$$\sigma = \frac{N_b c}{2\pi r \cos \delta_c}$$

Which is the ratio between the part of the circumference occupied by the blades of the turbine and the total circumference swept by the turbine.

Thanks to solidity we can write the axial coefficient, the torque coefficient and the power coefficient as follows:

$$C_x = \frac{dF_x^{tot}}{\frac{1}{2} \rho V_0^2 dA} = \frac{\sigma w^2}{V_0^2} (C_L \cos \phi + C_D \sin \phi)$$

$$C_M = \frac{dM^{tot}}{\frac{1}{2} \rho V_0^2 dA r \cos \delta_c} = \frac{\sigma w^2}{V_0^2} \frac{C_L \sin \phi - C_D \cos \phi}{\cos \delta_c}$$

Where  $dA = 2\pi r \cos^2 \delta_c dr$

Knowing that  $dP = dM^{tot} \cdot \Omega$

$$C_p = \frac{dM^{tot} \Omega}{0.5 \rho V_0^3 dA} = \frac{\Omega r C_M \cos \delta_c}{V_0} = \frac{x w^2}{V_0^2} \sigma K(C_L, C_D, \beta_\infty, \beta_c) = x(1-a)^2 \sigma K$$

Where K is a parameter which is function of  $C_L, C_D, \beta_\infty, \beta_c, \delta_c, Re$ .

This way to compute the power coefficient tells us that to extract the  $C_{p,max}$  at a given  $x$  we must impose a  $\sigma$ . So, at constant speed, if  $N_b$  increases, the tip speed ratio decreases; in the same way increasing the chord the tip speed ratio decreases to reach the maximum power coefficient. So, an increase in solidity has as consequence the reduction of the rotational speed at which we can have the maximum  $C_p$ .

Now it is time to define what we consider as efficiency for a wind turbine:

$$\eta = \frac{\text{power extracted by the turbine}}{\text{power released by the wind passing through the actuator disc}}$$

$$\eta = \frac{\Omega M}{F_x V_D} = \frac{\Omega r dF_y}{(1-a)V_0 dF_x}$$

$$\eta = \frac{dL \sin \phi - dD \cos \phi}{dD \sin \phi + dL \cos \phi} \cot g \phi$$



From this definition of efficiency, we see that increasing the drag force, the efficiency decreases, but not linearly.

We define than the coefficient:

$$\epsilon = \frac{D}{L}$$

We see that when  $\epsilon \rightarrow 0$  we have that  $\eta \rightarrow 1$ .

The definition of  $\eta$  we have used allow us to compute the real power coefficient in a very convenient way:

$$dC_p = \left( \frac{dPW_{blade}}{dPW_{limit}} \right) \cdot \left( \frac{dPW_{limit}}{0.5\rho V_0^3 dA} \right) = \eta_i dC_{p,max}$$

Now it is important to find a way to consider the effect of the number of blades and their tip effects. The tip effect is the phenomenon that sees air flows around the tip from the lower to upper surface, due to the fact that pressure on the suction side is lower than on the pressure side, reducing lift and hence the power production near the tip .

In this thesis the chosen used method is the one developed by Prandtl in 1979, he developed a correction factor  $F$  function of the number of blades, the angle of the relative wind, the position of the blade.

$$F = \frac{2}{\pi} \arccos(e^{-f})$$

$$f = \frac{N_b}{2} \frac{R-r}{r \sin \phi} = \frac{N_b}{2} \frac{1-\frac{r}{R}}{\frac{r}{R} \sin \phi}$$

It is notable that the Prandtl correction factor is always between 0 and 1, in particular:

- $F \rightarrow 1$  reducing the number of blades
- $F \rightarrow 1$  reducing the tip speed ratio

With this factor we can obtain the values of the axial force and the torque taking into account the number of blades and the tip losses just multiplying it times the values we obtained before, considering an infinite number of blades, so multiplying it to equations (1.31) and (1.32).

$$dT = F\rho V_0^2 4a(1-a)\pi r dr$$

$$dM = F4a'(1-a)\rho V_0 \pi r^3 \Omega dr$$

It is now possible to evaluate a new definition for the axial induction coefficient and the tangential induction coefficient. Equalling the definitions of the axial force and the

torque we obtained, introducing the definition of solidity and the Prandtl correction factor:

*axial momentum change = axial force*

$$4\pi dr \rho V_0^2 a(1-a)F = \frac{1}{2} N_b \rho w^2 c (C_l \cos \phi + C_d \sin \phi) dr$$

*angular momentum change = torque*

$$4\pi r^3 dr \rho \Omega V_0 a'(1-a)F = \frac{1}{2} N_b \rho w^2 c (C_l \sin \phi - C_d \cos \phi) r dr$$

Remembering that the solidity is defined as  $\sigma = \frac{cN_b}{2\pi r}$  (putting  $\delta_c = 0$ )

$$a = \frac{\sigma w}{4V_0 F} \left( \frac{C_l}{\tan \phi} + C_d \right)$$

$$a' = \frac{\sigma w}{4\Omega r F} \left( C_l - \frac{C_d}{\tan \phi} \right)$$

Which are different from the Glauert optimal values of  $a$  and  $a'$ .

Another important consideration to do to have coherent results with the real data, is to correct the value of the axial induction factor when it is higher than 0.5.

We have seen that, from the axial momentum balance at  $r$

$$dT \propto 4a(1-a) = C_x$$

And this means that the  $dT$  decreases for an increase of  $a$ , once  $a > 0.5$ , which is not physical.

To overcome this problem many different corrections have been proposed, which are shown in Figure 33.

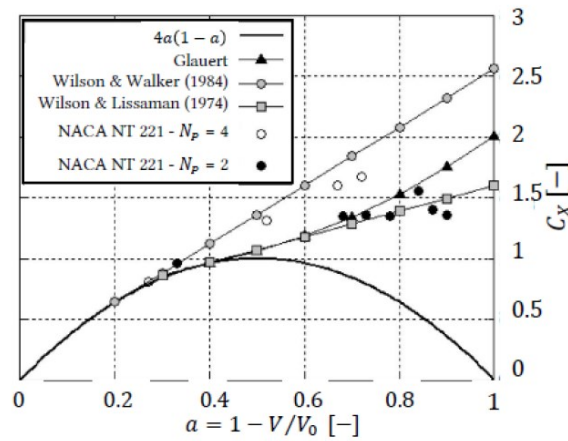


Figure 33: correction of a theories

The correction that will be followed in this thesis is the following:

$$C_x = C_{x,0} - 4(\sqrt{C_{x,0}} - 1)(1-a)$$

With  $C_{x,0} = C_x @ a = 1$

The correction is applied in case  $a > a_T$ , where  $a_T = 1 - \frac{\sqrt{C_{x,0}}}{2}$ .

### 9.3.2 Computational and aerodynamic issues in BEM evaluation

As mentioned at the beginning of this chapter, this thesis will focus on the steady state approach, with all the simplifications needed by the BEM algorithm. but it is important to highlight some effects that cause an increase in loads and a decrease in the power production expected with the BEM computations.

### 9.3.3 Non ideal steady State Aerodynamic Issues

These effects are typical also for a steady state situation but are not considered in the BEM equations. They are the degradation of the blade performance due to roughness on the surface, and stall condition that happen during rotational motion.

For what concerns roughness, it is worth a mention the fact that it can significantly increase the drag on the airfoil, bringing the power production of an airfoil a degradation up to 40%.

Stall effects during rotation are very difficult to predict since airfoil performances are usually measured in wind tunnels under non-rotating conditions. So, the rotation of the turbine itself can bring to unexpected stall conditions not forecasted during experiments.

### 9.3.4 Turbine wakes

BEM considers the induced velocities due to power production, the rotation of the turbine wake and the expanding wake downward the turbine, but the actual flow is much more complicated, and it can result in a 'skewed wake', with flow patterns not predictable by BEM [21].

Those effects concern the fact that the wake can be differentiated into far wakes and near waked, due to the different function of spatial distribution and intensity of the turbulence in the flow field. [25] The consequences are unpredictable behaviour of velocities and turbulence in turbine wakes, so an increase in fatigue loads. Another cause of a so called 'skewed wake' are the off-axis winds, that are wind that blows off the

direction perpendicular to the rotor. Those winds are due to yaw errors, or vertical wind components.

### 9.3.5 Unsteady aerodynamic effects

These effects are almost countless and all of them bring to a degradation of the turbine performances, some of them will be listed in this section.

*Tower shadow:* it is the condition in which the wind speed is decreased behind the tower due to the tower obstruction itself. This effect happens every rotation multiplied by the number of the blades of the turbine.

*Dynamic stall:* it is the condition in which a fast change in the wind speed (due to the tower shadow for example) cause a rapid detachment and reattachment of the air flow along the airfoil.

*Dynamic inflow:* it is the condition in which the steady state conditions are not satisfied due to the actuation of turbine regulations (pitch or yaw), or change in the rotor speed, without the ideal condition of the instantaneous time response considered in the BEM computations.

*Rotational samplings:* the fact that the wind as seen by the rotor is constantly changing as the rotor rotates, for examples turbulence eddies may be smaller than the rotor disc resulting in different winds at different part of the rotor disc. [21]

## 10 BEM EVALUATION OF THE STUDY-CASE TURBINE

---

### 10.1 CHOICE OF PROFILES AND DATA PROCESSING

This chapter will focus on the implementation of the BEM equations, presented before, in a case study.

The main airfoil used to conceive the blade, which will represent the primary section of the blade, has been chosen by the other participant of this project together with the Vestas supervisor, and it is the Nrel S809.

HAWT are designed using “families” of airfoils, that are different airfoils implemented in the same blade, at different radius, to achieve high performances of the overall blade. The family from which the entire blade will be derived is formed by the profiles S809, S810 and S811, for the primary part of the blade, the tip, and the root, respectively. [26]

Rotor Diameter	Category	Root	Primary	Tip
1-3 m	Thick	S835	S833	S834
3-10 m	Thick	S823	-	S822
10-20 m	Thin	<del>S804</del>	<del>S801</del>	<del>S802</del>
	Thin	<del>S804</del>	<del>S801</del>	<del>S803</del>
	Thin	S807	<del>S805</del>	<del>S806</del>
	Thin	S807	S805A	S806A
	Thin	S808	S805A	S806A
20-30 m	Thick	S821	S819	S820
	Thick	S811	S809	S810
	Thick	S814	S812	S813
20-40 m	Thick	S815	S812	S813
	-	S814	S825	S826
	-	S815	S825	S826
30-50 m	-	-	-	S829
	Thick	S818	S816	S817
	Thick	S818	S830	S831
40-50 m	Thick	S818	S830	S832
	Thick	S818	S827	S828

Figure 34: Nrel airfoil families [26]

The S-series airfoils are a special family of airfoils that have been developed by National Renewable Energy Laboratory (NREL) especially to be used in Horizontal Axis Wind Turbines (HAWT). Different airfoil families have been developed and divided depending on the efficiency they can achieve and the dimension of the rotor where they can be applied. [27]

The S809 has been studied to have a small variation over its parameters due to variations of the grit roughness and pitch oscillations [28].

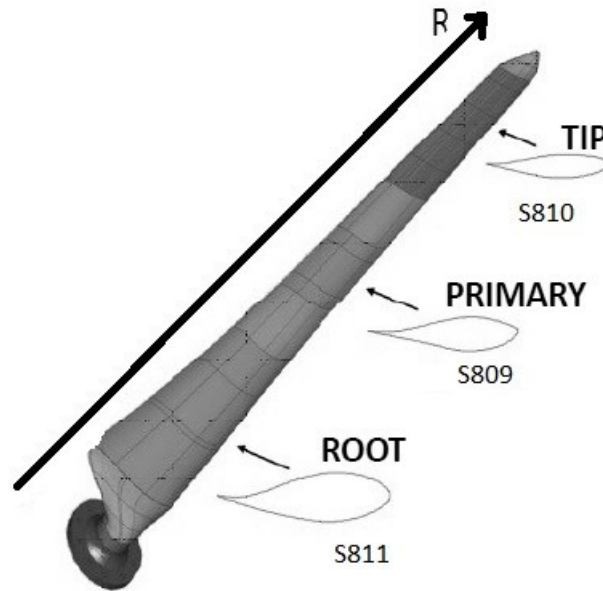


Figure 35: representation of the blade

S809

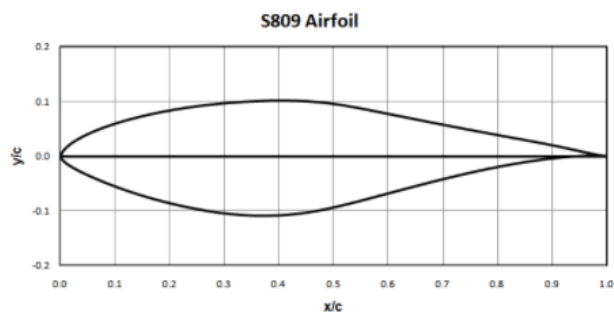


Figure 36: primary airfoil S809

Max thickness 21% at 39.5% chord.

Max camber 1% at 82.3% chord.

S810

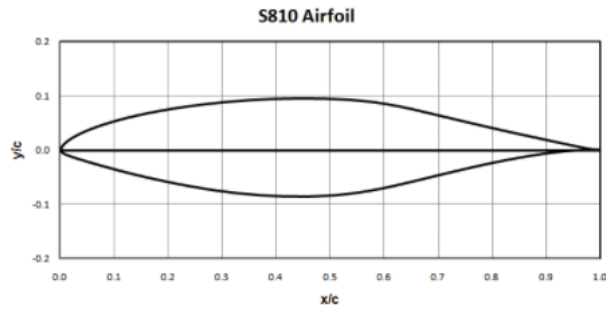


Figure 37: tip airfoil S810

Max thickness 18% at 44.2% chord.

Max camber 0.9% at 10.9% chord

S811

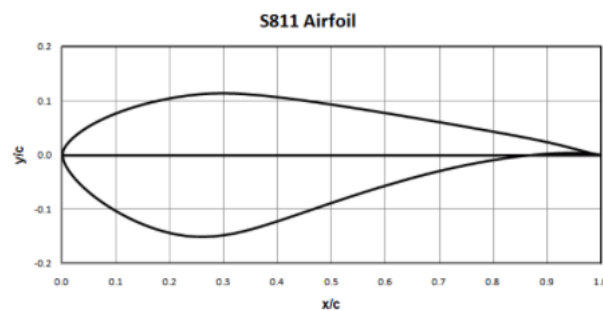


Figure 38: hub airfoil S811

Max thickness 26.3% at 27.4% chord.

Max camber 1.7% at 76.4% chord.

#### 10.1.1 Data Collection

After this first choice of the profiles, they have been divided again through the help of the program Xlfr5. XFLR5 is an analysis tool for airfoils, wings and planes operating at low Reynolds Numbers. It includes:

1. XFOIL's Direct and Inverse analysis capabilities
2. Wing design and analysis capabilities based on the Lifting Line Theory, on the Vortex Lattice Method, and on a 3D Panel Method. [29]

It has got a feature that allows to interpolate different profiles and have as outcome a profile which represents a linear interpolation of them. Eleven different profiles came out from this feature. They correspond to 0, 20, 40, 60, 80 per cent of the shape of the primary airfoil applied to the hub airfoil and the same percentage between the tip and the primary profiles. This operation enabled the creation of different profiles, then analysed with Xflr5 to find out more data, among them the values of CL and CD between the pitch angle of  $-6$  and  $+17^\circ$ , with a resolution of  $0.5$  degrees. This range of angles has been chosen due to problems of convergence of the program, that did not allow to overcome  $17^\circ$  in many cases. This condition, and the consequent lack of available data, cause the reduction of the original guess that was of  $25^\circ$ .

After that evaluation, every profile has been added of a flap, at 80% of the chord and with the angle of  $+10^\circ$  or  $-10^\circ$  and analysed again. This operation provided the data for every profile created for three positions of the flap ( $+10^\circ, 0^\circ, -10^\circ$ ) between the pitch angle of  $-6^\circ$  and  $17^\circ$ . Here is an example of the output for the S809 primary airfoil results.

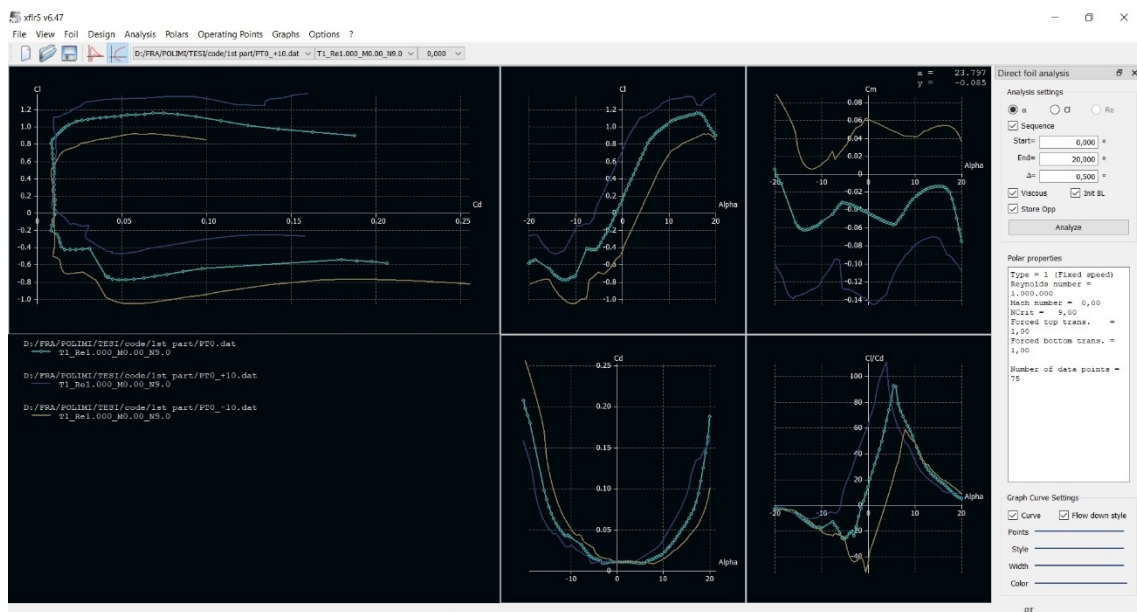


Figure 39: example of Xflr5 interview

All the data have been computed for different numbers of Reynolds, from 500.000 to 5.000.000 with a step of 500.000.

After this elaboration of data, an entire section of the MATLAB is dedicated to the importation and interpolation of data. In particular, Xflr5 exports all data in a txt file,



from which is possible to move data to MATLAB through a simple function. ANNEX

[A]

Here below an example of the output .txt file of Xflr5:

```
xflr5 v6.47
Calculated polar for: D:/FRA/POLIMI/TESI/code/1st part/PT10.dat
1 1 Reynolds number fixed          Mach number fixed
xtrf = 1.000 (top)          1.000 (bottom)
Mach = 0.000      Re = 2.000 e 6      Ncrit = 9.000
```

alpha	CL	CD	CDp	Cm	Top Xtr	Bot Xtr	Cpmin	Chinge	XCp
-6.000	-0.4214	0.02037	0.01503	-0.0415	0.6929	0.0086	-2.6459	0.0000	0.1417
-5.500	-0.3616	0.01664	0.01142	-0.0419	0.6719	0.0081	-2.5069	0.0000	0.1240
-5.000	-0.3160	0.01604	0.01085	-0.0418	0.6717	0.0110	-1.9320	0.0000	0.1076
-4.500	-0.2721	0.01694	0.01176	-0.0413	0.6714	0.0180	-1.3984	0.0000	0.0881
-4.000	-0.2336	0.01350	0.01176	-0.0413	0.6714	0.0180	-1.3984	0.0000	0.0881
-3.500	-0.1952	0.01009	0.00453	-0.0343	0.6708	0.0074	-1.5464	0.0000	0.0637
-3.000	-0.1452	0.00943	0.00378	-0.0341	0.6703	0.0062	-1.2010	0.0000	0.0031
-2.500	-0.0935	0.00876	0.00295	-0.0342	0.6697	0.0118	-0.9137	0.0000	-0.1304
-2.000	-0.0370	0.00858	0.00274	-0.0352	0.6691	0.0113	-0.6660	0.0000	-0.7322
-1.500	0.0197	0.00839	0.00261	-0.0363	0.6685	0.0148	-0.6404	0.0000	2.1281
-1.000	0.0769	0.00825	0.00252	-0.0375	0.6679	0.0179	-0.6144	0.0000	0.7437
-0.500	0.1182	0.00560	0.00152	-0.0377	0.6673	0.5473	-0.6150	0.0000	0.5700
0.000	0.1767	0.00553	0.00163	-0.0391	0.6667	0.5879	-0.6371	0.0000	0.4702
0.500	0.2358	0.00572	0.00197	-0.0404	0.6661	0.6182	-0.6597	0.0000	0.4190
1.000	0.2953	0.00569	0.00195	-0.0419	0.6647	0.6203	-0.6832	0.0000	0.3890
1.500	0.3549	0.00560	0.00186	-0.0434	0.6619	0.6222	-0.7082	0.0000	0.3688
2.000	0.4146	0.00525	0.00124	-0.0448	0.6394	0.5984	-0.7405	0.0000	0.3539
2.500	0.4728	0.00520	0.00121	-0.0460	0.6195	0.6166	-0.7675	0.0000	0.3428
3.000	0.4948	0.00748	0.00218	-0.0410	0.2996	0.6276	-0.7661	0.0000	0.3277
3.500	0.5238	0.00905	0.00297	-0.0374	0.1201	0.6299	-0.8241	0.0000	0.3157
4.000	0.5680	0.00970	0.00339	-0.0363	0.0670	0.6321	-0.9605	0.0000	0.3078
4.500	0.6170	0.01038	0.00392	-0.0358	0.1017	0.6395	-1.1433	0.0000	0.3013
5.000	0.6599	0.01063	0.00413	-0.0348	0.0281	0.6359	-1.3511	0.0000	0.2956
5.500	0.7172	0.01057	0.00436	-0.0360	0.0554	0.6377	-1.6055	0.0000	0.2926
6.000	0.7545	0.01143	0.00511	-0.0333	0.0782	0.6426	-1.8688	0.0000	0.2860
6.500	0.7805	0.01227	0.00581	-0.0290	0.0489	0.6434	-2.2815	0.0000	0.2784
7.000	0.8254	0.01235	0.00600	-0.0285	0.0197	0.6424	-2.8300	0.0000	0.2752
7.500	0.8625	0.01304	0.00670	-0.0266	0.0166	0.6433	-3.3663	0.0000	0.2709
8.000	0.8855	0.01446	0.00805	-0.0226	0.0022	0.6440	-3.6177	0.0000	0.2649
8.500	0.9182	0.01555	0.00929	-0.0204	0.0022	0.6445	-4.0502	0.0000	0.2608
9.000	0.9475	0.01692	0.01080	-0.0179	0.0024	0.6449	-4.4918	0.0000	0.2568
9.500	0.9731	0.01857	0.01265	-0.0152	0.0027	0.6452	-4.9062	0.0000	0.2528
10.000	0.9977	0.02031	0.01454	-0.0126	0.0031	0.6470	-5.3470	0.0000	0.2489
10.500	1.0136	0.02271	0.01715	-0.0092	0.0037	0.6507	-5.7049	0.0000	0.2446
11.000	1.0195	0.02607	0.02047	-0.0053	0.0038	0.6702	-6.0383	0.0000	0.2397
11.500	1.0234	0.03014	0.02502	0.0001	0.0048	0.6731	-6.0335	0.0000	0.2336
12.000	1.0315	0.03541	0.02502	0.0001	0.0048	0.6731	-6.0335	0.0000	0.2336
12.500	1.0409	0.04043	0.03570	0.0073	0.0054	0.6892	-6.3622	0.0000	0.2250
13.000	1.0307	0.04861	0.04447	0.0110	0.0062	0.6900	-6.1997	0.0000	0.2204
13.500	1.0127	0.05760	0.05395	0.0140	0.0066	0.6905	-5.9929	0.0000	0.2159
14.000	0.9491	0.06834	0.06510	0.0146	0.0069	0.6910	-5.7593	0.0000	0.2134
14.500	0.9038	0.08051	0.07762	0.0121	0.0071	0.6914	-5.5269	0.0000	0.2141
15.000	0.8631	0.09380	0.09119	0.0061	0.0071	0.6918	-5.3249	0.0000	0.2191
15.500	0.8291	0.10848	0.10611	-0.0031	0.0070	0.6921	-5.1317	0.0000	0.2286
16.000	0.7996	0.12477	0.12258	-0.0146	0.0068	0.6923	-4.8684	0.0000	0.2424
16.500	0.7572	0.15060	0.14847	-0.0283	0.0066	0.6924	-3.9551	0.0000	0.2614
17.000	0.7056	0.17985	0.14847	-0.0283	0.0066	0.6924	-3.9551	0.0000	0.2614

To enhance the resolution of the data, an entire part of the MATLAB code is dedicated to their interpolation.

The first interpolation is a linear one among the flap degrees, so to have data for each degree between -10 and +10. The chosen resolution is one degree. ANNEX [f1A]

Then, the second interpolation is among  $C_L$  and  $C_D$  coefficients, in this case too it is a linear interpolation to obtain values for 101 different profiles from the hub to the tip of the blade. ANNEX [f2A]

The last interpolation concerns the angle of attack, which was previously elaborated with a resolution of  $0.5^\circ$ , now it is linearly enhanced to  $0.1^\circ$ . ANNEX [f3A]

Below are depicted as an example the results of the profile number 75, which is between the primary and the tip part of the blade, with the flap angle of  $0^\circ$ .

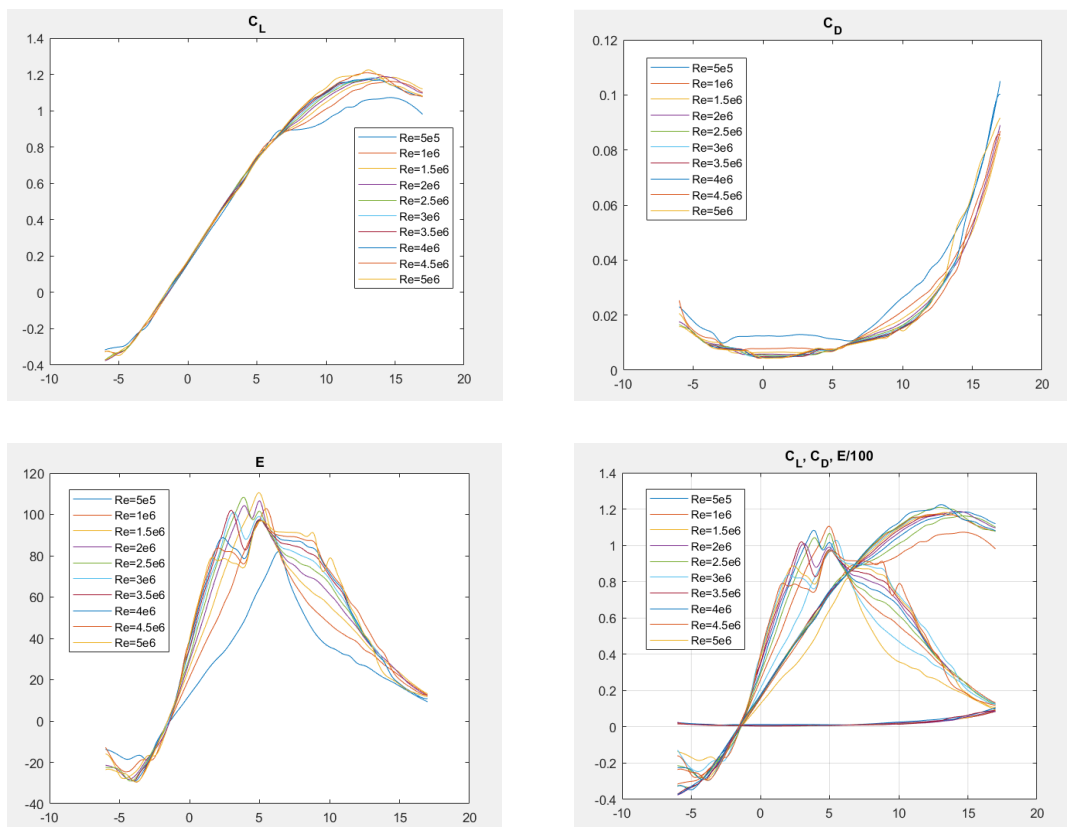


Figure 40:  $C_L$ ,  $C_D$ ,  $E$  values after interpolation, x-axis is the angle of attack

10.1.2 Design

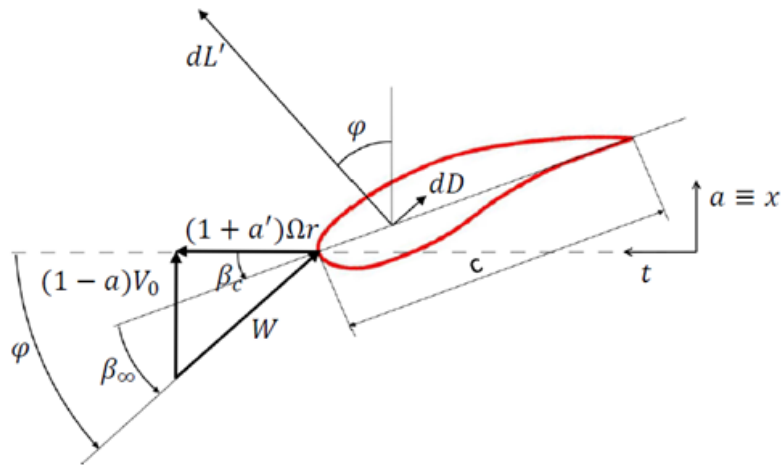


Figure 41: parameters on an airfoil

The design part of the program has got as objective to find the optimal chord, and with it all the parameters, for every considered section of the blade, at the designed speed of the turbine. ANNEX [B] As mentioned before, the total elements are 101.

The design parameters are:

$$V_0 = 8 \frac{m}{s} \quad D = 30 \text{ m} \quad \lambda = \frac{\Omega R}{V_0} = 7 \quad N_{bl} = 3$$

The value of the diameter of the turbine has been taken directly from Nrel guidelines of the used airfoils.

Hypothesis:

Coning angle and tilt angle are set at 0, the time delay is set at zero too. Consequently, all the formulas that present a  $\cos\delta_c$  have this parameter set to 1. The flap is considered absent, so the value of its opening is set to 0°.

The first assumption that is made is to consider the Glauert values for the axial induction factor ( $a$ ) and the BEM distribution for the tangential induction factor ( $a'$ ), and evaluate the optimal chord through the solidity converging on the Reynolds number. This operation is made using a dedicated function which returns the exact values of the  $C_L$  and  $C_D$  parameters depending on the  $Re$ . ANNEX [f1B]

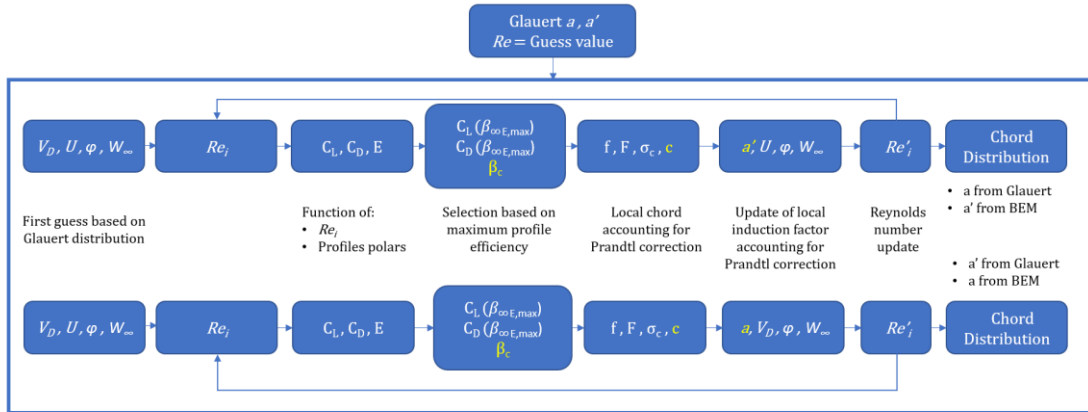


Figure 42: iterative computation to achieve the best chord distribution

The results obtained after this iterative process are the followings:

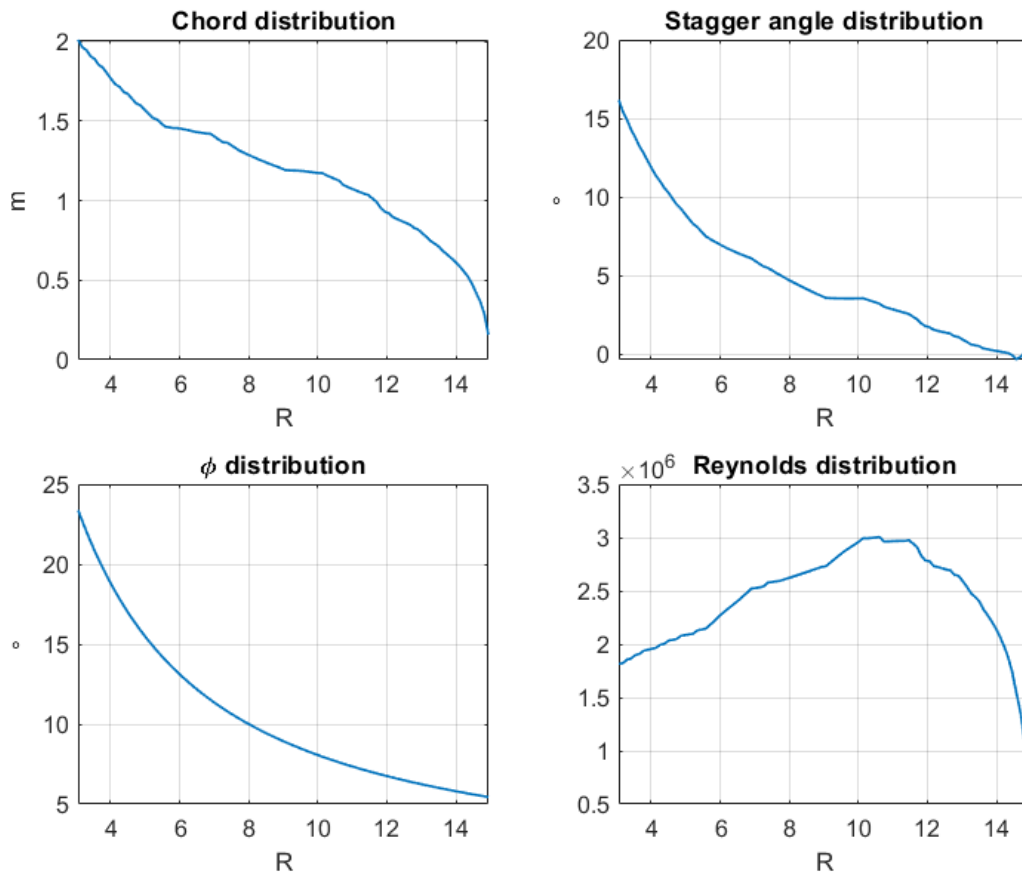


Figure 43: main results after the implementation of the first code

Then the exact same procedure is repeated unless using the BEM  $a$  distribution and the Glauert  $a'$  distribution, which provided very similar values unless for a slightly higher overall value for the chord.

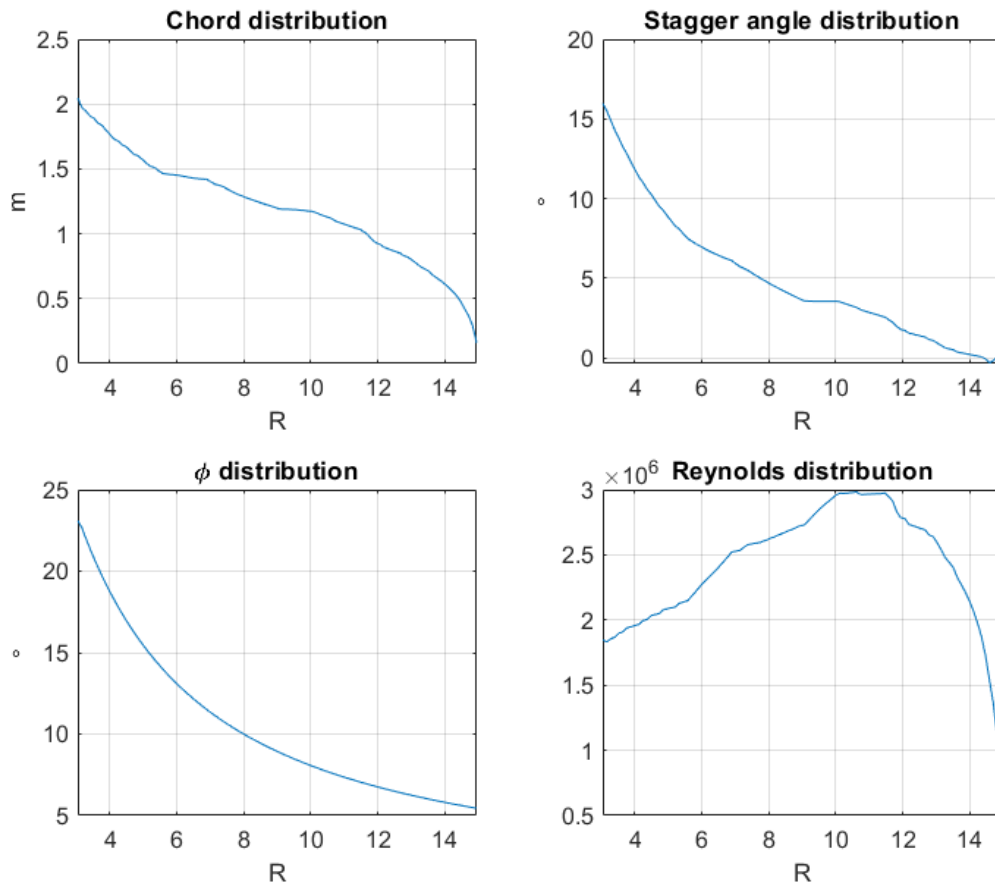


Figure 44: main results after the implementation of the second code

At last, the arithmetic average between the two results have been considered as the total outcome of this part of the code. This operation is necessary since it is possible to have two different equations to evaluate the chord, through  $a$  or  $a'$ , and this makes the problem mathematically not well posed, though physically it is. In all these computations we have considered the Prandtl's coefficient  $F$  to include in the computation the tip effects too.

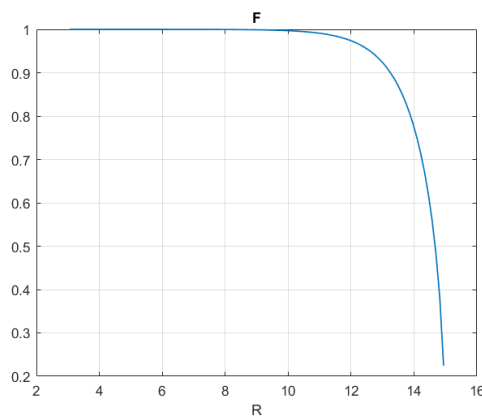


Figure 45: Prandtl coefficient  $F$  behaviour to include the tip effect

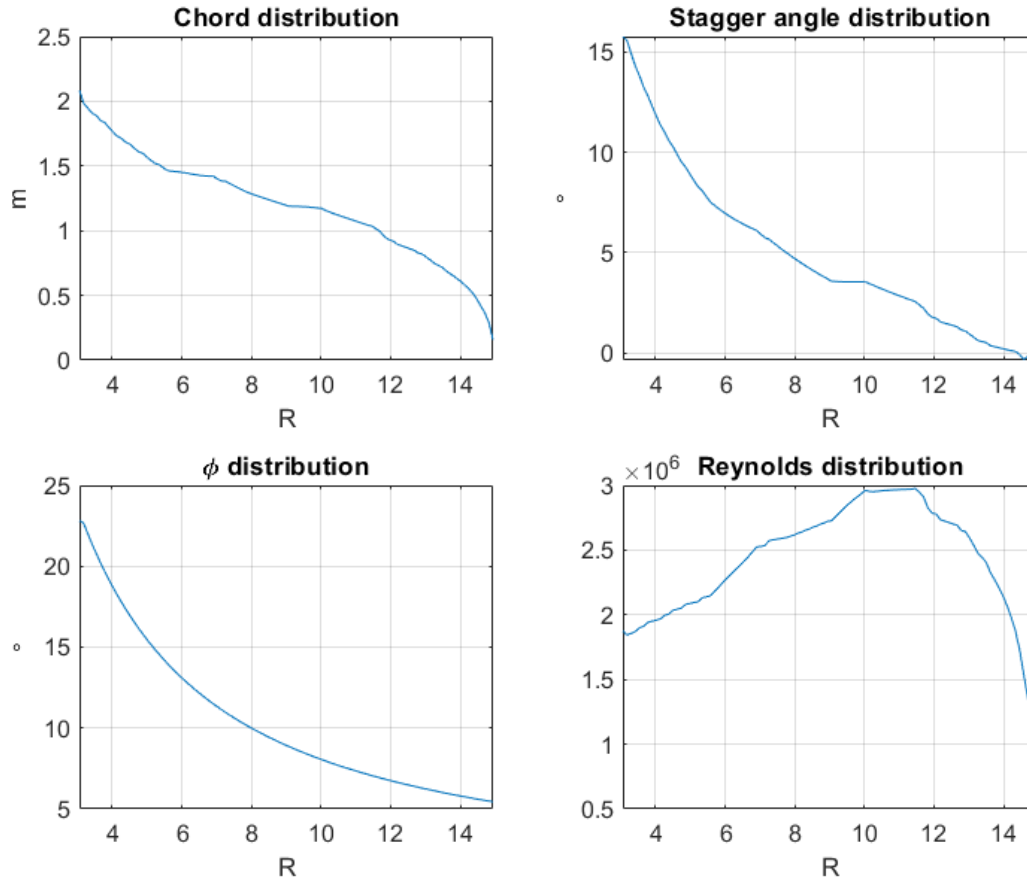


Figure 46: final averaged value

After this first evaluation of the chord some corrections should be made.

The first one is to check that  $\frac{C_{Max}}{R} \leq 0.12$  and to achieve it through a linearisation of the chord. This operation is compulsory to be done in order to make blades feasible to be built properly, without the creation of many difficulties in the process. This correction is made out with a convergence on the values of  $a$  and  $a'$ . In this way, the values of  $C_L$ ,  $C_D$ ,  $\beta_C$ ,  $\beta_\infty$ ,  $\phi$ ,  $W_\infty$ ,  $Re$  and  $F$  relative to the linearised chord have been calculated.

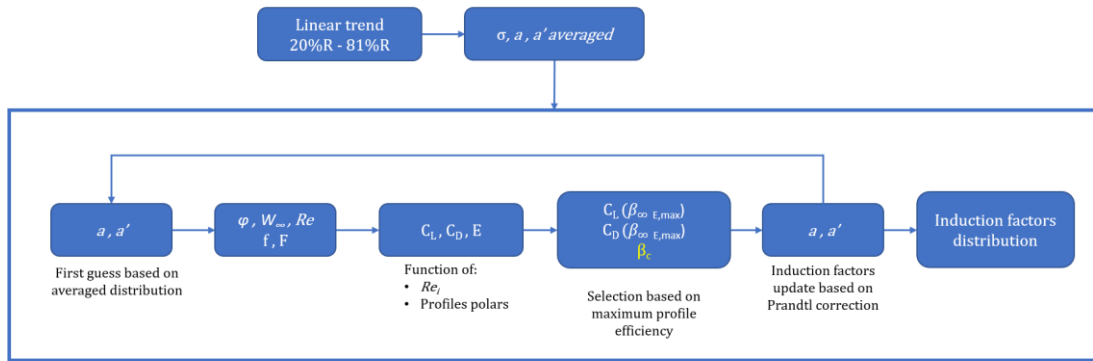


Figure 47: chord linearization procedure

The computation of axial and tangential induction factor has been made as:

$$a = \epsilon \tilde{a} + (1 - \epsilon)a \quad \text{and} \quad a' = \epsilon \tilde{a}' + (1 - \epsilon)a'$$

Where the  $\epsilon$  factor has only the role to help the conversion to happen.

After all these computations we end up with the optimal chord distribution of a feasible turbine and we can now evaluate the  $C_p$  value and the power coefficients from the force calculation or from the angular momentum balance calculation.

Choosing to linearise at 81% of the radius the obtained value of  $\frac{C_{Max}}{R} = 0.119 < 0.12$  is found. The resulting diagrams after this computation are showed in Figure 48.

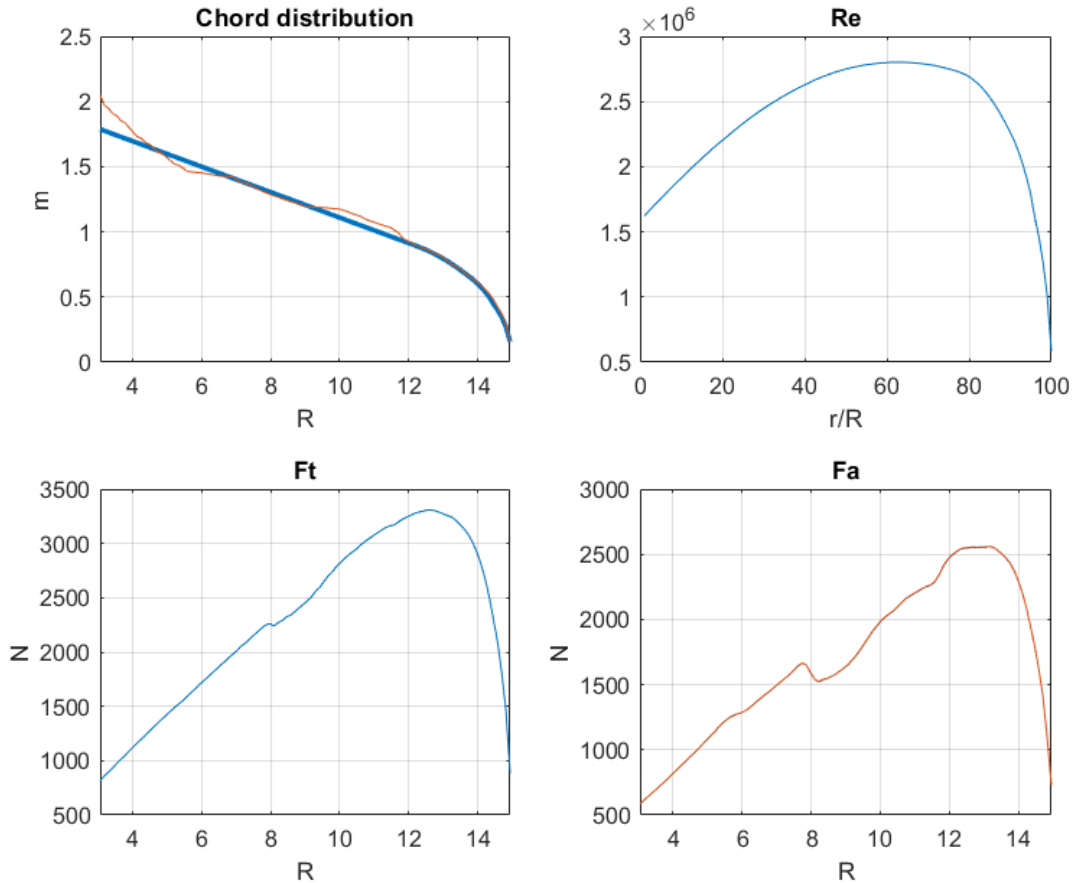


Figure 48: Final values of the corrected chord of the blade

The value of  $C_p$ , as described in the previous chapter, can be computer in two different ways: from force calculation and from the angular momentum balance. Its value happens to be:

$$C_p = \frac{N_b \Omega}{\pi R^2 2 V_0^3} \int_{R_{hub}}^R c W_\infty^2 (C_L \sin \phi - C_D \cos \phi) r dr = 0.4708$$

$$C_p = \frac{8}{\lambda^2} \int_{R_{hub}}^R c W_\infty^2 (C_L \sin \phi - C_D \cos \phi) r dr = 0.4711$$

The maximum cord, at the radius of the hub, has got the value of 1.787m while the smallest value of the chord is 0.1573m, at the very tip of the blade.

The maximum value of the Reynold number achieved at the design condition is 2.8015e+06.

The maximum thrust is of 2.564485e+03 N, while the maximum torque is of 3.304244e+03 N.



10.1.3 Off Design

It is essential in this part to consider a specific regulation strategy: here the selected regulation is a variable rotational speed generator plus pitch regulation strategy.

ANNEX [C]

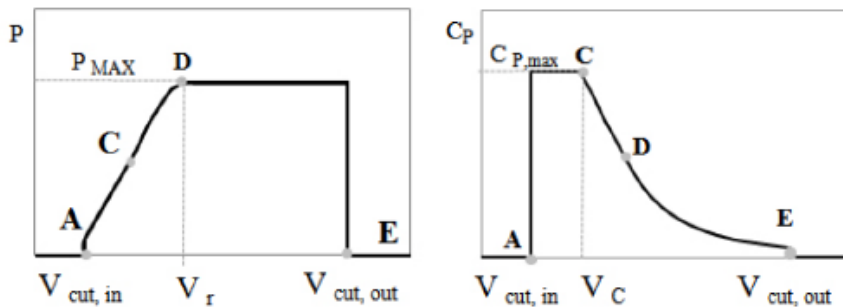
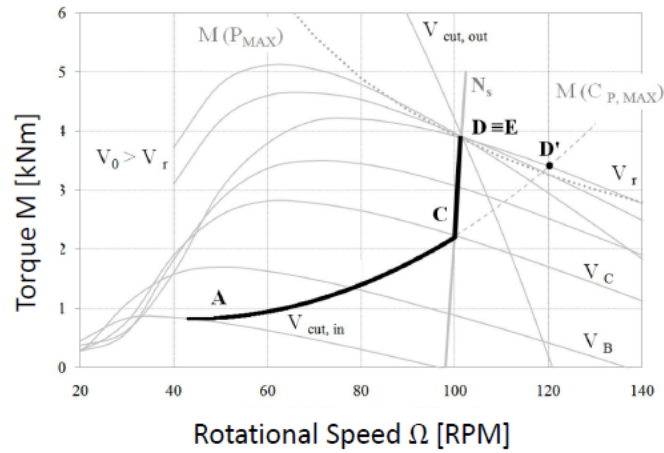


Figure 49: control strategy

The fixed parameters are:

$$V_{cut\ in\ or\ V_A} = 3.5 \frac{m}{s} \quad V_{rated\ or\ V_D} = 11 \frac{m}{s} \quad V_{cut\ out\ or\ V_E} = 20 \frac{m}{s}$$

$V_C$ , the wind speed at which the maximum rotational speed of the turbine is achieved, is chosen applying as constraint the maximum rotational speed of the blade at the tip at 70 m/s, so

$$\Omega_C = \frac{70 \frac{m}{s}}{15 m} = 4.6667 \text{ rpm} \quad V_C = 10 \frac{m}{s}$$

The code will be obviously divided into three different parts.

The first one is the part related to the wind speed between  $V_{cut\ in}$  and  $V_C$ , so the points A and C of the diagram in Figure 49. This part will see an increase of the torque with the wind speed and a variation of the rotational speed of the turbine, leaving fixed the pitch angle at the designed value. Once point C is achieved, the rotational speed together with the  $C_p$  are at their maximum, while the power output is not.

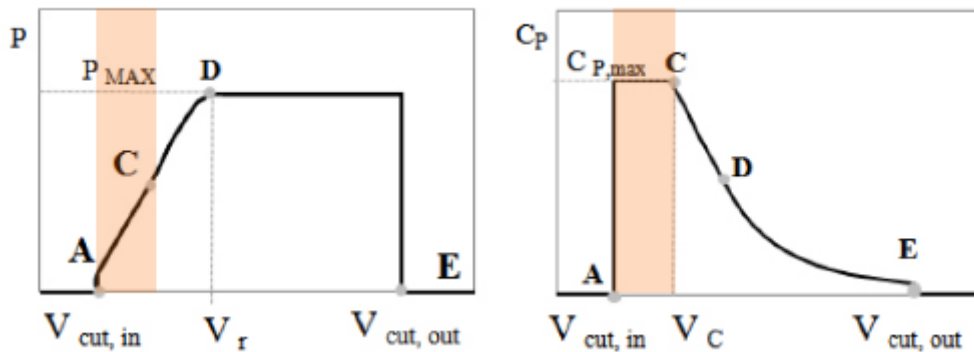


Figure 50: first part of the off-design evaluation

In this part the rotational speed  $\Omega$  is modified keeping the value of the tip speed ratio constant and the desired value  $\lambda = 7$ . The computation is based on a convergence on  $a$  and  $a'$  and a final check on the value of the  $C_p$ .

For each  $v \in [v_{cut,in}, v_C]$ :

- Compute  $\Omega$  from  $\lambda = \lambda_{des}$
- Guess values for  $a, a'$

For each  $R_j \in [R_{hub}, R]$ , given the geometry:

- Calculate  $W_\infty, \varphi, F$
- Calculate  $\beta_\infty, Re \rightarrow C_L, C_D$
- Calculate  $\tilde{a}, \tilde{a}'$  accounting for  $F$  and  $dD$  (BEM)
- Convergence criterion on  $a, a'$

- Calculate  $\dot{W}, C_p$  (check  $C_p \cong C_{p,max}$ )

Figure 51: iterative procedure of the first part

The second part is related to the wind speed between  $V_c$  and  $V_{rated}$ . From here the rotational speed of the turbine must be kept constant, which represents the maximum achievable rotational speed of the generator. The power will still increase due to the increase of the wind speed but the  $C_p$  will decrease to maintain the rotational speed

constant. This is achieved acting on the pitch angle, which will increase moved by the pitch regulation system placed at the base of the blade. Once the point D is achieved (the point at  $V_{rated}$ ) we have reached the maximum power output of the turbine.

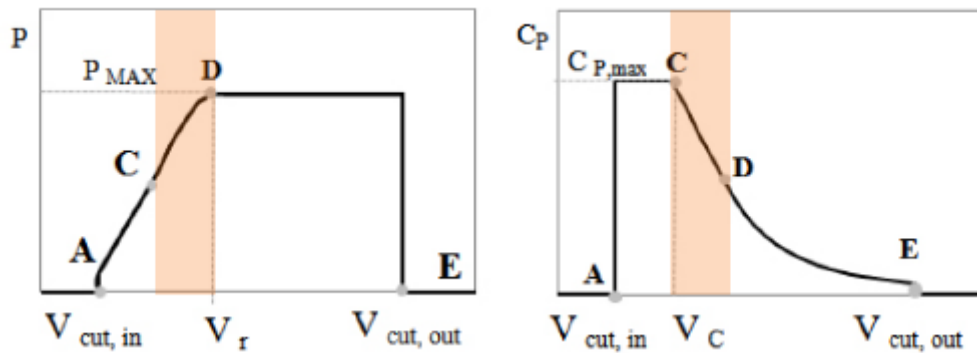


Figure 52: second part of the off-design evaluation

In this part the code is based on a convergence on  $a$  and  $a'$  with a check on the stall of the blade, this constraint is set at the value of 20%, which is the maximum acceptable amount of the blade that stalls. If this constraint is not respected, the pitch angle is increased, of course, with a resolution of  $0.1^\circ$ .

```

For each  $v \in [V_c, V_{rated}]$  :
  ○ Pitch variation vs. design:  $\Delta\beta_c = 0$ 
    • Guess values for  $a, a'$ 
      For each  $R_j \in [R_{hub}, R]$ , given the geometry and  $\Omega$ :
        ▪ Calculate  $\varphi, W_\infty, F$ 
        ▪ Calculate  $\beta_\infty, Re \rightarrow C_L, C_D$ 
        ▪ Calculate  $\tilde{a}, \tilde{a}'$  accounting for  $F$  and  $dD$ 
        ▪ Convergence criterion on  $a, a'$ 
        ▪  $\varepsilon = C_L/C_D < 0.95 \varepsilon_{max}$ ? If so, local stall
      • Stalled blade < 20%? If not, increase  $\Delta\beta_c$  and restart with new  $\beta_c$ 
    ○ Calculate  $\dot{W}, C_p$ 
  
```

Figure 53 :iterative procedure of the second part

The third part is between the wind speeds of  $V_{rated}$  and  $V_{cut\ off}$ , so between the points D and E of Figure 49. Here the objective is to maintain constant the power output of the turbine since the maximum value achievable has already been reached at the  $V_{rated}$  keeping on increasing the pitch angle and reducing the  $C_p$ . The same logic is used in the

code, applying a maximum tolerance on the output power of the machine, and converging on  $a$  and  $a'$ . The maximum value of the rated power, and so the choice of the rated speed, is usually determined by the generator.

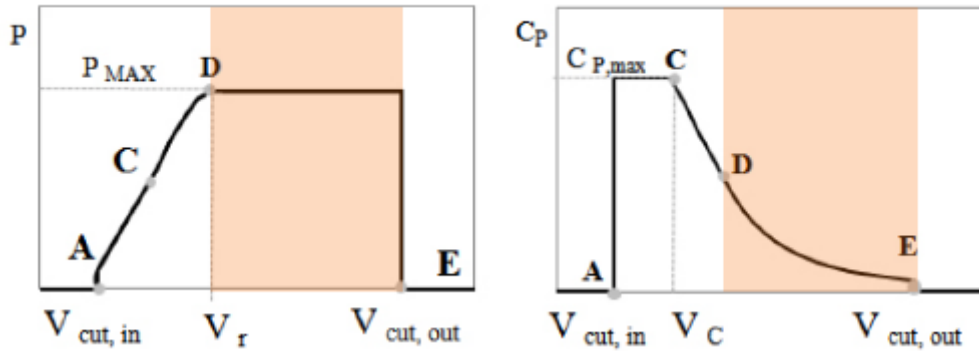


Figure 54: third part of the off-design evaluation

Also in this last part the iterative code is based on the convergence of  $a$  and  $a'$ , with a last check on the output power, which should be closer to the rated one than an acceptable tolerance. Every iteration sees a variation of the pitch control that helps to achieve the goal of a constant power output.

```

For each  $v \in [v_r, v_{cut,out}]$ :
  o Pitch variation:  $\Delta\beta_c = 0$ 
    • Guess values for  $a, a'$ 
      For each  $R_j \in [R_{hub}, R]$ , given the geometry and  $\Omega$ :
        • Calculate  $\varphi, W_\infty, F$ 
        • Calculate  $\beta_\infty, Re \rightarrow C_L, C_D$ 
        • Calculate  $\tilde{a}, \tilde{a}'$  accounting for  $F$  and  $dD$ 
        • Convergence criterion on  $a, a'$ 
      • Calculate  $\dot{W}, C_p$ 
      •  $|\dot{W} - \dot{W}_{rated}| < \text{toll}$  ? If not, increase  $\Delta\beta_c$  and restart
  
```

Figure 55: iterative procedure of the third part

The results of this computations are highlighted in these graphics, considering a blade with no flap at its trailing edge.

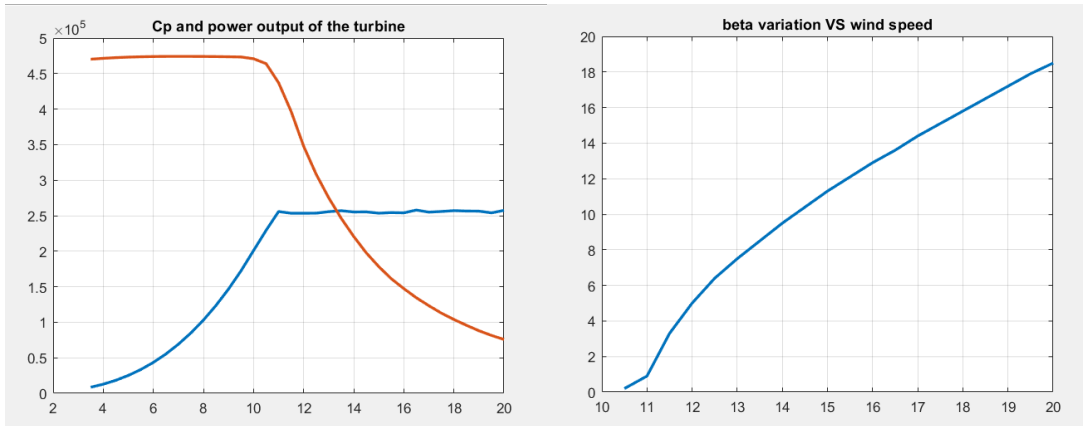


Figure 56:  $C_p$  and power graphics in the left picture, pitch variation in the right picture vertical axis for power output is in kW, for pitch regulation in  $^\circ$

Also, the axial force acting on the turbine is computed, and it follows the expected behaviour:

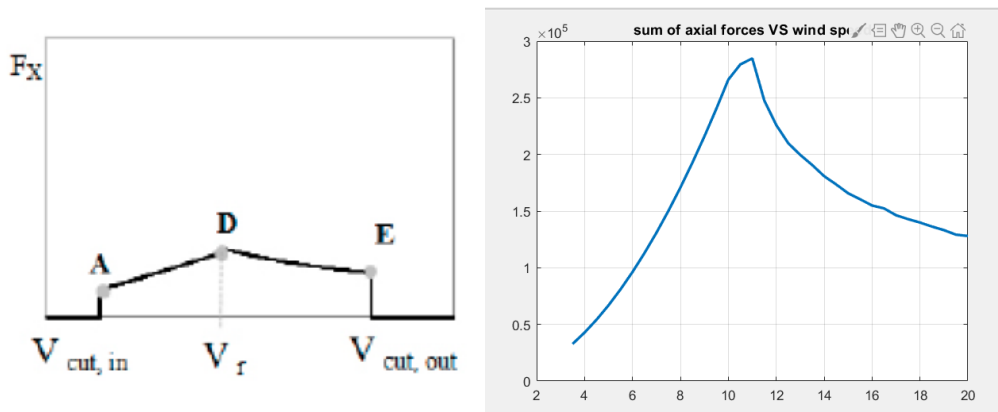


Figure 57: axial force, x-axis is the mean wind speed [m/s], y-axis is in N

max pitch variation =  $18.5^\circ$

$$P_{rated} = 256 \text{ kW}$$

$$\text{axial force @ } 11 \frac{m}{s} = 2.85 \times 10^5 \text{ N}$$

In the followings the presence of the flap is implemented in the algorithm and some results are worth of considerations. Some different strategies of the activation of the flap control and the pitch regulation are investigated to evaluate the effect the flap has got on the actual power output of the turbine.

## 10.2 INCLUSION OF THE FLAP

Now will be presented a first attempt to install the smart regulation system of the flap. Those configurations are only small experiments to see how the flap can interact with a turbine working properly, in a steady state condition. The presented flap is built on the outer half of the radius of the blade and the motion is in both directions, with an amplitude of 10 degrees. The flap is hinged at the 80% of the chord, and it is modelled thanks to Xflr5.

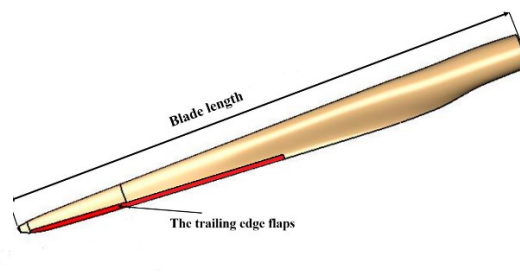
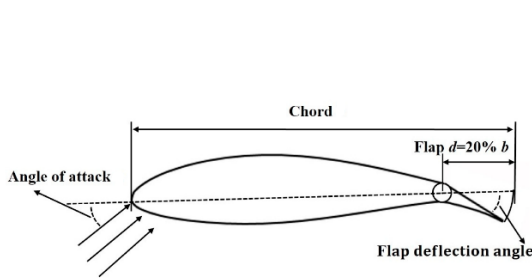


Figure 58: schematisation of the flap [30]

Figure 59: flap location on the blade [30]

### 10.2.1 Turbine flap orientation but with no pitch regulation

As already mentioned, these configurations are just an attempt to see how far the flap technology can effectively control the power output of the turbine. So, in this one, the same wind speed range is considered, the flap is activated and free to move between its amplitude of  $-10^\circ$  and  $+10^\circ$ , but the pitch regulation is not implemented. The turbine has always a variable rotational speed.

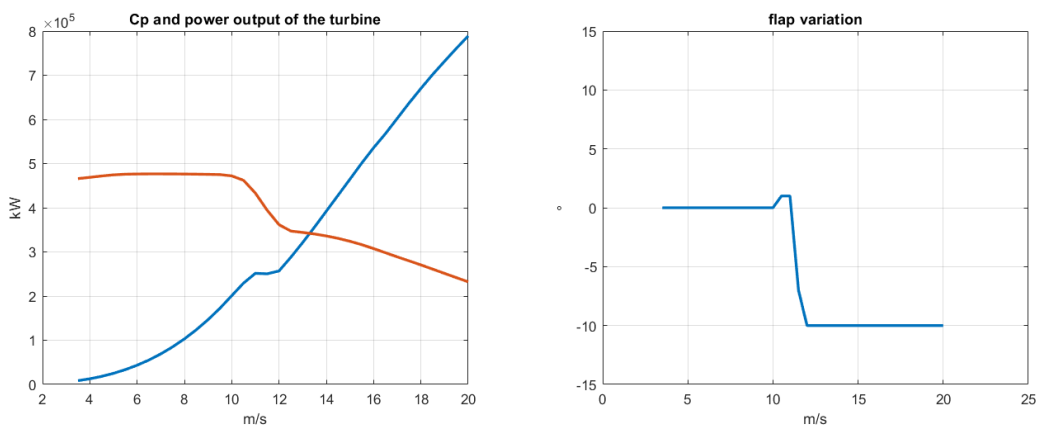


Figure 60: power and Cp output in case 1, with the flap motion

As expected, the flap orientation cannot really influence the power output. Despite the attempt of the flap to control it we can see a huge variation between the  $V_{rated}$  and the speeds beside it. The flap is trying to reach the maximum power generation at 11 m/s starting from zero degree and moving abroad, while it is trying to keep the power inside a small tolerance range for every speed beside the rated one. We can also see that after a wind speed of 12 m/s it cannot reach an effective control on the power and it increases very rapidly, despite the flap is oriented at  $-10^\circ$ , the position that should guarantee the higher dissipation of the power of the wind. Another important aspect that deserves to be mentioned is the impossibility for the turbine to reach the same  $P_{rated}$  as before, due to the lack of the pitch regulation.

$$P_{rated}(P_{11m/s}) = 251 \text{ kW}$$

Without the pitch orientation is than impossible to achieve an effective control on the machine at wind speeds that overcome the rated one. In this case it would force us to consider as  $V_{cut\ off}$  equal to 12 m/s and shut down the turbine once this speed is exceeded, wasting a huge amount of exploitable energy.

**10.2.2 A turbine which introduces the pitch regulation only after having exploited the flap orientation at its maximum.**

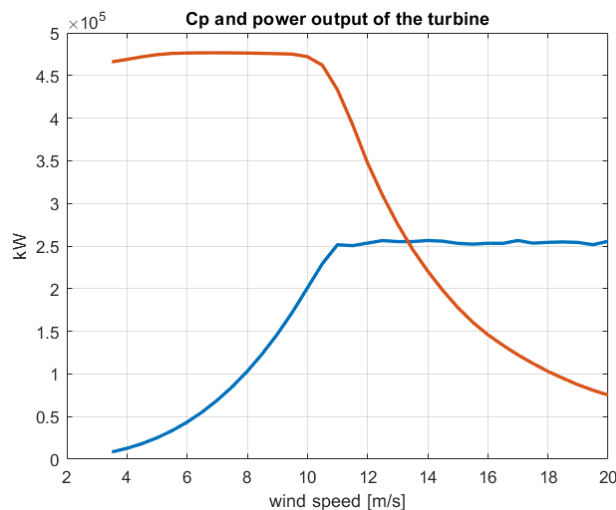


Figure 61: Cp and power output

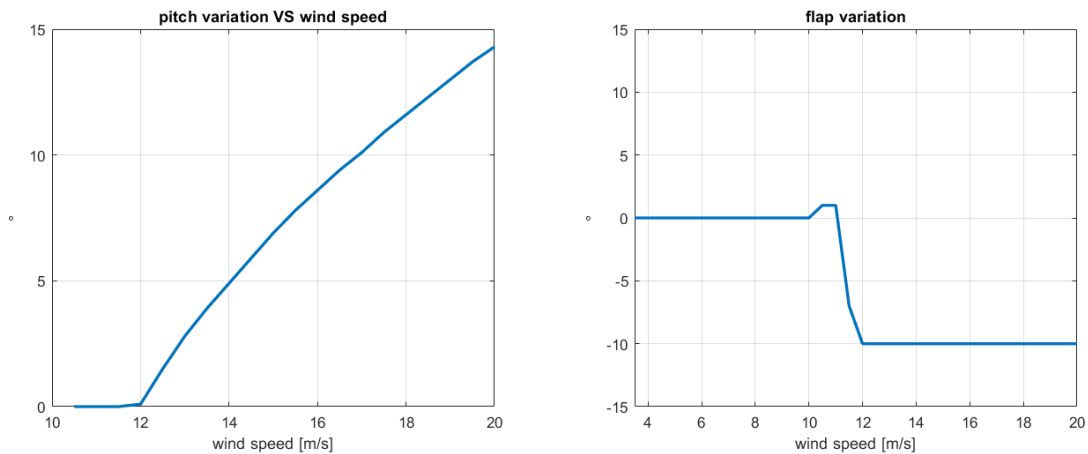


Figure 62: flap variation and pitch control activation

In this case the objective is to reduce at its minimum the use of the pitch regulation, trying to exploit the flap control in all its potential, without wasting the wind power after having reached the speed of 12 m/s, so still using the pitch regulation. The algorithm is trying to reach the rated power only adjusting the flap starting from the position at  $0^\circ$  and moving abroad, so to find a solution that does not stall the blade and that is not too far from the solution at  $0^\circ$  for the flap, allowing it to move again in case it is necessary. Only after having reached the maximum rotation of the flap the pitch regulation is considered. As we can see in these graphs, it is the same situation we saw in the previous case until 12 m/s, but thanks to the exploitation of the pitch regulation it is than possible to achieve good results in terms of power output until we reach  $V_{cut\ off}$ . The rotation of the blade is reduced, if compared to the rotation in the case with the absence of the flap, from  $18.5^\circ$  to  $14.3^\circ$ , which means a reduction of  $4.2^\circ$  in the adjust of the pitch angle. The delayed use of the pitch regulation makes it impossible to reach the same  $P_{rated}$  at the rated speed of 11 m/s as in the previous case.

$$P_{rated} = 251 \text{ kW}$$



10.2.3 A turbine with a combined configuration of the flap orientation and the pitch regulation

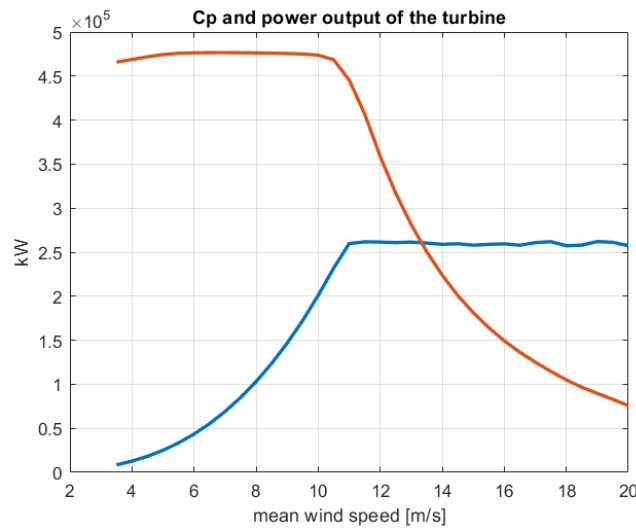


Figure 63: Cp and power output

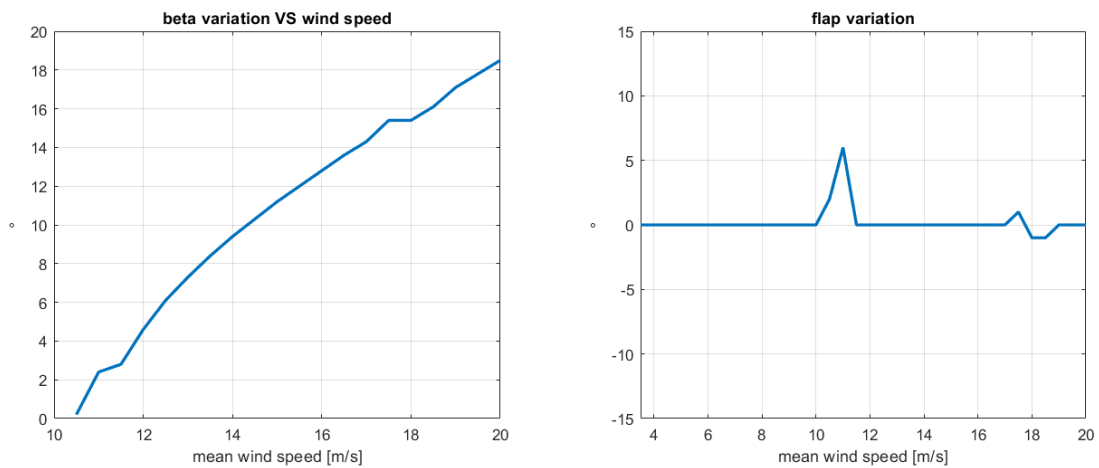


Figure 64: flap variation and pitch regulation

In this configuration the objective is to achieve a good configuration between these two technologies. The algorithm aims for the configuration that gives the maximum power output until  $P_{rated}$  is reached. Then for the configuration that guarantees the output power in a range of  $\pm 2.5$  kW from the rated wind speed to the cut-off speed, keeping the flap as close as possible to the value of  $0^\circ$  of motion. It may seem strange the flap orientation is not all at  $0^\circ$  between  $V_{rated}$  and  $V_{cut\ off}$  as it was in the first case, the reason is that the tolerance range has been narrowed around the  $P_{rated}$  from  $\pm 5$  kW to  $\pm 2.5$  kW and there was no possibility for the flap, at speeds between 17 m/s and 19 m/s to produce a power so close to the rated one if stuck at  $0^\circ$ .

$$P_{rated} = 260 \text{ kW} \quad \text{max pitch variation} = 18.5^\circ$$

As we can see, the  $P_{rated}$  is just slightly higher compared to the case where the flap is not present, this confirms the small effect the flap has on the global power output of the turbine.

A condition that all the configurations have in common is the maximum power output between  $V_{cut\ in}$  and  $V_C$  which is guaranteed for the flap stuck at  $0^\circ$ . This is since the blades are designed to achieve the maximum  $C_p$  in that configuration (flap angle equal to  $0^\circ$ ) at the speed of  $8 \frac{m}{s}$  which is in the named range.

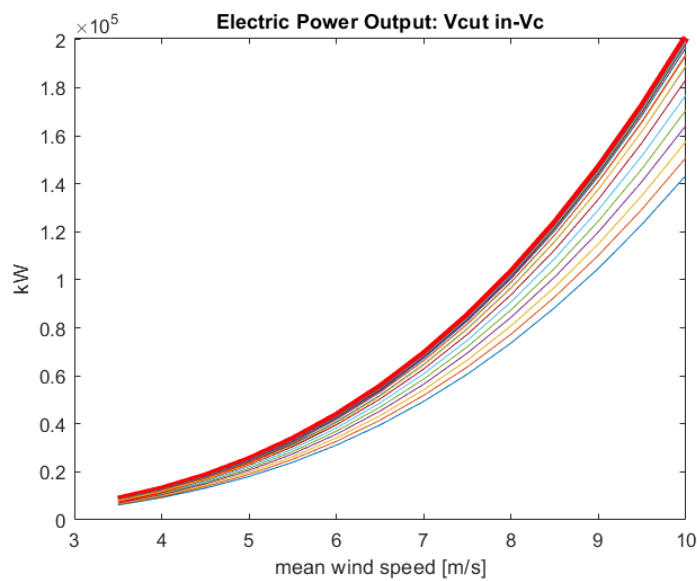


Figure 65: power output between  $V_{cut-in}$  and  $V_C$

In this plot we can see the power output between  $V_{cut\ in}$  and  $V_{rated}$  for every position of the flap, and the line corresponding to  $0^\circ$  is the one highlighted in red. This condition has the important consequence to make the turbine capable of working as expected in the wind speeds between  $v_{cut-in}$  and  $v_{rated}$  leaving the flap at  $0^\circ$ , therefore able to move only in case of unexpected load, due for example to gusts.

### 10.3 IMPLEMENTATION OF THE GUST

Since we saw that the presence of the flap cannot really affect the power production of the turbine, or at least it cannot enhance it, the main reason why this technology should be implemented is to better cope with an environment that presents gusts. Thanks to the fast flap motion, every blade of the turbine can temporarily modify the profile to better bear with the gust being subjected to a lower strain.

To verify this concept a simple configuration of a gust has been implemented in the code and the analysis will tell us how the turbine responds to it.

Since the BEM algorithm exploits and studies the effect of only the wind speed facing the turbine, the gust will be than outlined as a sudden increase of the axial speed, which implies the hypothesis of an instant respond of the turbine to the gust, in terms of adjust of the flap and the yaw control. Both the conditions without the gust and with the gust are considered in steady state conditions, so to use the same algorithm for both.

As depicted in the figure below the red vector represent the gust and  $\mu$  its incidence angle with respect to the main direction of the wind.



Figure 66: schematisation of the gust

The results show the consequences of a gust of 1 m/s vector acting with an angle of 45°: it results in an increase of the axial wind speed of  $1 \cdot \cos(45^\circ) = 0.7071 \text{ m/s}$ .

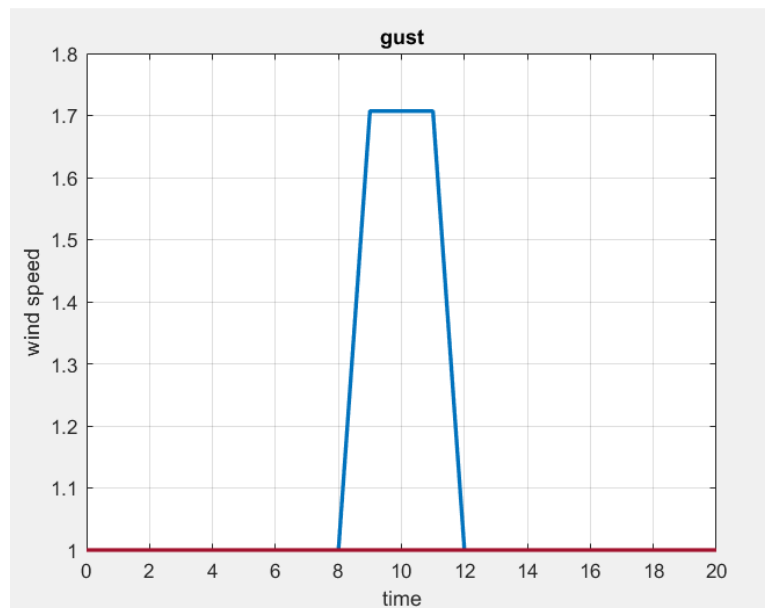


Figure 67: wind speed increment with the presence of the gust

### 10.3.1 Gust with no flap

Firstly, it should be investigated what could happen in the case we apply the gust to a turbine which does not have any kind of smart control implemented. So, the pitch and the yaw angle remain fixed at the angle they would be with no gust, and there is no flap to be activated.

The gust is applied on all the speed range.

It is important to highlight that the yaw angle and the pitch angle will be set fixed at the value computed in the case of absence of the gust in every case, since they are two slow kinds of control and cannot be activated promptly to face a gust. In the following graph we can see this effect on the pitch angle, which is exactly the same as before. Obviously, the gust has been implemented only in the off-design part of BEM computations, while the design part has been kept the same as the case with no gust. This implies the hypothesis of a turbine that should work properly without the activation of the flap if no gust is present in the environment.

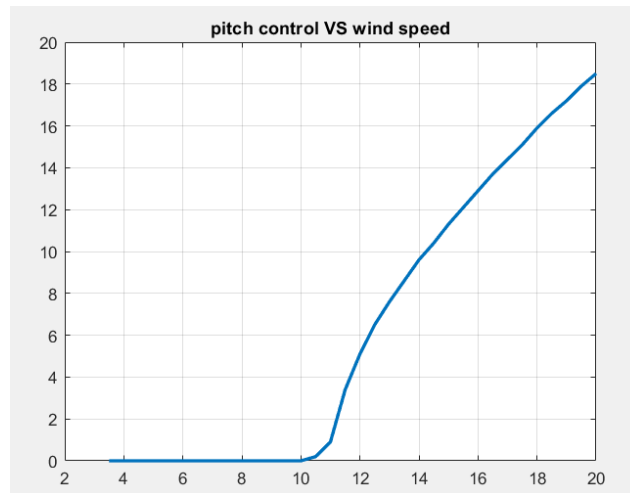


Figure 68: pitch control

In all the diagrams shown from this chapter on the wind speed depicted in the horizontal axis is the one that does not consider the gust so that a comparison with the previous case would be easier to do.

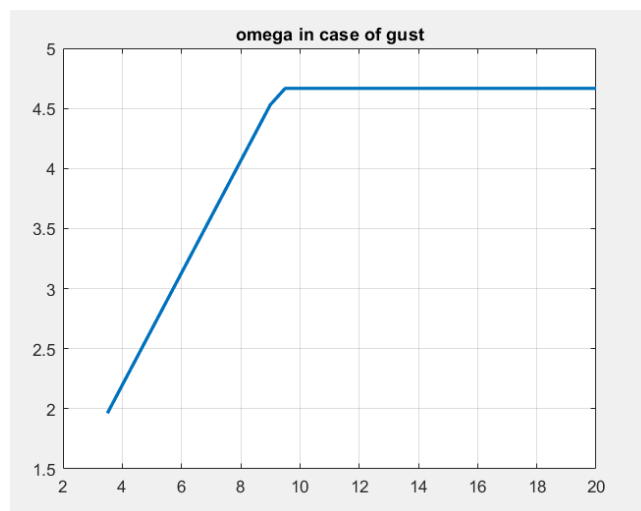


Figure 69: rotational speed of the turbine

In Figure 66Figure 69 we can see the first effect of the gust in the new steady state condition:  $V_C$  is achieved at a lower rotational speed. As explained in the previous chapter,  $V_C$  is the wind velocity at which the turbine reaches its maximum rotational speed. Of course, the maximum allowed rotational speed of the turbine has remained the same as in the case without the gust, since it depends on the components of the turbine (i.e., the electric generator) and structural limits of the turbine, for instance forces that act on the blade.

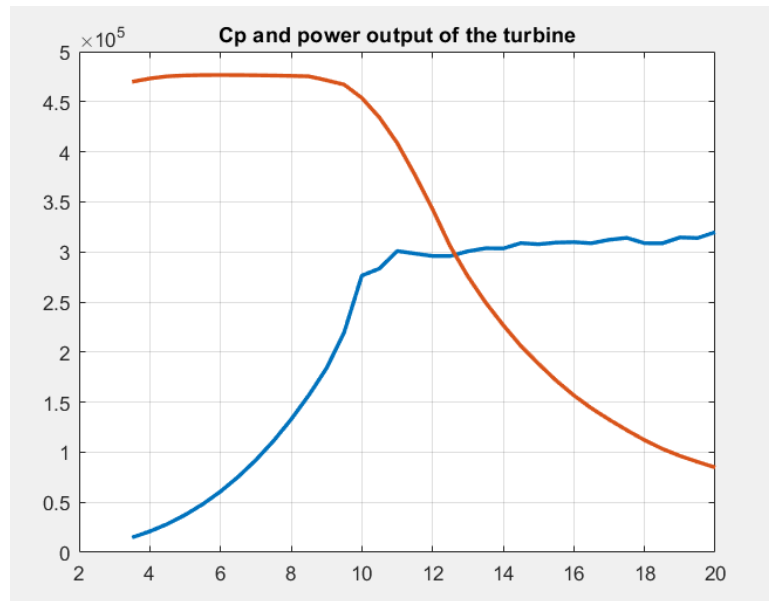


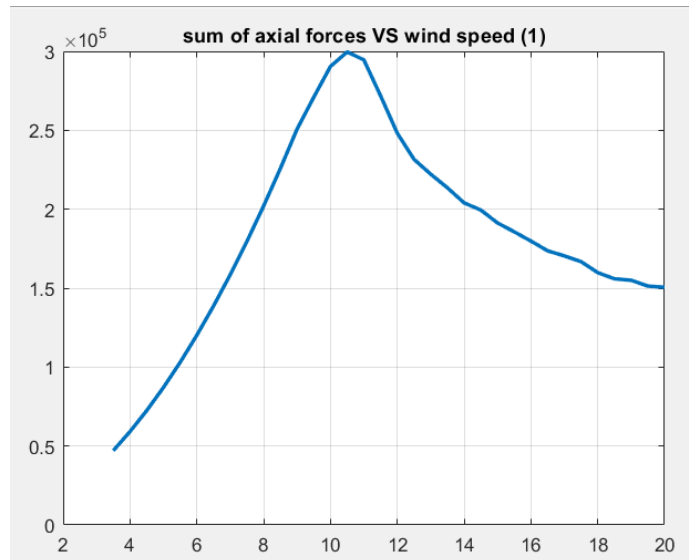
Figure 70: power output and  $C_p$  of the turbine

Figure 70 shows the power output and its  $C_p$  along all the range of wind velocities, from  $V_{cut.in}$  to  $V_{cut-out}$ . Comparing these results to the ones of the previous chapter, we can highlight different things. The first one is the rated power of the turbine, which is higher, due to the higher speed of the wind in case of gust.

$$P_{rated} = 300 \text{ kW}$$

Then, always talking about the power, we notice that it starts from a higher value at the cut-in velocity and increases at a higher rate than before. Furthermore, once the turbine has reached the rated rotational speed, we see the power to increase even faster, until it reaches the  $V_C$  speed, at 10 m/s. Computations have been kept the same as the previous case, so that computations follow the same rule and the algorithm changes at the same wind velocity as before. The “unstable” behaviour of the power between 9.5 m/s and 11 m/s is due to the obligation of the turbine to be stuck at the pitch control variation computed before. We see that this obligation generates another effect on the output power after the rated speed. In this range of velocities, the power should be kept as close to the rated one as possible, but we can see that it is increasing, since the pitch rotation computed before is not enough to cope with the increase of the wind speed in this condition and to keep the power output of the turbine constant.

For what concern the  $C_p$ , it follows the expected behaviour, almost the same as before.



*Figure 71: axial force acting on the blade.*

Another strong effect can be seen in the results of the axial force acting on the blade. The maximum reached value is now of  $3 \times 10^5$  N, 5.2 % more than the previous case. And it is reached at 10.5 m/s, and not anymore at 11 m/s, as we could have expected. This can be explained always looking at the pitch control variation, which starts to be consistent after 10.5 m/s, allowing the blade to better cope in terms of axial thrust with the increase in the wind velocity and to move the maximum value of the axial force in the region where the pitch regulation is not rotating enough the blades.

### 10.3.2 Gust with flap control

This section focuses on the main objective of this thesis: the effects of a smart flap control on the output values of a turbine in an environment with the presence of gusts.

The gust implemented is the same presented in the first section of this chapter, with an intensity of one meter per second and an incidence angle of 45 degrees.

As before, the yaw regulation is considered perfect, therefore no time delay is present in the simulation, and the parameters of the turbine are unchanged in the design values. The pitch regulation too has been kept as the values computed in the first case, the one which does not consider an environment with gusts.

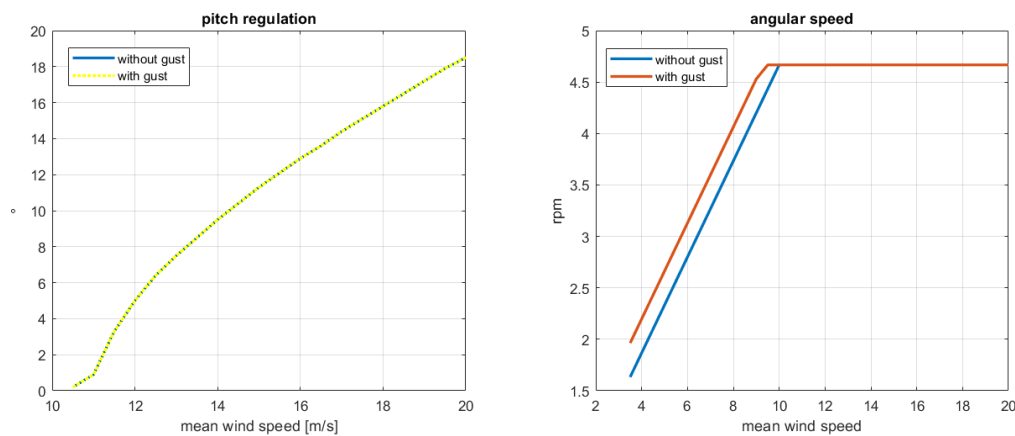


Figure 72: pitch regulation and rotational speed

As we can see in Figure 72, the beta variation, which stands for the pitch regulation, matches between the case without gust (blue line) and the one without (yellow dotted line). As already mentioned, this is due to the hypothesis that the pitch regulation is too slow to be activated to face the effect of a gust, which is a real condition, therefore it is kept equal to the one computed in the case without gusts.

In the same figure, in the right position, we can see that, exactly as the case in the first section of the chapter, the rotational speed varies in a different way compared to the variation in the case with no gust. Now it reaches the maximum allowed rotational speed at a lower wind speed, since it is meant to be increased of the value added by the gust. This fact caused before, in the case with no flaps, an unexpected behaviour in the power output of the turbine, due to the fixed pitch control at the condition of a calm environment.



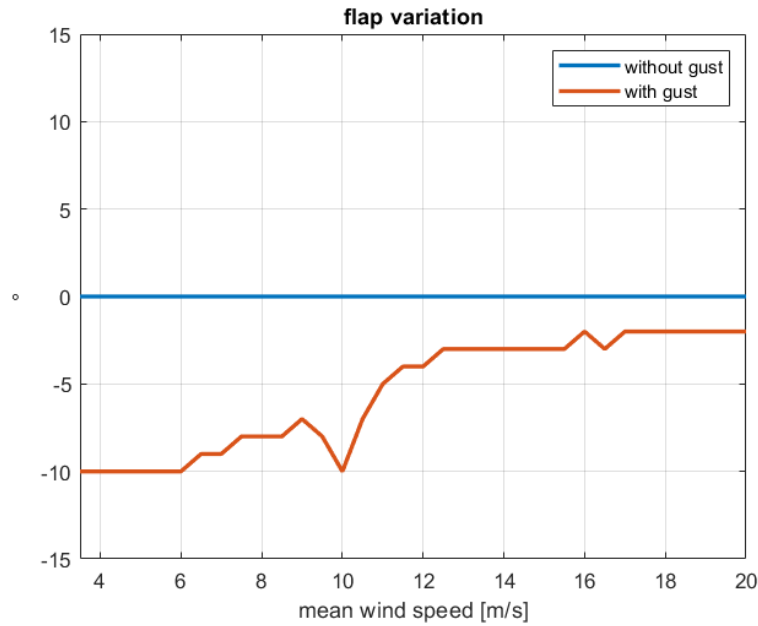


Figure 73: flap variation at different wind speed

Figure 73 shows the way the flap reacts on the presence of the gust. We see that in case of no gust the flap is not actuated, as the blue line highlights the angle of rotation is kept at the value of zero degree. The red line is the one that shows us the rotation around its hinge when sensors read a gust. The objective of the algorithm is not to enhance the power output of the turbine but to keep it as close as possible to the power production of a turbine in an environment without gusts, so to make easier its prediction. The negative rotation is in the direction in which the flap dissipates some of the energy of the wind while the positive direction tents to increase the performances of the airfoil. In the case-study the angle is always negative since the implemented gust increases the velocity of the wind and so its intrinsic kinetic energy. The variation of the angle of rotation of the flap is due to different reasons. Near the cut-in velocity the flap is oriented at its maximum angle since the gust has a great relative value on the original wind speed:

$$\frac{0.7071}{3.5} = 20\%$$

So going to a higher wind speed keeping the same value of the gust, make it less effective in terms of relative variation of the kinetic speed of the wind, and so make the variation more easily manageable by the flap and require a smaller angular variation.

Between the cut-in velocity and 9.5 m/s the turbine can manage to reach the same value of power output as the turbine with no gust using both the increase of the rotational speed and the flap motion, while the pitch regulation, fixed at the no-gust computation values, starts its motion at 10.5 m/s. We can see that these factors have an effect in the flap orientation. Between 9 and 10 m/s, in fact, the flap is increasing again the angle, passing from  $-7^\circ$  to  $-10^\circ$ , and we can see this inversion of the variation coincide with the wind speeds at which the turbine reaches its maximum angular velocity without having the possibility to activate the pitch regulation. After the value of 10 m/s the flap can better control the power output of the turbine thanks to the activation of the pitch regulation, which starts to happen at a mean wind speed of 10.5 m/s, therefore we see that the flap is now starting to reduce the opening angle around its hinge.

The results in terms of power and  $C_p$  are shown in Figure 74.

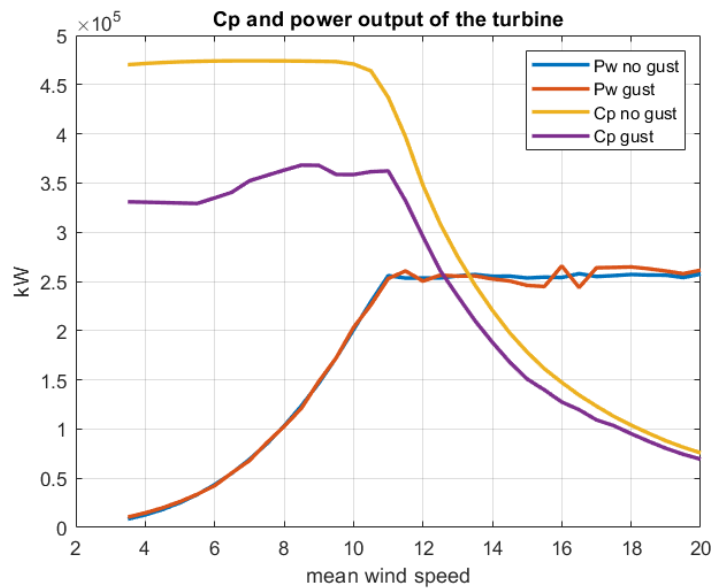


Figure 74: power output and  $C_p$  comparison

In the above picture we see how well can be managed the power output of the turbine. It can be kept almost equal to the one computed in case of constant wind speed (blue line), as the percentage variation plot describes.

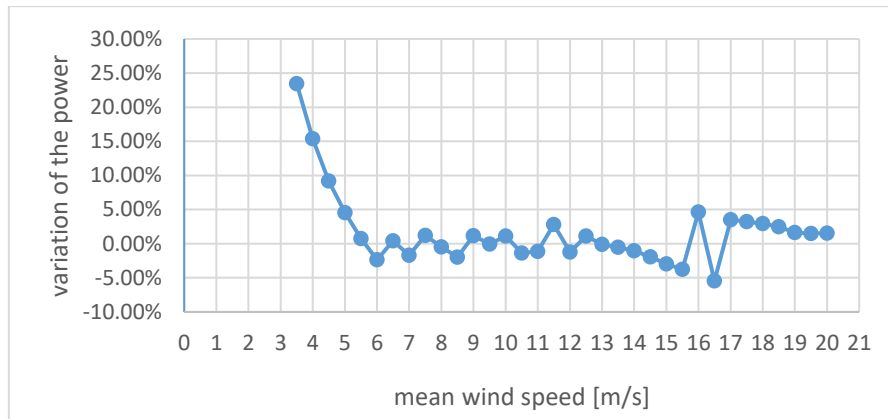


Figure 75: percentage variation on power production

Obviously, the percentage variation is higher in the area where the wind speeds are closer to the value of the gust, so near the cut-in speed, even if in absolute values the variation of the power output is not so high. We can see that, after a mean wind velocity of 5 m/s, the variation is always lower than 5% in absolute value. This value is exceeded only at 16 m/s and 16.5 m/s, that matches with the flap variation between  $-3^\circ$  and  $-2^\circ$ . This error can be easily reduced considering a smaller resolution of the flap variation angle, which has been considered of one degree in this thesis, a very high value, due to computation limit of the calculator.

For what concerns the power coefficient, it follows an expected behaviour. It decreases compared to the value of the case with no gust since the effective energy of the wind that is exploited through the turbine reduces: the flap is always dissipating some of its kinetic energy being at a negative degree rotation in the whole range. Then, of course, the value of  $C_p$  keeps being smaller but with a smaller difference going up with the wind velocities: this is because the gust has always the same value and has a smaller and smaller relative effect on the mean wind speed. It is interesting to highlight how it follows the trend of the flap too. Before the rated speed of the wind, in the portion of wind speed range where the  $C_p$  is supposed to stay almost constant, the  $C_p$  increases while the flap decreases its negative angle and decreases when it moves in the opposite direction.

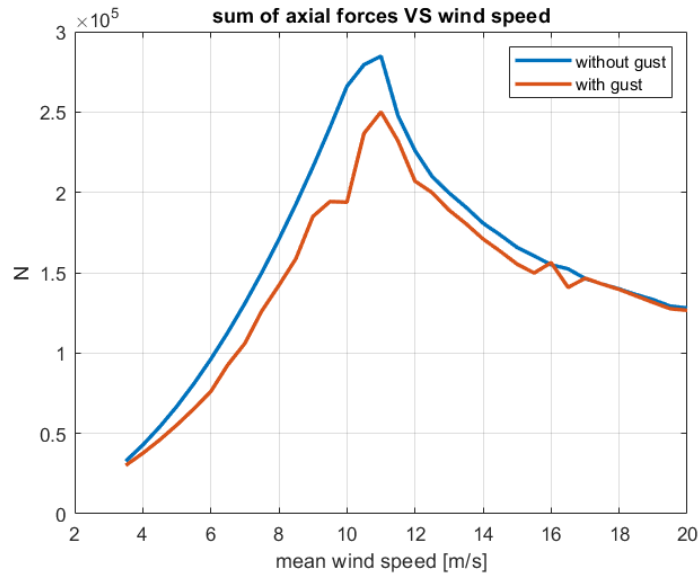


Figure 76: axial force acting on the turbine

For what concerns the axial force, Figure 76 shows a huge variation after the introduction of the flap. We see that it decreases despite the wind speed is increasing due to the gust. The only portion where the increase in wind speed manage to compensate the effect of the gust is at 16 /s and from 17 m/s until the cut-off velocity, once the relative value of the gust is lower than 4.4% of the mean wind speed.

But the main comparison to be made in terms of axial strain is between the two cases that experience the presence of the gust: the one without the flap and the one with the smart control regulation.

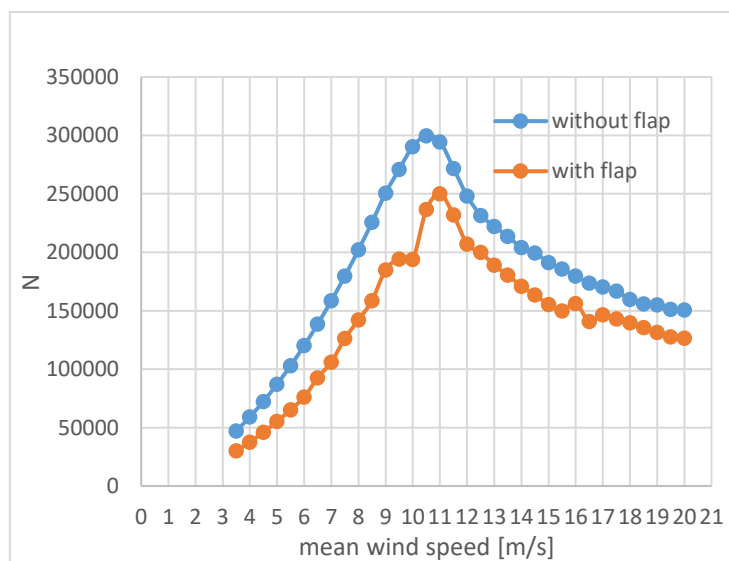


Figure 77: axial forces

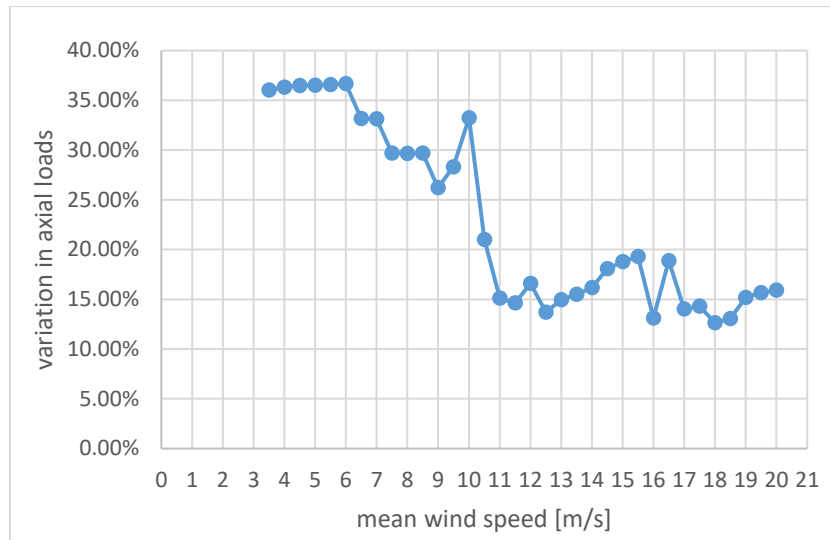


Figure 78: percentage differential on axial force

Figure 77 and Figure 78 show this comparison. It is clear that the difference between the two conditions is now higher than the previous case, when the presence of the gust was not considered in the case with no flap. In this case the two values of the axial forces never match, as they did before in the wind speed range between 17 m/s and the cut-off velocity. The variation in percentage of the axial forces acting on the three blades (these forces refer to the entire turbine) is going from the higher value of 36.6% at 6 m/s to the lower of 12.6% at the speed of 18 m/s. These differences are very big and highlights the validity of this solution having as objective the reduction of the strains affecting the turbine in case of gusts. Also, this result shows the limitation that is introduced considering a resolution of the motion of the flap of 1 degree. It is evident that the variation of the axial force follows the variation of the flap with big differences coinciding with the motion of the flap. These values can be made smoother increasing the resolution and bringing it for example to a value of 0.1 degree. Afterwards a linear interpolation in retrospect will be made to reduce this error.

## 11 ECONOMIC FEASIBILITY ANALYSIS

---

In this chapter of the thesis the economic feasibility of the project will be studied. This first analysis will be an important step in the choice to continue or not with the development of this project.

The case that will be studied to have valuable economic data for the project is the following:

A reference turbine will be considered together with another one which can produce more. In particular, the second one will be a turbine exactly the same as the reference one unless the length of the blades, which will be more. The second turbine will suffer the same value of axial strains as the reference one thanks to the presence of the flap. In this case Opex and Capex will be modified, and the output threshold value will be the difference in the Capex value between the two turbines (considered part of a wind farm). Lifespan of the two turbines will be the same.

### 11.1 ECONOMIC PARAMETERS

The economic coefficient that will be considered to see whether the project should be convenient or not are the Net Present Value (NPV), the Internal Rate of Return (IRR), the Payback Time (PBT) and the Levelized Cost Of Electricity (LCOE). All of them are commonly used in the economic evaluation of projects and allow good results despite having only some available starting data.

#### 11.1.1 Net Present Value

The first parameter, the NPV, is obtained bringing all the cash flow at a discounted value. Moreover, to make all of these cash flows comparable, they must refer to the same instant in time. It is straightforward that a positive value of the NPV refers to a good investment while a negative value refers to a bad investment. As a drawback this coefficient is not a good parameter alone to confront different investments since it appears to have a higher value the bigger is the dimension of the investment itself. Another issue is related to the discount rate, the choice of which is critic. The NPV, generally, relies heavily on

assumptions and estimates, this is the reason why all of them must be clearly defined, so that the result can be read giving it the correct value.

$$NPV = \sum_{t=1}^n \frac{R_t}{(1 + r_{disc})^t}$$

Where  $R_t$  is the net cash inflow minus outflows during the single period  $t$ ,  $r_{disc}$  is the discount rate and  $t$  the number of time periods. In the computations of the case-study it is computed summing all the discounted cash flows. Cash flows are computed as a fraction of the Capex (capital expenditure) for the first two years, when the wind farm is built but does not produce any revenue so far, while it is computed as a difference among revenues, Opex (operational expenditures) and taxes for the other time periods.

$$CF_{i=-1,0} = X_{-1,0} \cdot CAPEX$$

$$CF_{i>0} = R(i) - OPEX(i) - T(i)$$

Where  $X_{-1}$  and  $X_0$  are two numbers between 0 and 1 following the condition  $X_{-1} + X_0 = 1$ ,  $R(i)$  are the revenues at time  $i$ ,  $T(i)$  are the taxes at time  $i$ .

Opex changes through the years as varies the inflation:

$$OPEX(i + 1) = OPEX(i) * (1 + r_{infl})$$

Here we can observe that the  $r_{infl}$ , the inflation rate, typical of the location of the plant, can affect a lot the expenditures over the year experienced by the project.

$$T(i) = profit(i) * r_{tax}$$

Taxis too changes through the years following the tax rate,  $r_{tax}$ . This value can vary due to political choices and market fluctuations.

$$DCF(i) = CF(i) * (1 + r_{disc})^{-1}$$

Here  $DCF(i)$  stands for the Discounted Cash Flow at period,  $r_{disc}$  is the discount rate.

$$CDCF(i) = \sum_{j=0}^i DCF(i)_j$$

$$NPV = \sum_i DCF(i)$$

Of course, the difference between the Cumulative Discounted Cash Flow (CDCF) and the Net Present Value is the fact that the NPV is always computed considering all the time periods.

### **11.1.2 Internal Rate of Return**

The second parameter, the IRR, is the value of the discount rate that, if exists, make the value of the Net Present Value to be equal to zero. The Internal Rate of Return is more effective than the NPV to confront different investments, with different life-time too, but it is usually considered less effective than the NPV to consider the profitability or not of an investment. Even if it is used as instrument to compare projects with different lifespans or amount of required capital, its first condition to be considered an effective parameter is that it must be higher than the Weighted Average Cost of Capital (WACC). WACC can be considered as the threshold value of internal rate of return at or under which a project cannot be considered attractive anymore. Since the definition of IRR, the formula it relies on is the same formula of the NPV and, generally speaking, since it represents the annual return that makes the NPV equal to zero, the higher the IRR, the more desirable an investment is to undertake. For us, it will be a meaningful parameter, because the comparison will be between the existing plant with a modified version of the same. [31]

### **11.1.3 Payback Period**

The third parameter that is going to be observed in this chapter is the Payback Time, which simply is the year at which the cumulative discounted cash flow becomes positive for the first time. Therefore, it represents the amount of time it takes to recover the cost of the investment. Of course, the shorter this value is the more attractive the investment is. A drawback is that this method fails to account for the time value of money, so, the longer is the period of the investment, the greater is the inaccuracy of this parameter.

### **11.1.4 Levelized cost of energy**

This parameter is usually computed to compare the cost of energy in different production options. It can be useful to compare different technologies too. In this thesis it will be a parameter that could help us understand how the trailing edge flap can affect the economy of a wind farm.



$$LCOE = \frac{ICC * FCR + O\&Mcost}{E} + LL$$

Where ICC stands for Initial capital cost (€ or £) and FCR is the Fixed Charge Rate (%). Obviously E stands for the annual energy production (kWh) and O&Mcost represents the annual operation and maintenance cost (€ or £), LL represents the land lease (€ or £).

FCR itself is a function of the discount rate chosen in the computation of the DCF:

$$FCR = \frac{r_{disc}}{1 - (1 + r_{disc})^{-n}}$$

$n$ = estimated lifetime of the wind farm in years, 20.

Land lease is considered negligible and so put at a value of £0.

Another computation that is more commonly used in the estimation of the LCOE is the following simplified version, commonly used in the wind industry to evaluate the feasibility of future projects:

$$LCOE = \frac{\sum_{t=1}^n \frac{I_t + M_t + F_t}{(1 + r)^t}}{\sum_{t=1}^n \frac{E_t}{(1 + r)^t}}$$

With:  $I_t$ =Investment expenditures in the year t (including financing)

$M_t$  =Operations and maintenance expenditures in the year t

$F_t$  =Fuel expenditures in the year t

$E_t$  =Electricity generation in the year t

$r$  =Discount rate

$n$  =Life of the system in years [32]

This last version for the computation of LCOE, under the suggestion of Mr. Vronsky, will be used, since it is the formula typically used in Vestas too.

### 11.1.5 Procedure

The followed procedure starts with the implementation of the Discount Cash Flow (DCF) approach. This is a static approach, which in the end considers only the value of

the NPV and suggests starting the project if it is positive, and, in case of multiple projects, to start with the one with the higher value. This approach has three limitations: the first one is about time, the investor is supposed to make all his decisions immediately, with no possibility of modifications during the project's life. Then, it does not consider the possible fluctuations in the cash flow. Finally, the use of the actualisation coefficient to express the risk can bring to misleading, since this factor itself is affected by estimation errors. [33] The first step consists of fixing the investor's choices: the technology to use (in this case the offshore wind energy), the budget and the plant location. Then, these data are elaborated to find out the exact values necessary for the computation of the above-mentioned economic parameters. After that, the Discount Cash Flow analysis is made, and the output of the second step are used to evaluate the indicators NPV, IRR and PBT, the first useful data for the investor. [33]

The analysis is based on an existing wind farm, this allows me to have information about the actual power curve of the turbines which constitute the wind farm (computations allowed the use of the power curve at an air density of  $1.12 \frac{kg}{m^3}$ ) and to operate through a Weibull wind distribution to make an effective study of this technology. The frequency wind distribution here obtained is called  $f(v)$  and does not have a unit of measurement while the electric power  $P_{el}$  is calculated as kW.

Then, it is convenient to compute the power of the wind, in particular the theoretical power associated to the wind that interacts with the surface swept by the turbine:

$$P_{wind} = \dot{m} * E_{kinetic} = \rho A_D V_0 * \frac{V_0^2}{2} = \frac{1}{2} \rho V_0^3 A_D$$

Having computed  $P_{wind}$  it is now straight forward the computation of the power coefficient just by doing:

$$C_p = \frac{P_{el}}{P_{wind}}$$

After that, in order to make some economic consideration, it is necessary the definition of some parameters. The first parameter we must take into account is the availability efficiency from which we can obtain the availability hours of operation of the wind farm.

$$\eta_{available} = \frac{h_{available}}{h_{year}}$$

It is necessary to highlight that this definition has an important intrinsic hypothesis: the hours of stop have the same probability to happen for each wind velocity.

Following, it is finally possible to evaluate the electric energy generation through one year of the selected turbine by doing:

$$E = P_{el} \cdot f(v) \cdot h_{available}$$

As we can see the unit of measurement is in kWh. Before passing to the evaluation of the economic parameters, other two coefficients are worth of computation, they will help evaluate the differences between the two different configurations of the plants in subject. They are the equivalent hours, which represents the number of hours the plant (turbine) should work at nominal power to produce the electric energy evaluated just above, and the capacity factor, which is the ratio among equivalent hours and the total amount of hours in a year.

$$h_{eq} = \frac{E}{P_{nom}}$$

$$C_F = \frac{h_{eq}}{h_{year}}$$

## 11.2 REFERENCE SITE

The reference site that is the one of Barrow, in Cumbria, England. It has been chosen since it hosts Vestas turbines and, due to its age, it is a potential site which can see the installation of the trailing edge flap on the next generation of turbines that will fit it, if there will be.



Figure 79: map of Barrow wind farm

This wind farm has been performing since July 2006 and the 20 years of lifetime assumed are almost reached. It has a capacity of 90 MW, reached through 30 Vestas V-90 turbines capable to reach a nominal power of 3 MW apiece. The swept area is of 6362 meters and the depth of water at which turbines are fixed is of 15÷20 meters, the distance from the shore is of 12.8 km. [34]

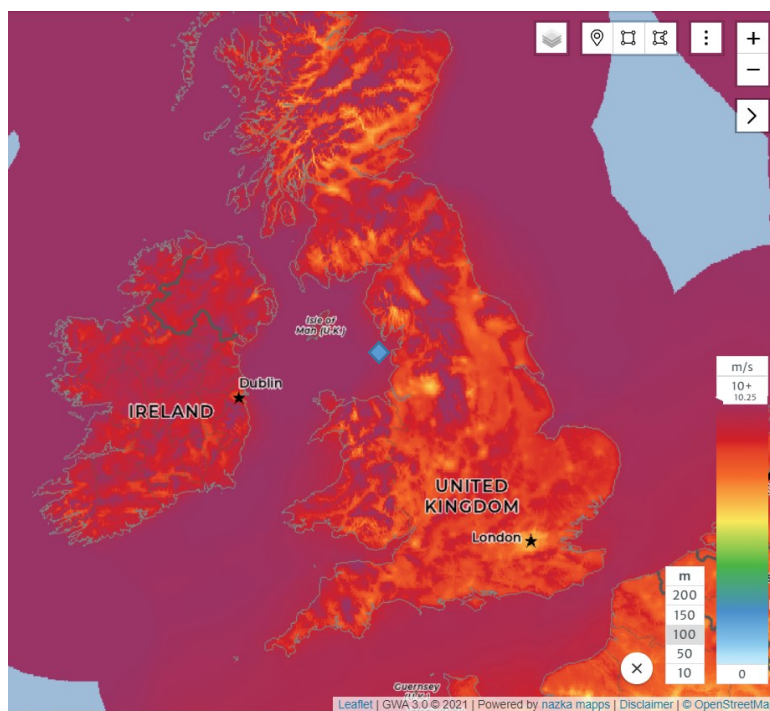


Figure 80: UK wind mean speed at 100m

As we can see in Figure 80 wind speed in the Barrow location is high, and the presence of a huge wind farm is easily justified (mean wind speed > 9m/s). [35]

The Capital Expenditures (CAPEX) of the barrow wind farm is of £1367/kW, which brings to a total CAPEX of the wind farm of around 123.030.000£ and a CAPEX for one of its Vestas V-90 turbines of 4.101.000£.

The Operating Expenditure (OPEX) is of about £10/MWh produced by the wind farm, which brings to a value of 110.618£ for the first year. Both Capex and Opex may seem pretty high, but they are very highly affected by the long distance of the wind farm from the shore.

As we have seen in the previous paragraphs, three important parameters are needed to evaluate some economic coefficients, the value of which has to be decided (or computed) before the DCF evaluations:  $r_{infl}$ ,  $r_{tax}$ ,  $r_{disc}$ .

The inflation rate is computed making an average between the Hodrick Prescott mean and the arithmetic mean of the growth rate of the Gross Domestic Product (GDP) Per Capita in the United Kingdom along the years 1960 and 2019. The output value is 1.71, which makes the inflation rate to have the value of  $r_{infl} = 0.0171$ .

For the evaluation of the tax rate  $r_{tax}$  the corporate tax rate has been used [36]. This is a form of taxation that every company that has a profit must pay in the United Kingdom. The government website allowed to find the value of the Corporate Tax Rate backward to 2006. In particular, the values of the mentioned tax from the year 2006 to 2014 were computed through the government calculator [37] while the values starting from the year 2015 were known [38]. For the years going from 2021 and 2025 the hypothesis of a tax rate equal to 20% is estimated.

Year	Rtax
2004	-
2005	-
2006	0.3
2007	0.3
2008	0.28
2009	0.28
2010	0.28
2011	0.21
2012	0.2
2013	0.2
2014	0.2
2015	0.2
2016	0.2
2017	0.19
2018	0.18
2019	0.18
2020	0.17
2021	0.2
2022	0.2
2023	0.2
2024	0.2
2025	0.2

*TABLE 6: TAX RATE IN UK*

The discount rate  $r_{disc}$  has been found having a value of 7.25%. [39]

**11.2.1 The turbine**

As mentioned before the turbine used in the Barrow wind farm are thirty 3 MW Vestas V-90 turbines.

This turbine is equipped with a variable speed generator and a pitch control system (as the one hypnotized in the MATLAB BEM analysis made in the previous part of the thesis) to ensure a stable energy generation. [40]

The technical information of the turbine with the resulting power curve are the following:

V90 – 3.0 MW, 60 Hz, Mode 0												
Wind Speed [m/s]	Air Density [kg/m <sup>3</sup> ]											
	0.97	1	1.03	1.06	1.09	1.12	1.15	1.18	1.21	1.225	1.24	1.27
4	53	56	59	61	64	67	70	72	75	77	78	81
5	142	148	153	159	165	170	176	181	187	190	193	198
6	271	281	290	300	310	319	329	339	348	353	358	368
7	451	466	482	497	512	528	543	558	574	581	589	604
8	691	714	737	760	783	806	829	852	875	886	898	921
9	995	1028	1061	1093	1126	1159	1191	1224	1257	1273	1289	1322
10	1341	1385	1428	1471	1515	1558	1602	1645	1688	1710	1732	1775
11	1688	1740	1794	1849	1903	1956	2010	2064	2118	2145	2172	2226
12	2010	2074	2137	2201	2265	2329	2392	2454	2514	2544	2573	2628
13	2310	2382	2455	2525	2593	2658	2717	2771	2817	2837	2856	2889
14	2588	2662	2730	2790	2841	2883	2915	2940	2958	2965	2971	2981
15	2815	2868	2909	2939	2960	2975	2984	2990	2994	2995	2996	2998
16	2943	2965	2979	2988	2993	2996	2998	2999	2999	3000	3000	3000
17	2988	2994	2997	2998	2999	3000	3000	3000	3000	3000	3000	3000
18	2998	2999	3000	3000	3000	3000	3000	3000	3000	3000	3000	3000
19	3000	3000	3000	3000	3000	3000	3000	3000	3000	3000	3000	3000
20	3000	3000	3000	3000	3000	3000	3000	3000	3000	3000	3000	3000
21	3000	3000	3000	3000	3000	3000	3000	3000	3000	3000	3000	3000
22	3000	3000	3000	3000	3000	3000	3000	3000	3000	3000	3000	3000
23	3000	3000	3000	3000	3000	3000	3000	3000	3000	3000	3000	3000
24	3000	3000	3000	3000	3000	3000	3000	3000	3000	3000	3000	3000
25	3000	3000	3000	3000	3000	3000	3000	3000	3000	3000	3000	3000

Wind speed as 10 minutes average value at hub height and perpendicular to the rotor plane

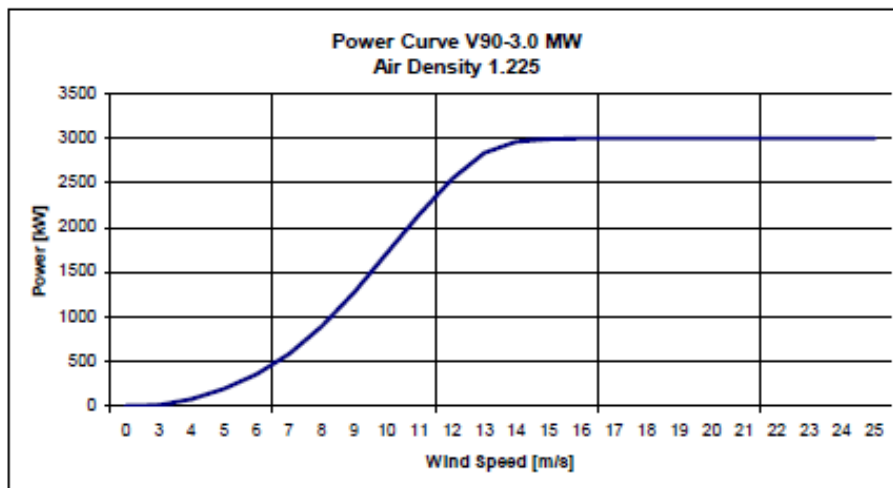


Figure 81: power curve of the Vestas V90 3MW

**Rotor**

Diameter: 90 m

Swept area: 6.362 m<sup>2</sup>

Speed, nominal power: 16.1 RPM Speed, Dynamic operation range

rotor: 9.9 - 18.4 RPM

Rotational direction: Clockwise (front view)

Orientation: Upwind

Tilt: 6°

Blade coning: 4°

Number of blades: 3

Aerodynamic brakes: Full feathering

### **Hub**

Type: SG Cast Iron

Material: GJS-400-18U-LT

Weight: 8000 kg

### **Blades**

Principle: Airfoil shells bonded to supporting beam

Material: Fibreglass reinforced epoxy and carbon fibres

Blade connection: Steel root inserts

Air foils: RISØ P + FFA-W3

Length: 44 m

Chord at blade root: 3.512 m

Chord at blade tip: 0.391 m

Twist (blade root/blade tip): 17.5°

### **Bearings**

Type: 4-point ball bearing

### **Sensors**

#### **Lightning Detector**

Appellation: Lightning detector

Signal: Optical Analogue

#### **Wind Sensor**

Appellation: Ultrasonic wind sensor, (2 units)

Signal: RS485/optical

Accuracy: +/- 0.1 m/s, less than 5 m/s

+/- 2 %, more than 5 m/s

#### **Movements and Vibrations**

Appellation: Accelerometer, tower

Signal: RS485

#### **Generator**

Generator 60 Hz



Rated power: 3.0 MW

Type: Asynchronous with wound rotor,  
slip rings and VCRS

Voltage: 1000 VAC

Frequency: 60 Hz

No. of poles: 4

Class of protection: IP54

Rated speed: 1758

Rated power factor,  
default at 1000 V: 1.0

Power factor range at  
1000 V: 0.98CAP - 0.96IND

### 11.2.2 Reference wind distribution

The first parameter to choose is the power curve that could fit in the best way the Barrow conditions. To do this, a computation of the density of the air in the chosen site has been made:

$$\rho = \frac{\left( 101300 \left( 1 - \left( 0.0065 * \frac{altitude}{2880} \right)^{\frac{9.80665}{0.0065} * 287.15} \right) \right)}{287.15 * (288 - 0.0065 * altitude)}$$

With an altitude value of 90 meters, the value that come is  $\rho = 1.2274 \frac{kg}{m^3}$ . The chosen power curve of the V-90 3MW turbine is consequently the one computed at an air density of  $1.225 \frac{kg}{m^3}$ . [41]

The reference wind distribution, so the factor that describes the wind behaviour and its probability to have a determined speed in the selected site, is computed through the Weibull distribution. [42]

$$f_w = \frac{k}{c} \left( \frac{v}{c} \right)^{k-1} e^{-\left( \frac{v}{c} \right)^k}$$

$k$ =shape factor

$c$ = scale factor

$v$ = distribution of the wind from 0 m/s to 25 m/s

The Weibull  $k$  value, or Weibull shape factor, is a parameter that reflects the breadth of a distribution of wind speeds. Lower  $k$  values correspond to broader distributions of wind speed, meaning that winds tend to vary over a large range of speeds. Higher  $k$  values correspond to narrower wind speed distributions, meaning that wind speeds tend to stay within a narrow range.

In the following the selected value for the shape factor has been set to 1.5, under the suggestion of the Vestas co-relator of this Master Thesis Mr. Tomas Vronsky, while the shape factor has been computed as follow:

$$v_m = c \Gamma\left(\frac{1}{k} + 1\right)$$

Where  $v_m$  is the mean wind speed in Barrow, which is equal to 9.15 m/s [34], and  $\Gamma$  is the gamma function, which returns the value of:

$$\Gamma(n) = \int_0^{\infty} t^{n-1} e^{-t} dt$$

Then it is possible to calculate the cumulative Weibull distribution simply by doing:

$$F(v) = 1 - \exp\left(-\left(\frac{v}{c}\right)^k\right)$$

Both the function  $f(v)$  and  $F(v)$  assumes the given value in case the result is higher or equal to zero while are put equal to zero in case the result is negative.

The obtained value for  $c$  is equal to 10.1357 and a final Weibull distribution as follows:

$v$ [m/s]	$f(w)$	$F(w)$
0	0	0
1	1.858676	0.009337
2	3.614192	0.036829
3	5.172875	0.080963
4	6.458803	0.139374
5	7.41985	0.209053
6	8.030845	0.286601
7	8.29363	0.368506
8	8.23427	0.451398
9	7.898013	0.532267
10	7.342896	0.608628
11	6.632907	0.678609
12	5.831605	0.740982
13	4.996865	0.795131
14	4.177164	0.840971
15	3.40954	0.878849
16	2.719113	0.909421
17	2.119878	0.933536
18	1.61637	0.952138
19	1.205813	0.966174
20	0.880373	0.976538
21	0.629242	0.984029
22	0.440387	0.989331
23	0.30186	0.993005
24	0.202678	0.995499
25	0.133322	0.997158

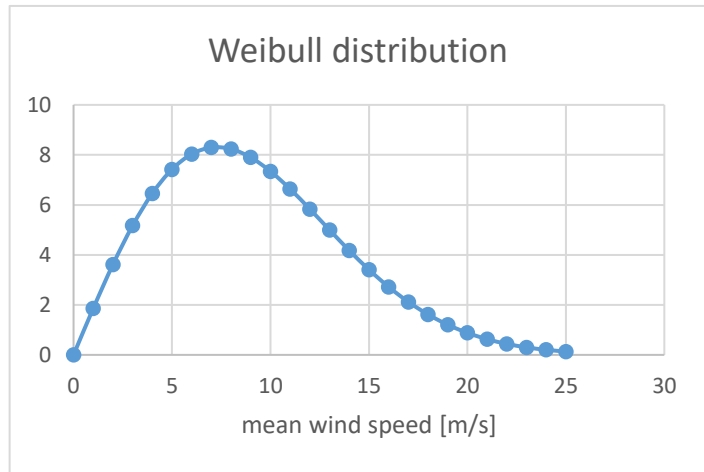


Figure 83:: weibull wind distribution

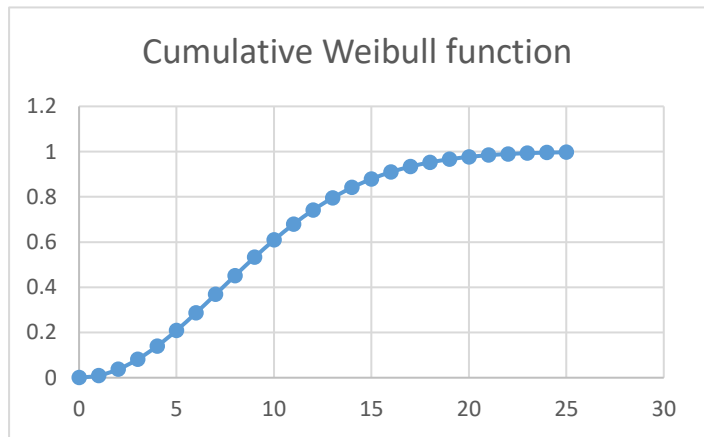


Figure 82: cumulative weibull wind distribution

Table 7: weibull wind distribution

### 11.2.3 Incentives

As said at the beginning of this chapter, the Barrow wind farm is operational since 2006, and in that year, in UK, the incentives were based on Tradable Green Certificates (TGCs). This particular type of incentives work like this: the government defines targets for Renewable Sources of Energy (RES-E) deployment and fix a party of the supply chain with a minimum value it must achieve. After that, a TGCs market is defined, and their price is fixed following the economic laws of demand and supply. In this way the revenues of the plant are double: they come both from selling the energy and from the market support mechanism. For example, the average price obtained for electricity from wind in the power auction in February 2007 was 7.36 p/kWh (£73.6/MWh), while the

average ROC price in April 2007 was £47.50/MWh. [43] Furthermore, there is an obligation on suppliers to purchase a percentage of electricity produced by renewable energy sources. It is important to mention that these certificates are not different from source to source, so not to create unsteadiness in the market, and avoid the creation of many small different markets one for each technology. [44] UK is calling the Green Certificates as Renewable Obligation Certificates (ROC) and is founding its support scheme on four sections:

- Compulsory targets with ROC system for energy suppliers. If not achieved, it implies a “buy-out” price set at 33.24 £/MWh (around 48.20 €/MWh) adjusted annually coupling the retail price index.
- Climate Change Levy on electricity: 4.3 £/MWh (approx. 6.3 €/MWh) that does not affect the electricity produced by RES-E.
- Grants scheme: special funds like the New Opportunities Fund are created to incentivise RES-E.
- Regional diversification of the strategy to achieve the goal set by international agreements, to better comply with them.

ROC auctions are held quarterly every year, starting from the first of April. In April the 1<sup>st</sup> of 2006 the auction set the ROC price to an average of 40.65 £.

The Renewable Obligation scheme is guaranteed to run until at least 2027. The target supply increases every year starting from a level of 3% in the year starting in April the 1<sup>st</sup> 2002 until it reaches the maximum value of 15.4% in April the 1<sup>st</sup> 2015. [44]

As mentioned earlier, there are two income streams available for renewable generators. The first is the standard wholesale price of electricity, which value is normally in the region of £20 to £30 per MWh. The other income stream is from selling the renewable obligation certificates (ROCs). Generators of renewable energy are given one Renewables Obligation Certificate (ROC) per each MWh of electricity generated from renewables, than, ROCs are submitted to the official agency to demonstrate their compliance with the RO targets. The ROCs have value because otherwise electricity suppliers have to pay a penalty of £30 per every MWh (2002 prices) of renewable

electricity that they fail to supply. In addition, this penalty is recycled as an extra reward in respect of each ROC that is issued and then cashed in. Hence if there is an undersupply of ROCs, their market value increases (theoretically), encouraging more expensive generation to be developed to meet the gap in the renewable electricity market. The value of one ROC, including recycled value is about £45-£50 (i.e. per MWh), and this value seems likely to remain at current high levels because the RO targets will be underachieved. The RO is designed as a competitive mechanism, since the more the RES-E generated, the less will be the value of the ROCs, and vice-versa. [45] However, in practice this market is not so easy to understand. For instance, fines paid by suppliers failing to meet their quota are recycled to suppliers that have met their quota, thus increasing the income of the latter. In addition, many suppliers in the market have vested interest in ensuring that competitive pressures do not drive down the value of ROCs. If that were to happen, the value of their own investments in renewable energy schemes would be reduced. Although the official target for the RO is 10.4% of RES-E by 2010 and 15% by 2015, the real proportions will probably be about 7% by 2010 and about 10-11% by 2015. Hence there will be a deficit of RES-E for many years, and so wind power developers are likely to receive good income streams in the long term, despite the outward appearance of market uncertainty (Toke, to be published, 2006). As showed in the following picture, these predictions have turned out to be true:

**Chart 6: Electricity generation capacity of UK renewable assets derated for intermittency, 2000 to 2019.**

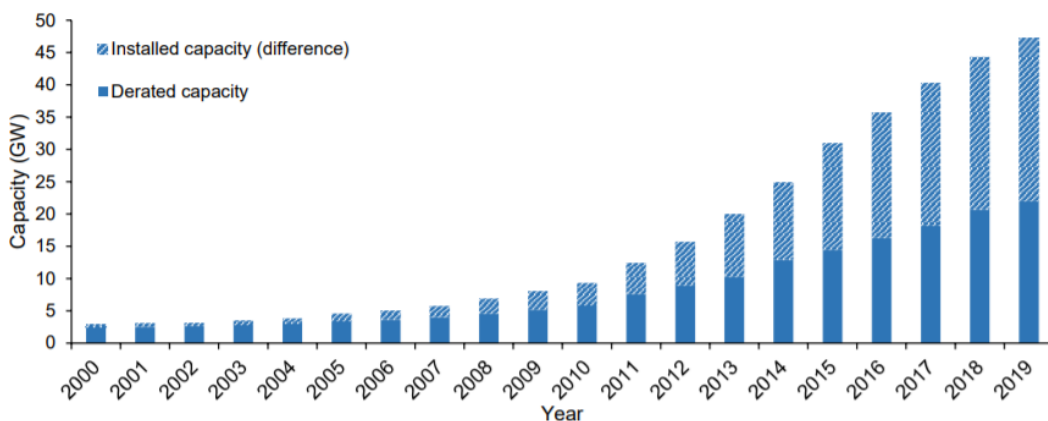


*Figure 84: renewable energy generation in UK [46]*

On the other hand, the full value of the wholesale price plus the ROCs is usually not passed onto the generators. Conventional developers are financed by banks which want the security of guaranteed rates per kWh set down as part of long-term contracts with a

major (and creditworthy) electricity supplier. In return for the security, the electricity suppliers take a significant proportion of the value of the wholesale price and ROCs. At the present time (end 2004) it seems that 15 years contracts are available from at least one major electricity supplier for a fixed price of 5 p/kWh for both the electricity and the ROCs [45]. The price due to banks can be neglected in the computation in this thesis since it is referred to small wind farms owned by different privates. The project considered here is a big wind farms with country's interests in it, banks are involved too of course, but in a more complicated way which is not part of the project of this MSc Thesis. The wind farm of Barrow has financed through the ROC subsidy regime. [47] At the end, the evaluation of revenues, which must consider both the wholesale price of electricity ( $el_{price}$ ) and the ROC benefit in the computation, has been done as follow:

$$R(i) = ROC_{price} \cdot n^{\circ}_{ROC} + el_{price} \cdot AEP$$

The formula of revenues computed for each year relies the electricity price to the annual energy produced by the turbine while the ROC benefit is related to the number or ROCs given to the plant. This value is established just by considering that one ROC is given for each MWh of energy produced by the plant.

11.2.4 Computation

year	R(i)	E(i)	Amortization	Profit
-1	0	2050000	0	
0	0	2050000	0	
1	667268.24	101101.2	341666.6667	224500.3279
2	672323.31	102830.1	341666.6667	227826.559
3	677378.37	104588.5	341666.6667	231123.227
4	682433.43	106376.9	341666.6667	234389.8266
5	687488.49	108196	341666.6667	237625.8434
6	692543.56	110046.1	341666.6667	240830.7545
7	697598.62	111927.9	341666.6667	244004.0281
8	702653.68	113841.9	341666.6667	247145.123
9	677378.37	115788.6	341666.6667	219923.1144
10	682433.43	117768.6	341666.6667	222998.192
11	687488.49	119782.4	341666.6667	226039.4119
12	743094.18	121830.7	341666.6667	279596.8196
13	748149.24	123914	0	624235.2438
14	753204.31	126032.9	0	627171.3769
15	758259.37	128188.1	0	630071.2763
16	763314.43	130380.1	0	632934.3224
17	768369.49	132609.6	0	635759.885
18	773424.56	134877.2	0	638547.3231
19	778479.62	137183.6	0	641295.9849
20	783534.68	139529.5	0	644005.2073
tot	14396818	6486794	4100000	7910023.847

Table 8: first part of computations

Table 8 displays the first part of the computations that will result in the evaluation of the economic parameters presented before. As mentioned in the previous paragraph revenues are computed as  $R(i) = ROC_{price} \cdot n^{\circ}_{ROC} + el_{price} \cdot AEP$ . The wholesale price of electricity  $el_{price}$  has been computed considering a starting value of £20/MWh and then increased every year of £0.5/MWh. A similar computation has been made to evaluate the ROC price, which has been kept between £40/MWh and £50/MWh after a research over its prices along the years. The number of ROC achieved by the V90-3MW Vestas' turbine is 10.603 per year, since its AEP is of 10.603.302 kWh.

After that, the expenditures  $E(i)$  have been computed. For the first two years (the year -1 and 0), the years of construction of the plant, they are represented by the Capex divided into the two different years, after the wind farm is built, the value of the expenditures is represented by the Opex actualised at the current year.

$$E(i)_0 = \frac{E(i)_i}{(1 + r_{infl})^i}$$

The fourth column is just to represent the amortisation of the initial investment, in the computation has been assumed a constant amortisation over the first 12 years of operation of the wind farm.

Amortisation is important to compute the profits, which state in the last column of and are computed as follows:

$$P(i) = R(i) - E(i) - Amortisation$$

Rtax	T(i)	CF(i)	DCF(i)	CDCF(i)	
-	0	-2050000.0	-2198625	-2198625	1
-	0	-2050000.0	-2050000	-4248625	2
0.3	67350.1	498816.9	465097.3	-3783527.66	3
0.3	68347.97	501145.3	435681.4	-3347846.26	4
0.28	64714.5	508075.4	411847.3	-2935998.93	5
0.28	65629.15	510427.3	385784.5	-2550214.47	6
0.28	66535.24	512757.3	361347.7	-2188866.74	7
0.21	50574.46	531923.0	349514.3	-1839352.45	8
0.2	48800.81	536869.9	328918.2	-1510434.23	9
0.2	49429.02	539382.8	308119.1	-1202315.1	10
0.2	43984.62	517605.2	275691.2	-926623.91	11
0.2	44599.64	520065.2	258276.4	-668347.464	12
0.2	45207.88	522498.2	241943.8	-426403.67	13
0.19	53123.4	568140.1	245294.5	-181109.162	14
0.18	112362.3	511872.9	206061.7	24952.5135	15
0.18	112890.8	514280.5	193035.8	217988.318	16
0.17	107112.1	522959.2	183024.1	401012.41	17
0.2	126586.9	506347.5	165231.1	566243.52	18
0.2	127152	508607.9	154749.4	720992.927	19
0.2	127709.5	510837.9	144921.1	865914.04	20
0.2	128259.2	513036.8	135706.2	1001620.27	21
0.2	128801	515204.2	127067.2	1128687.44	22
0.2185	1639171	6270853.209	1128687.439		

Table 9: second part of the computations

Table 9 is the following of the previous computations. Here the taxation rate  $r_{Tax}$  considered in the computation of taxes is listed. It changes through the years decreasing from 0.3 in 2006 to 0.2 in 2020, then it is kept constant. Taxes act on the profits and are simply computed as:

$$T(i) = P(i) \cdot r_{tax}$$



The cash flow  $CF(i)$  just represents the effective motion of money seen by the wind farm. For the first two years is composed just by the expenditures of those years changed in sign. After 2006, when the farm start to operate, the cash flow is computed as:

$$CF(i) = R(i) - E(i) - T(i)$$

One of the last passages is the implementation of the discount rate  $r_{disc}$ , which is simply inserted into the cash flow with the same actualising formula used before to have the discounted cash flow.

$$DCF(i) = CF(i) \cdot (1 + r_{disc})^{-i}$$

The last passage is the calculation of the Cumulative Discounted Cash Flow, which sum all the previous  $DCF(i)$  up:

$$CDCF(i) = \sum_{n=0}^i DCF(n)$$

The economic parameters for this reference case assume the following values:

$$PBT_{ref} = 15 \text{ years}$$

$$NPV_{Ref} = 1128687,439$$

$$IRR_{Ref} = 10.30\%$$

$$LCOE_{Ref} = 0.0773 \frac{\text{£}}{\text{kWh}}$$

One first thing that can be noticed, before going through the comparison with other turbines, is the consistency of the LCOE final value with the typical values reached by this technology.

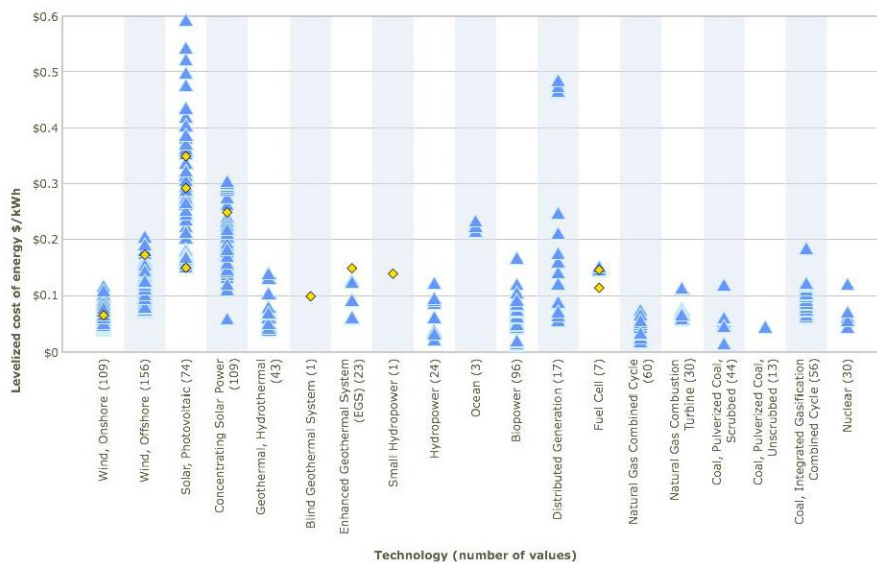


FIGURE 85: TYPICAL LCOE FOR DIFFERENT TECHNOLOGY [32]

### 11.3 TURBINE WITH FLAP

This case is comparing two wind farms having turbines which are exactly the same unless their dimension. In particular, the second turbine has been defined starting from the reference one and progressively increasing the diameter. As studied on MATLAB, it is possible to achieve the same value of axial loads the two different turbines are subjected to, with a diameter of one of the two turbines bigger than 20% compared to the reference one. This result is due to the presence of the Trailing Edge Flap on the blades of the second turbine, which enhance the overall performances of the turbine. The case studied on MATLAB considers a reference HAWT with a diameter of 30 meters and, as it can be seen in the picture below, it suffers slightly the same axial strains as the turbine having a diameter of 36 meters and the trailing edge flap.

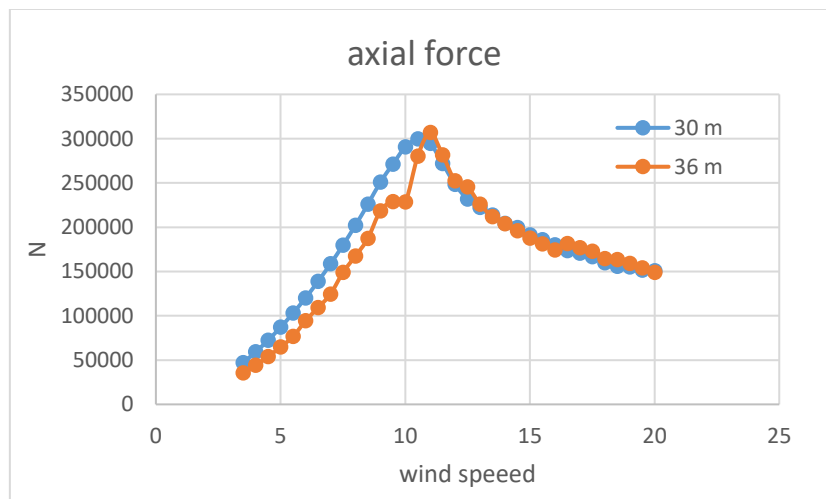


Figure 86: axial forces acting on the two turbines

From the same computations made on MATLAB it is obtained the difference in power production that these two turbines can achieve in a steady state conditions and with the presence of a gust having the module of 1 m/s and an angle of 45° between itself and the main direction of the wind.

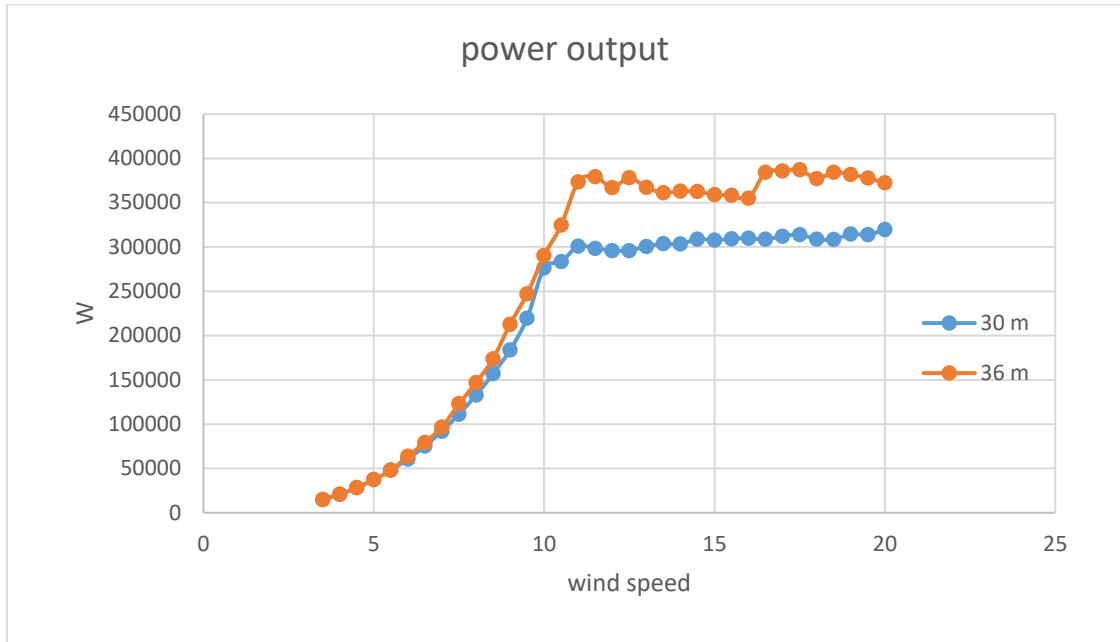


Figure 87: power output of the two turbines

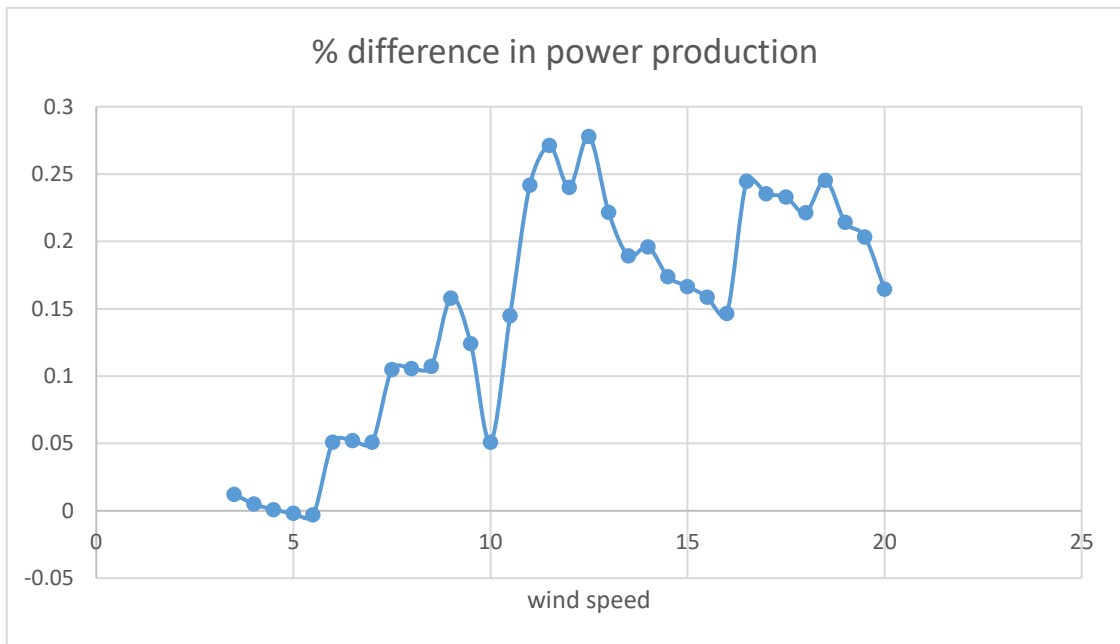


Figure 88: difference in power production

Figure 87 and Figure 88 depict the difference in power production between the two turbines. The difference starts to be effective once the main wind speed overtakes the value of 6 m/s and the power increases more than 5%. The final average increase of power production is of about 14.7%.

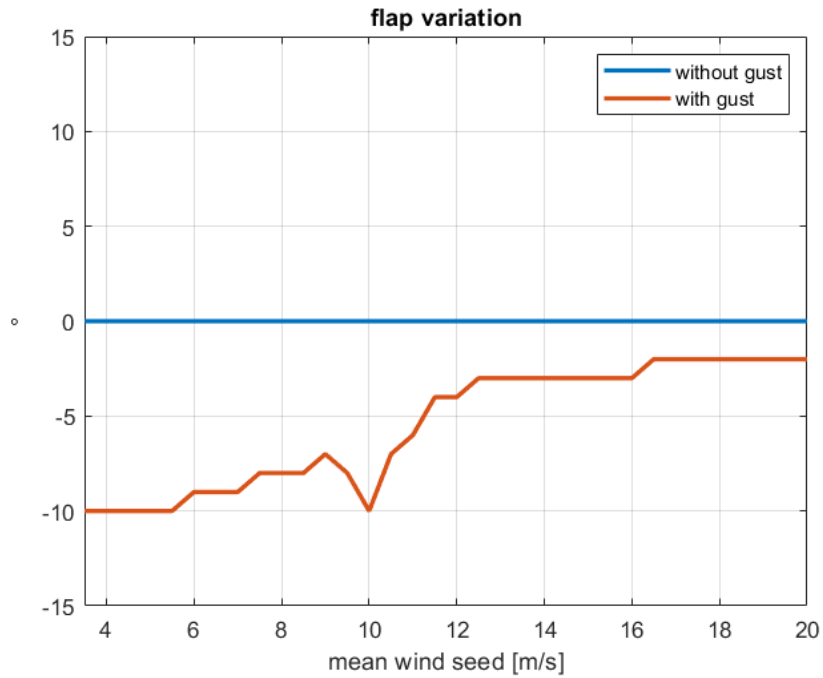


Figure 89: flap orientation

In Figure 89 is clear that the different steps the power production's variation is performing are essentially due to the flap motion. This effect is again due to the low resolution used in the flap motion, 1 degree, which is not enough to have a smooth power output from the turbine. A higher resolution, for instance 0.1°, could easily achieve this objective, so an interpolation has been made in retrospect to consider this fact and to work with a more real value of power output. Figure 90 represents the difference in power production that will be considered afterwards:

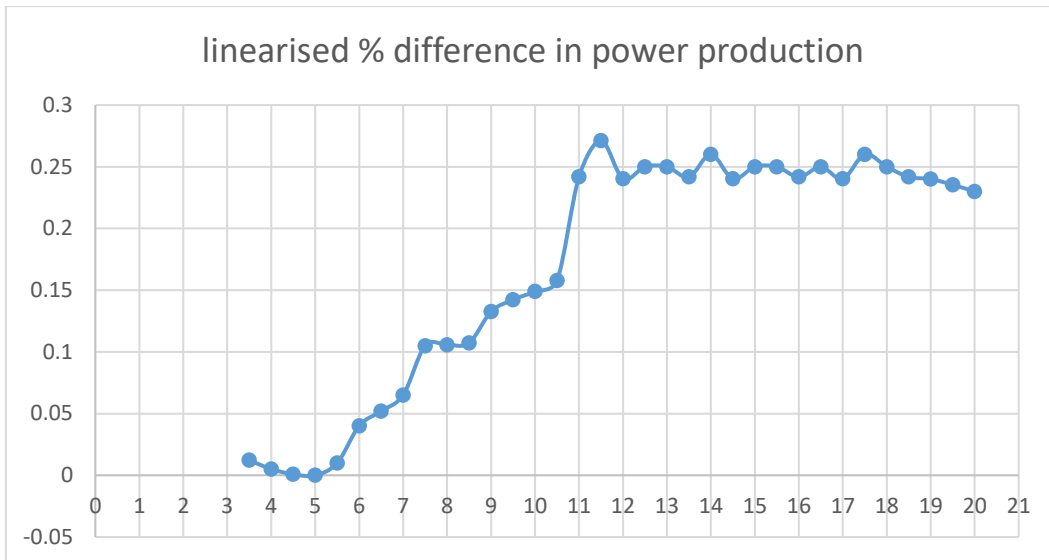


Figure 90: linearised percentage value of the difference in power output of the two turbines

These values, as they are, in percentage, can be used to compute the difference in power production of every kind of turbine after the implementation of the Trailing Edge Flap system, and it will be used in the reference turbine of Barrow to estimate the output power of the 90MW-Vestas turbine with the hypothesis of the presence of the flap.

The output of the total estimation in this case will be the Capex difference that brings to the same value of the IRR of the reference state. This difference will represent the maximum capital expenditure feasible to install a trailing edge flap expecting an economic positive return.

But, as expected, the turbine Capex will see an increase even without considering the trailing edge flap. The estimation of the Capital Expenditures of an offshore wind farm is a crucial problem in the economic analysis, since its value is the one that affects the most the LCOE of the entire wind farm [48].

Many different estimations can be found in literature to solve this problem, some of them use a linear trend to evaluate the Capex of an estimated project, some other use component scaling [41], or even other more complicated scaling methods. All of this bring to a very uncertainty in the final LCOE estimated value. This uncertainty could end up in difficulties for wind turbines Original Equipment Manufacturer (OEM), which is seeing the LCOE decreasing rapidly since 2016. [49]

In this thesis, the following formula will be used, presented in a study of 2018 which uses the same LCOE formula used in this thesis [50]. Moreover, this formula has been chosen since it refers exactly to offshore wind farms.

$$CAPEX = -1.485 \cdot 10^{11} \cdot P_{WT}^{0.001} + 2.353 \cdot 10^6 \cdot WD + 2.530 \cdot 10^6 \cdot D + 2.451 \cdot 10^6 \cdot P_{WF} + 1.487 \cdot 10^{11}$$

Where  $P_{WT}$  = power of the wind turbine [MW]

$P_{WF}$  = power of the wind farm [MW]

$WD$  = water depth [m]

$D$  = distance from the shore [km]

Since the two turbines confronted will end up in the same wind farm (Barrow), the exact Capex of the existing wind farm is the starting point, it is just necessary to compute the difference of the two Capexs and then sum it to the original one, and find the final Capex of the estimated, bigger, turbine. So, being the same wind farm, the two factors which include water depth and distance from the shore disappear and the final difference in Capex between the two wind farms is:

$$\begin{aligned} \Delta CAPEX &= -1.485 \cdot 10^{11} \cdot 3.6^{0.001} + 1.485 \cdot 3^{0.001} - 2.451 \cdot 10^6 \cdot 90 + 2.451 \cdot 10^6 \cdot 108 \\ &= 17011017 \text{ £} \end{aligned}$$

The estimate Capex of the bigger wind farm is than

$$CAPEX_{108MW} = 123.000.000 + 17.011.017 = 140.011.017 \text{ £}$$

So that the estimated Capex for one 3.6MW turbine is

$$CAPEX_{3.6MW} = 4.667.034 \text{ £}$$

This value is 13.8% higher than the Capex of the V90-3MW turbine, which is consistent with the increase of 20% of its diameter, since the expected the cost to increase with a lower speed than the dimension of the turbine.

It has been decided to compute the Opex of the new machine keeping the same percentage they represent in the first case. This is not strictly correct, since they should decrease in percentage with the increase of the dimensions, but this solution has been

chosen to consider some possible costs related to the presence of the new Training Edge Flap technology in this turbine.

$$\frac{OPEX_{3MW}}{CAPEX_{3MW}} = 2.59\% \rightarrow OPEX_{3.6MW} = 2.59\% \cdot CAPEX_{3.6MW} = 120.876,00 \text{ €}$$

Since the comparison has been done starting from 2006, the discount rate  $r_{disc}$ , the inflation rate  $r_{infl}$  and the tax rates  $r_{tax}$  have been kept the same as the reference case.

The Weibull wind distribution too has not changed, and so the previous computations are considered in the 3.6MW too.

The number of availability hours during a year is decreased. This is done to consider a small decrease in the global reliability due to the presence of the Trailing edge flap. The consider variation of the  $h_{availability}$  value that has been chosen is -200 h.

Due to the fact the comparison between the two wind farms has been made considering 2006 as first year for both, the estimation of the ROC economic benefit has been computed in the same way as before.

From all these new assumptions, a new economic study has been made, computing the NPV, the IRR, the PBT and the LCOE again for this new hypothetical case.

year	R(i)	E(i)	Amortization	Profitti
-1	0	2333517	0	
0	0	2333517	0	
1	789168.35	115083.6	388919.4911	285165.2128
2	795146.9	117051.6	388919.4911	289175.8305
3	801125.45	119053.2	388919.4911	293152.7966
4	807104	121089	388919.4911	297095.5357
5	813082.54	123159.6	388919.4911	301003.4625
6	819061.09	125265.6	388919.4911	304875.9816
7	825039.64	127407.7	388919.4911	308712.4876
8	831018.19	129586.3	388919.4911	312512.3647
9	801125.45	131802.3	388919.4911	280403.6978
10	807104	134056.1	388919.4911	284128.4273
11	813082.54	136348.4	388919.4911	287814.6165
12	878846.57	138680	388919.4911	351247.0875
13	884825.12	141051.4	0	743773.6989
14	890803.67	143463.4	0	747340.2677
15	896782.22	145916.6	0	750865.5916
16	902760.77	148411.8	0	754348.9654
17	908739.31	150949.6	0	757789.6717
18	914717.86	153530.9	0	761186.981
19	920696.41	156156.3	0	764540.151
20	926674.96	158826.5	0	767848.4271
tot	17026905	7383924	4667033.893	9642981.256

Table 10: first part of computations of the 3.6MW turbine

As can be seen in the table above the computations were the same as before, but with all the hypothesis explained in the previous paragraphs. Revenues are bigger than the previous case since the expected energy output of the turbine along a year, keeping the same Weibull wind distribution, is higher: 11957096.24 kWh/y. Expenditures are higher too, since they strongly depend on the Opex of the turbine, and they are conceived as the same percentage of the Capex as before. The amortisation has been done in the same way, dividing the Capex for 12 years. The total sum of amortisation corresponds to the Capex value. All of this brings to higher profits for each year.



Rtax	T(i)	CF(i)	DCF(i)	CDCF(i)	
-	0	-2333516.947	-2502696.93	-2502696.93	1
-	0	-2333516.947	-2333516.95	-4836213.87	2
0.3	85549.56	588535.14	548750.7133	-4287463.16	3
0.3	86752.75	591342.5725	514096.3785	-3773366.78	4
0.28	82082.78	599989.5047	486353.1701	-3287013.61	5
0.28	83186.75	602828.2768	455621.7126	-2831391.9	6
0.28	84280.97	605641.9841	426804.9712	-2404586.93	7
0.21	64023.96	629771.5166	413808.3114	-1990778.61	8
0.2	61742.5	635889.4812	389583.4821	-1601195.13	9
0.2	62502.47	638929.3829	364984.5273	-1236210.61	10
0.2	56080.74	613242.4494	326630.3241	-909580.281	11
0.2	56825.69	616222.233	306030.2484	-603550.033	12
0.2	57562.92	619171.1843	286708.4065	-316841.626	13
0.19	66736.95	673429.632	290753.2727	-26088.3536	14
0.18	133879.3	609894.4331	245521.6297	219433.276	15
0.18	134521.2	612819.0195	230022.3434	449455.619	16
0.17	127647.2	623218.441	218112.6141	667568.234	17
0.2	150869.8	603479.1723	196927.0941	864495.328	18
0.2	151557.9	606231.7374	184452.5035	1048947.83	19
0.2	152237.4	608949.5848	172754.7205	1221702.55	20
0.2	152908	611632.1208	161786.2351	1383488.79	21
0.2	153569.7	614278.7417	151502.3847	1534991.17	22
0.2185	2004519	7638462.715	1534991.171		

Table 11: second part of computations for the 3.6MW turbine

Table 11 shows us the other part of computations to achieve some economic results for this case. As said before, the same tax rate has been used, to end up with two comparable computations. Taxes so are higher than before, since the tax rate has been kept the same while profits have increased. After that, the Cash Flow, the discounted cash flow and the cumulative discounted cash flow have been calculated and with them, the new values of NPV, IRR, PBT and LCOE.

$$PBT_2 = 15 \text{ years}$$

$$NPV_2 = 1534991,171$$

$$IRR_2 = 10.85\%$$

$$LCOE_2 = 0.0744 \frac{\text{€}}{\text{kWh}}$$

The final computation that must be done before performing some conclusion is the evaluation of the Weighted Average Cost of Capital (WACC). The reference company for this computation will be the owner of the Barrow wind farm: Orsted. This value

represents a threshold that must be lower than the IRR, only this condition can make a project economically valuable for the selected company. WACC is a function of the assets of the company, the equity, its financial performances, the market behaviour and the tax regime. [51]

The result for 2006 is a WACC of 8.81%.

Looking at the values of the following years it can be said that the obtained value is consistent with the data:

WACC	2007	2008	2009	2010	2011	2012	2013	2014	2015	2016	2017
Risk Free rate	4,8%	4,6%	4,5%	4,4%	4,1%	3,9%	3,5%	3,2%	3,0%	2,7%	2,3%
Weighted Unlevered Beta	1,25	0,97	0,77	0,86	0,95	0,94	0,88	0,81	0,85	0,73	0,55
Relevered Beta	1,52	1,14	1,17	1,32	1,33	1,28	1,27	1,18	1,47	0,95	0,67
Implied Market Risk Premium	4,4%	6,4%	4,4%	5,2%	6,0%	5,8%	5,0%	5,8%	6,1%	5,7%	5,1%
<b>Cost of Equity</b>	<b>11,4%</b>	<b>11,9%</b>	<b>9,6%</b>	<b>11,2%</b>	<b>12,1%</b>	<b>11,3%</b>	<b>9,8%</b>	<b>10,1%</b>	<b>12,0%</b>	<b>8,1%</b>	<b>5,7%</b>
Pre-tax Cost of Debt	4,5%	4,5%	4,5%	4,5%	4,5%	4,5%	4,5%	4,5%	4,5%	4,5%	3,8%
Corporate Tax Rate	25%	25%	25%	25%	25%	25%	25%	25%	22%	22%	22%
<b>Cost of Debt</b>	<b>3,4%</b>	<b>3,4%</b>	<b>3,4%</b>	<b>3,4%</b>	<b>3,4%</b>	<b>3,4%</b>	<b>3,4%</b>	<b>3,4%</b>	<b>3,5%</b>	<b>3,5%</b>	<b>3,0%</b>
Market Value of Equity	78%	81%	59%	58%	65%	68%	62%	62%	52%	73%	78%
Market Value of Debt	22%	19%	41%	42%	35%	32%	38%	38%	48%	27%	22%
Implied D/E	29%	23%	69%	71%	54%	48%	60%	61%	93%	37%	29%
<b>Historical WACC</b>	<b>9,60%</b>	<b>10,28%</b>	<b>7,07%</b>	<b>7,95%</b>	<b>9,05%</b>	<b>8,71%</b>	<b>7,40%</b>	<b>7,56%</b>	<b>7,89%</b>	<b>6,84%</b>	<b>5,12%</b>

Figure 91: WACC of Orsted computed from annuals reports 2007-2017 [52]

From these results it is important to see that:

$$PBT_{ref} = PBT_2$$

$$NPV_{ref} < NPV_2$$

$$IRR_{ref} < IRR_2$$

$$LCOE_{ref} > LCOE_2$$

So, considering everything that has been said at the beginning of this chapter, all the data tell us that this second case would be preferable from an economical point of view, and both the IRRs are bigger than the computed WACC, which tells us that both the project could be worth of being implemented.

But the objective of this thesis was not only related to the feasibility or not of this solution. The objective is to find which is the maximum price allowed for the trailing edge flap system in order to have a competitive turbine from an economic point of view. To achieve it, it has been computed the variation of the Capex value fixing the IRR value of the second case to the one of the reference case. The choice to use the IRR as comparative value has been made since the two turbines that compared in this work are

different in many ways, and a relative value would be better to achieve a consistent result. Using the NPV would not bring to the correct results since it depends a lot on the initial investment and so a higher NPV in this second case is very expected.

After this evaluation, the final results are:

$$\begin{aligned} PBT_2 &= 15 \text{ years} \\ NPV_2 &= 1336985,79 \\ IRR_2 &= 10.30\% \\ LCOE_2 &= 0.0772 \frac{\text{£}}{\text{kWh}} \end{aligned}$$

As expected, the  $NPV_2$  remains higher than  $NPV_{Ref}$ , while the LCOE is slightly smaller (almost negligible difference). The final Capex result is:

$$CAPEX_2 = 4.847.097,00 \text{ £/turbine}$$

Which means a difference in Capex compared to the previous value of

$$\Delta_{CAPEX} = 4.847.097 - 4.667.034 = 180.063,00 \text{ £/turbine}$$

So, under all the hypothesis described in the previous paragraphs, the trailing edge flap system can be considered economically valuable only if its cost is smaller than 180.063 £ for each turbine of the wind farm of Barrow.

This value is an important achievement at this initial point of the project. It must of course be considered with all the hypothesis that have been made, but can truly affect the next decisions of the project. The total price of the complete trailing edge flap smart control system can have an important role in the choice of the actuator to use for example. It was showed that depending on the technology its cost and its power consumption can vary a lot. On the other hand, this value can be considered too low, and so there can be an effort in the next phases of the project to try to change the hypothesis that have been made. The length of the blade where the flap is installed for example can be reduced, the percentage of the chord where to hinge it can be changed to have a different influence of the flap in the output of the turbine etc. This result can therefore be considered as a first step in the economic study of this technology and can start to affect the next choices in order to conceive a cost-effective system to be installed on turbines.

## 12 FUTURE DEVELOPMENTS

---

Britain is already leading the way in the domain of wind energy. Over the last 30 years, it has shown that economic success and environmental responsibility go hand in hand. It expanded its GDP by 75 per cent while cutting emissions by 43 per cent. The low-carbon industries already support over 460,000 jobs, from electric vehicle manufacturing in the Midlands and the North East to the thriving offshore wind industry centred on the Humber and the Tees. In 2019, Britain became the first major economy to adopt a legally binding obligation to reach net zero greenhouse gas emissions by 2050.

UK is currently developing some important power plans to enhance the green energy field in the country. The declared goal is to achieve the zero-emission condition by 2050 together with the creation of 60 thousand jobs related to this sector.

The path to achieve this bold objective is strictly related to the offshore wind sector since UK has claimed to aim for being the world leader in clean wind energy, with the creation of jobs, to reduce the carbon emission and increasing exports of energy.

UK already has got the largest offshore wind capacity in the world, and already covers 10% of the electricity demand thanks to it, but it is investing 160 million pounds to increase ports and infrastructures across communities near the wind farms. This investment is predicted to create around two thousand jobs in the short term related to the construction of this infrastructures, and other sixty-thousand by 2030 directly or indirectly connected to the wind energy sector.

This action of the Government has got another objective: to make for UK factories of wind turbines easier to win orders so that they are able to invest in themselves and start to compete in the global market, now full of just some big manufacturers, increasing their competitiveness.

All these actions can make UK one of the leader countries in the challenge of the reduction (or zeroing) of emissions by 2050 around the world.

The tangible objectives are:

- Make the offshore sector so big that it will be able to produce more than all the electricity needed by UK's households by 2030. This means a power value of 40GW.
- Enhance research and production of floating offshore wind farms. The aim here is to achieve a power nominal value of 1 GW related only to this branch of the wind energy by 2030. To understand how big this objective is, nowadays the global production of floating wind is fifteen times smaller. Thank to this UK thinks it can lead the green revolution even after this decade, thanks to capacity to exploit winds where they are strongest.
- Modifying the new contracts and auctions in the English energy market, setting stricter targets to the percentage of energy produced by green sources, trying to keep the cost low and to provide enough energy to satisfy the request. [53]

These points were defined as milestones for the UK's government despite the explosion of the COVID-19 sanitary emergency, and lead to the definition of the final document that describes the future plans for UK: The Ten Point Plan for a Green Industrial Revolution. [54] The title has been chosen to highlight the great importance that has been given to this next years, a new Revolution is going to happen, as big as, or even more, that the industrial revolution that hit UK two centuries ago. As it was at that time, Britain wants to lead the world in this revolution once more. With this plan Britain mobilises 12 billion to place green jobs at the heart of its economic revival, offshore wind farms remain one of the leading means, together with nuclear plants and hydrogen technologies. The aim is to have enough energy to power household keeping the bills low. Beside this, this plan aims to harness nature's ability to adsorb carbon dioxide by establishing new National Parks and making the existing ones bigger, enhancing biodiversity. This will bring to new possible solutions to make us and the other living creatures to adapt to the changes that are occurring in the world.

The declared objective for Britain with this plan is to reduce UK emissions by 180 million tonnes of carbon dioxide equivalent ( $Mt CO_2e$ ) between 2023 and 2032, together with the achievement of a net zero by 2050.

## 12.1 TEN POINTS PLAN

As already written, UK is already the leading country in the world for offshore wind, therefore, it constitutes a critical source of renewable energy. The specific aim for this technology is to quadruple the offshore wind capacity by 2030 reaching a capacity of 40 GW, including 1 GW of innovative floating offshore wind in the windiest parts of the country. Thanks to government support and market behaviour the cost of offshore industry has fallen by two thirds in the last five years; in the next year, the British Government aim to double the amount of renewables procured through the next Contract for Difference Auction. The contract for difference scheme is the current support mechanism for green technologies in Britain. It guarantees a regulated price of electricity to successful generators. These contracts are allocated through auctions with the aim of allocating support to those projects with the lowest cost, protecting the investments in renewable sources from volatile wholesale prices. [55] The investment in the wind industry consists of £160 million into modern ports and manufacturing infrastructure, providing high quality employment in coastal regions. More stringent requirement will be asked for supply chain, so to help to attract inward investments into manufacturing in the UK and increase the global competitiveness and expertise. Together with this the network infrastructure will be increased in dimension and updated with the latest technologies, like energy storage systems. An Offshore Transmission Network Review will be implemented to set out a new strategy to connect offshore wind farms in a clean and cost-effective way. This first point of the plan is expected to create up to 60 thousand jobs and to reduce by 5% the emission of  $CO_2$  (2028 data) between 2023 and 2032, which represents around 21 Mt $CO_2$ e.

Offshore wind is just one of the technologies UK wants to improve to achieve its net-zero result. As said at the beginning of this chapter there are other 9 points it wants to develop, they focus on the fields of hydrogen, nuclear power, zero-emission vehicles, zero-emission public transportation, Green Jets and ships, greener buildings, Carbon Capture, Usage and Storage (CCUS), protection of the natural environment, green finance.

## 13 CONCLUSIONS

---

In this Master of Science thesis, I had the opportunity to be part of a project proposed by Vestas which aims to the development of an optimum trailing edge flap smart control regulation for horizontal axis wind turbines' blades. This technology is needed to better cope with the increase of request of clean energy by governments and customers without keeping on increasing the diameter of the blades of turbines. Specifically, I studied through a BEM method code, developed with MATLAB, how a trailing edge flap applied on the outer 50% of a blade, can affect the power production of the turbine and how it can alleviate the axial strains experienced by the turbine. The flap is hinged at the 80% of the chord of the airfoil and the chosen profiles are the Nrel S811, S809, S810. The results show that the power is not very much affected by the presence of the flap even if it can help a lot in keeping the power output as the expected value in case of gusts, avoiding the use of brakes and preventing possible unbalances on the grid. But, as the results show, the presence of the flap cannot preclude the installation of a pitch regulation system to be able to produce power until the cut off wind speed. For what concerns axial strains, they are hugely reduced, of an average of 22.8%, with peaks of about 36% in case of gusts. Those results are very important since the flap regulation is way faster in response time than the pitch regulation and can cope very well with the events that are too fast for the pitch regulation. To represent this situation, in this thesis the pitch regulation has been kept at the value computed in case of constant mean wind speed while the flap has hypnotized to have a zero delay in its response time. Gusts are an example, the pitch regulation rotates depending on the mean wind speed of a 10-minute time, the flap can move continuously reading the variation in speed and direction of the wind, saving the blade from a huge amount of loads. Starting from these results I performed an economic feasibility analysis to see which could be the maximum price of this technology to be economically convenient. The chosen way to do it was applying the trailing edge flap regulation to the existing turbine Vestas V-90 operating in the wind farm of Barrow, developing a turbine with the same characteristics unless the presence of the flap. The resulting turbine has been chosen increasing its diameter until the amount of axial strain experienced by the bigger turbine in case of gust were as close as

possible to the axial strains experienced by the original turbine in case of the same gust. The result of this computation is an increase in diameter of 20%, which brings to an increase of power production of 25%. The economic analysis has been done using the DFC approach, computing the NPV, the IRR and the LCOE of the two configurations. After then the second configuration has been forced to have the same IRR of the original plan and the resulting difference in Capex has determined the maximum allowable price per turbine of the trailing edge flap system. The result was a difference in the Capex price of £180.063,00/turbine, with a slightly smaller LCOE after having compared the two cases at the same IRR. The last control has been done comparing the IRR to the WACC of the Orsted Company, the owner of the plant, in 2006 to verify the effective convenience of the investment. All the results highlight the cost-effectiveness of the configuration having a bigger diameter and the Trailing edge flap system installed.



## 14 ANNEX [A]

---

```

%% Data gathering
%%%%%%%%%%%%%%%%%%%%%%%%%%%%%%%%%%%%%%%%%%%%%%%%%%%%%%%%%%%%%%%%%%%%%%%%
%%%%%%%%%%%%%%%%%%%%%%%%%%%%%%%%%%%%%%%%%%%%%%%%%%%%%%%%%%%%%%%%%%%%%%%%
clc
clear
close all

%% General
rH = 0.2;          rP = 0.6;          rT = 1.0;    %rad(ii) rP fixed at
50% of the blade due to dInterp3
minDeg=-6;        maxDeg=17;          %minAlphaValue
stepD=0.5;        %alphaResolution
ReMin=0.5;        ReMax=5;           %Re range
stepRe=0.5;
NN=100;           %spatialStep
minFlap=-10; maxFlap=10; stepFlap=1;
%% Extension
alphaD=minDeg:stepD:maxDeg;
ReN=ReMin:stepRe:ReMax;
Flap=minFlap:stepFlap:maxFlap;

%% HP portion
%CL lascialo così e a seconda gli applico quello che ho bisogno

CL=zeros(length(alphaD),11,length(ReN), length(Flap)); %11=
number of rofiles created by xFoil
CD=zeros(length(alphaD),11,length(ReN), length(Flap));

% HP00
%I save all the data in the position 11 (the one that matches with
the
%angle 0)
for ii=1:length(ReN)
    if round(ReN(ii))==ReN(ii)
        string=('HP00_T1_Re%s.000_M0.00_N9.0.txt');
        a=num2str(round(ReN(ii),1,'decimals'));
        filename = sprintf(string,a);
    else
        string=('HP00_T1_Re%s00_M0.00_N9.0.txt');
        a=num2str(round(ReN(ii),3,'decimals'));
        filename = sprintf(string,a);
    end
    delimiterIn = ' ';
    headerlinesIn = 11;
    A = importdata(filename,delimiterIn,headerlinesIn);
    % A = refined(A.data(:,1:3),stepD); %allunga i dati con un
botto di gradi
    for jj=1:length(Flap)
        CL(:,1,ii,jj)=A.data(:,2); %here I put HP data in all
the angles (HP doesn'thave a flap, so values are the same for
every flap angle)
        CD(:,1,ii,jj)=A.data(:,3);
    end
end

```

```

disp('HP00')
end

%HP20
for ii=1:length(ReN)
    if round(ReN(ii))==ReN(ii)
        string=('HP20_T1_Re%s.000_M0.00_N9.0.txt');
        a=num2str(round(ReN(ii),1,'decimals'));
        filename = sprintf(string,a);
    else
        string=('HP20_T1_Re%s00_M0.00_N9.0.txt');
        a=num2str(round(ReN(ii),3,'decimals'));
        filename = sprintf(string,a);
    end
    delimiterIn = ' ';
    headerlinesIn = 11;
    A=importdata(filename,delimiterIn,headerlinesIn);
    %   A = refined(A.data(:,1:3),stepD);
    %   CL(:,2,ii) = A.data(13,2);
    %   CD(:,2,ii) = A.data(13,3);
    for jj=1:length(Flap)
        CL(:,2,ii,jj)=A.data(:,2);    %here I put HP data in all
the angles (HP doesn'thave a flap, so values are the same for
every flap angle)
        CD(:,2,ii,jj)=A.data(:,3);
    end
    disp('HP20')
end

%HP40
for ii=1:length(ReN)
    if round(ReN(ii))==ReN(ii)
        string=('HP40_T1_Re%s.000_M0.00_N9.0.txt');
        a=num2str(round(ReN(ii),1,'decimals'));
        filename = sprintf(string,a);
    else
        string=('HP40_T1_Re%s00_M0.00_N9.0.txt');
        a=num2str(round(ReN(ii),3,'decimals'));
        filename = sprintf(string,a);
    end
    delimiterIn = ' ';
    headerlinesIn = 11;
    A=importdata(filename,delimiterIn,headerlinesIn);
    %   A = refined(A.data(:,1:3),stepD);
    for jj=1:length(Flap)
        CL(:,3,ii,jj)=A.data(:,2);    %here I put HP data in all
the angles (HP doesn'thave a flap, so values are the same for
every flap angle)
        CD(:,3,ii,jj)=A.data(:,3);
    end
    disp('HP40')
end
%

%HP60

```

```

for ii=1:length(ReN)
    if round(ReN(ii))==ReN(ii)
        string=('HP60_T1_Re%s.000_M0.00_N9.0.txt');
        a=num2str(round(ReN(ii),1,'decimals'));
        filename = sprintf(string,a);
    else
        string=('HP60_T1_Re%s00_M0.00_N9.0.txt');
        a=num2str(round(ReN(ii),3,'decimals'));
        filename = sprintf(string,a);
    end
    delimiterIn = ' ';
    headerlinesIn = 11;
    A=importdata(filename,delimiterIn,headerlinesIn);
    % A = refined(A.data(:,1:3),stepD);
    for jj=1:length(Flap)
        CL(:,4,ii,jj)=A.data(:,2); %here I put HP data in all
the angles (HP doesn'thave a flap, so values are the same for
every flap angle)
        CD(:,4,ii,jj)=A.data(:,3);
    end
    disp('HP60')
end
%

%HP80
for ii=1:length(ReN)
    if round(ReN(ii))==ReN(ii)
        string=('HP80_T1_Re%s.000_M0.00_N9.0.txt');
        a=num2str(round(ReN(ii),1,'decimals'));
        filename = sprintf(string,a);
    else
        string=('HP80_T1_Re%s00_M0.00_N9.0.txt');
        a=num2str(round(ReN(ii),3,'decimals'));
        filename = sprintf(string,a);
    end
    delimiterIn = ' ';
    headerlinesIn = 11;
    A=importdata(filename,delimiterIn,headerlinesIn);
    % A = refined(A.data(:,1:3),stepD);
    for jj=1:length(Flap)
        CL(:,5,ii,jj)=A.data(:,2); %here I put HP data in all
the angles (HP doesn'thave a flap, so values are the same for
every flap angle)
        CD(:,5,ii,jj)=A.data(:,3);
    end
    disp('HP80')
end

% PT0
for ii=1:length(ReN)
    if round(ReN(ii))==ReN(ii)
        string=('PT0_T1_Re%s.000_M0.00_N9.0.txt');
        string=('S809_T1_Re%s.000_M0.00_N9.0.txt');
        string=('PT02_T1_Re%s.000_M0.00_N9.0.txt');
        a=num2str(round(ReN(ii),1,'decimals'));

```

```

        filename = sprintf(string,a);
    else
        string=('PT0_T1_Re%s00_M0.00_N9.0.txt');
%       string=('S809_T1_Re%s.000_M0.00_N9.0.txt');
%       string=('PT02_T1_Re%s.000_M0.00_N9.0.txt');
        a=num2str(round(ReN(ii),3,'decimals'));
        filename = sprintf(string,a);
    end
    delimiterIn = ' ';
    headerlinesIn = 11;
    A=importdata(filename,delimiterIn,headerlinesIn);
%     A = refined(A.data(:,1:3),stepD);
    CL(:,6,ii,11) = A.data(:,2);
    CD(:,6,ii,11) = A.data(:,3);
    disp('PT0')
end

% PT0_UP
for ii=1:length(ReN)
    if round(ReN(ii))==ReN(ii)
        string=('S809_UP_T1_Re%s.000_M0.00_N9.0.txt');
        a=num2str(round(ReN(ii),1,'decimals'));
        filename = sprintf(string,a);
    else
        string=('S809_UP_T1_Re%s00_M0.00_N9.0.txt');
        a=num2str(round(ReN(ii),3,'decimals'));
        filename = sprintf(string,a);
    end
    delimiterIn = ' ';
    headerlinesIn = 11;
    A=importdata(filename,delimiterIn,headerlinesIn);
%     A = refined(A.data(:,1:3),stepD);
    CL(:,6,ii,1) = A.data(:,2);
    CD(:,6,ii,1) = A.data(:,3);
    disp('PT0_UP')
end

% PT0_DOWN
for ii=1:length(ReN)
    if round(ReN(ii))==ReN(ii)
        string=('S809_DOWN_T1_Re%s.000_M0.00_N9.0.txt');
        a=num2str(round(ReN(ii),1,'decimals'));
        filename = sprintf(string,a);
    else
        string=('S809_DOWN_T1_Re%s00_M0.00_N9.0.txt');
        a=num2str(round(ReN(ii),3,'decimals'));
        filename = sprintf(string,a);
    end
    delimiterIn = ' ';
    headerlinesIn = 11;
    A=importdata(filename,delimiterIn,headerlinesIn);
%     A = refined(A.data(:,1:3),stepD);
    CL(:,6,ii,21) = A.data(:,2);
    CD(:,6,ii,21) = A.data(:,3);
    disp('PT0_DOWN')
end

```

```

% PT2
for ii=1:length(ReN)
    if round(ReN(ii))==ReN(ii)
        string=('PT2_T1_Re%s.000_M0.00_N9.0.txt');
        a=num2str(round(ReN(ii),1,'decimals'));
        filename = sprintf(string,a);
    else
        string=('PT2_T1_Re%s00_M0.00_N9.0.txt');
        a=num2str(round(ReN(ii),3,'decimals'));
        filename = sprintf(string,a);
    end
    delimiterIn = ' ';
    headerlinesIn = 11;
    A=importdata(filename,delimiterIn,headerlinesIn);
%     A = refined(A.data(:,1:3),stepD);
    CL(:,7,ii,11) = A.data(:,2);
    CD(:,7,ii,11) = A.data(:,3);
    disp('PT2')
end

% PT2_UP
for ii=1:length(ReN)
    if round(ReN(ii))==ReN(ii)
        string=('PT2_UP_T1_Re%s.000_M0.00_N9.0.txt');
        a=num2str(round(ReN(ii),1,'decimals'));
        filename = sprintf(string,a);
    else
        string=('PT2_UP_T1_Re%s00_M0.00_N9.0.txt');
        a=num2str(round(ReN(ii),3,'decimals'));
        filename = sprintf(string,a);
    end
    delimiterIn = ' ';
    headerlinesIn = 11;
    A=importdata(filename,delimiterIn,headerlinesIn);
%     A = refined(A.data(:,1:3),stepD);
    CL(:,7,ii,1) = A.data(:,2);
    CD(:,7,ii,1) = A.data(:,3);
    disp('PT2_UP')
end

% PT2
for ii=1:length(ReN)
    if round(ReN(ii))==ReN(ii)
        string=('PT2_DOWN_T1_Re%s.000_M0.00_N9.0.txt');
        a=num2str(round(ReN(ii),1,'decimals'));
        filename = sprintf(string,a);
    else
        string=('PT2_DOWN_T1_Re%s00_M0.00_N9.0.txt');
        a=num2str(round(ReN(ii),3,'decimals'));
        filename = sprintf(string,a);
    end
    delimiterIn = ' ';
    headerlinesIn = 11;
    A=importdata(filename,delimiterIn,headerlinesIn);
%     A = refined(A.data(:,1:3),stepD);

```

```

CL(:,7,ii,21) = A.data(:,2);
CD(:,7,ii,21) = A.data(:,3);
disp('PT2_DOWN')
end

% PT4
for ii=1:length(ReN)
    if round(ReN(ii))==ReN(ii)
        string=('PT4_T1_Re%s.000_M0.00_N9.0.txt');
        a=num2str(round(ReN(ii),1,'decimals'));
        filename = sprintf(string,a);
    else
        string=('PT4_T1_Re%s00_M0.00_N9.0.txt');
        a=num2str(round(ReN(ii),3,'decimals'));
        filename = sprintf(string,a);
    end
    delimiterIn = ' ';
    headerlinesIn = 11;
    A=importdata(filename,delimiterIn,headerlinesIn);
    % A = refined(A.data(:,1:3),stepD);
    CL(:,8,ii,11) = A.data(:,2);
    CD(:,8,ii,11) = A.data(:,3);
    disp('PT4')
end

% PT4_UP
for ii=1:length(ReN)
    if round(ReN(ii))==ReN(ii)
        string=('PT4_UP_T1_Re%s.000_M0.00_N9.0.txt');
        a=num2str(round(ReN(ii),1,'decimals'));
        filename = sprintf(string,a);
    else
        string=('PT4_UP_T1_Re%s00_M0.00_N9.0.txt');
        a=num2str(round(ReN(ii),3,'decimals'));
        filename = sprintf(string,a);
    end
    delimiterIn = ' ';
    headerlinesIn = 11;
    A=importdata(filename,delimiterIn,headerlinesIn);
    % A = refined(A.data(:,1:3),stepD);
    CL(:,8,ii,1) = A.data(:,2);
    CD(:,8,ii,1) = A.data(:,3);
    disp('PT4_UP')
end

% PT4_DOWN
for ii=1:length(ReN)
    if round(ReN(ii))==ReN(ii)
        string=('PT4_DOWN_T1_Re%s.000_M0.00_N9.0.txt');
        a=num2str(round(ReN(ii),1,'decimals'));
        filename = sprintf(string,a);
    else
        string=('PT4_DOWN_T1_Re%s00_M0.00_N9.0.txt');
        a=num2str(round(ReN(ii),3,'decimals'));
        filename = sprintf(string,a);
    end
end

```

```

    delimiterIn = ' ';
    headerlinesIn = 11;
    A=importdata(filename,delimiterIn,headerlinesIn);
%   A = refined(A.data(:,1:3),stepD);
    CL(:,8,ii,21) = A.data(:,2);
    CD(:,8,ii,21) = A.data(:,3);
    disp('PT4_DOWN')
end

% PT6
for ii=1:length(ReN)
    if round(ReN(ii))==ReN(ii)
        string=('PT6_T1_Re%s.000_M0.00_N9.0.txt');
        a=num2str(round(ReN(ii),1,'decimals'));
        filename = sprintf(string,a);
    else
        string=('PT6_T1_Re%s00_M0.00_N9.0.txt');
        a=num2str(round(ReN(ii),3,'decimals'));
        filename = sprintf(string,a);
    end
    delimiterIn = ' ';
    headerlinesIn = 11;
    A=importdata(filename,delimiterIn,headerlinesIn);
%   A = refined(A.data(:,1:3),stepD);
    CL(:,9,ii,11) = A.data(:,2);
    CD(:,9,ii,11) = A.data(:,3);
    disp('PT6')
end
% PT6_UP
for ii=1:length(ReN)
    if round(ReN(ii))==ReN(ii)
        string=('PT6_UP_T1_Re%s.000_M0.00_N9.0.txt');
        a=num2str(round(ReN(ii),1,'decimals'));
        filename = sprintf(string,a);
    else
        string=('PT6_UP_T1_Re%s00_M0.00_N9.0.txt');
        a=num2str(round(ReN(ii),3,'decimals'));
        filename = sprintf(string,a);
    end
    delimiterIn = ' ';
    headerlinesIn = 11;
    A=importdata(filename,delimiterIn,headerlinesIn);
%   A = refined(A.data(:,1:3),stepD);
    CL(:,9,ii,1) = A.data(:,2);
    CD(:,9,ii,1) = A.data(:,3);
    disp('PT6_UP')
end

% PT6_DOWN
for ii=1:length(ReN)
    if round(ReN(ii))==ReN(ii)
        string=('PT6_DOWN_T1_Re%s.000_M0.00_N9.0.txt');
        a=num2str(round(ReN(ii),1,'decimals'));
        filename = sprintf(string,a);
    else
        string=('PT6_DOWN_T1_Re%s00_M0.00_N9.0.txt');

```

```

        a=num2str(round(ReN(ii),3,'decimals'));
        filename = sprintf(string,a);
    end
    delimiterIn = ' ';
    headerlinesIn = 11;
    A=importdata(filename,delimiterIn,headerlinesIn);
%     A = refined(A.data(:,1:3),stepD);
    CL(:,9,ii,21) = A.data(:,2);
    CD(:,9,ii,21) = A.data(:,3);
    disp('PT6_DOWN')
end

% PT8
for ii=1:length(ReN)
    if round(ReN(ii))==ReN(ii)
        string=('PT8_T1_Re%s.000_M0.00_N9.0.txt');
        a=num2str(round(ReN(ii),1,'decimals'));
        filename = sprintf(string,a);
    else
        string=('PT8_T1_Re%s00_M0.00_N9.0.txt');
        a=num2str(round(ReN(ii),3,'decimals'));
        filename = sprintf(string,a);
    end
    delimiterIn = ' ';
    headerlinesIn = 11;
    A=importdata(filename,delimiterIn,headerlinesIn);
%     A = refined(A.data(:,1:3),stepD);
    CL(:,10,ii,11) = A.data(:,2);
    CD(:,10,ii,11) = A.data(:,3);
    disp('PT8')
end

% PT8_UP
for ii=1:length(ReN)
    if round(ReN(ii))==ReN(ii)
        string=('PT8_UP_T1_Re%s.000_M0.00_N9.0.txt');
        a=num2str(round(ReN(ii),1,'decimals'));
        filename = sprintf(string,a);
    else
        string=('PT8_UP_T1_Re%s00_M0.00_N9.0.txt');
        a=num2str(round(ReN(ii),3,'decimals'));
        filename = sprintf(string,a);
    end
    delimiterIn = ' ';
    headerlinesIn = 11;
    A=importdata(filename,delimiterIn,headerlinesIn);
%     A = refined(A.data(:,1:3),stepD);
    CL(:,10,ii,1) = A.data(:,2);
    CD(:,10,ii,1) = A.data(:,3);
    disp('PT8_UP')
end

% PT8_DOWN
for ii=1:length(ReN)
    if round(ReN(ii))==ReN(ii)

```



```

        string=('PT8_DOWN_T1_Re%s.000_M0.00_N9.0.txt');
        a=num2str(round(ReN(ii),1,'decimals'));
        filename = sprintf(string,a);
    else
        string=('PT8_DOWN_T1_Re%s00_M0.00_N9.0.txt');
        a=num2str(round(ReN(ii),3,'decimals'));
        filename = sprintf(string,a);
    end
    delimiterIn = ' ';
    headerlinesIn = 11;
    A=importdata(filename,delimiterIn,headerlinesIn);
%   A = refined(A.data(:,1:3),stepD);
    CL(:,10,ii,21) = A.data(:,2);
    CD(:,10,ii,21) = A.data(:,3);
    disp('PT8_DOWN')
end

% PT10
for ii=1:length(ReN)
    if round(ReN(ii))==ReN(ii)
        string=('PT10_T1_Re%s.000_M0.00_N9.0.txt');
        a=num2str(round(ReN(ii),1,'decimals'));
        filename = sprintf(string,a);
    else
        string=('PT10_T1_Re%s00_M0.00_N9.0.txt');
        a=num2str(round(ReN(ii),3,'decimals'));
        filename = sprintf(string,a);
    end
    delimiterIn = ' ';
    headerlinesIn = 11;
    A=importdata(filename,delimiterIn,headerlinesIn);
%   A = refined(A.data(:,1:3),stepD);
    CL(:,11,ii,11) = A.data(:,2);
    CD(:,11,ii,11) = A.data(:,3);
    disp('PT10')
end

% PT10_UP
for ii=1:length(ReN)
    if round(ReN(ii))==ReN(ii)
        string=('PT10_UP_T1_Re%s.000_M0.00_N9.0.txt');
        a=num2str(round(ReN(ii),1,'decimals'));
        filename = sprintf(string,a);
    else
        string=('PT10_UP_T1_Re%s00_M0.00_N9.0.txt');
        a=num2str(round(ReN(ii),3,'decimals'));
        filename = sprintf(string,a);
    end
    delimiterIn = ' ';
    headerlinesIn = 11;
    A=importdata(filename,delimiterIn,headerlinesIn);
%   A = refined(A.data(:,1:3),stepD);
    CL(:,11,ii,1) = A.data(:,2);
    CD(:,11,ii,1) = A.data(:,3);
    disp('PT10_UP')
end

```

```

% PT10_DOWN
for ii=1:length(ReN)
    if round(ReN(ii))==ReN(ii)
        string=('PT10_DOWN_T1_Re%s.000_M0.00_N9.0.txt');
        a=num2str(round(ReN(ii),1,'decimals'));
        filename = sprintf(string,a);
    else
        string=('PT10_DOWN_T1_Re%s00_M0.00_N9.0.txt');
        a=num2str(round(ReN(ii),3,'decimals'));
        filename = sprintf(string,a);
    end
    delimiterIn = ' ';
    headerlinesIn = 11;
    A=importdata(filename,delimiterIn,headerlinesIn);
%     A = refined(A.data(:,1:3),stepD);
    CL(:,11,ii,21) = A.data(:,2);
    CD(:,11,ii,21) = A.data(:,3);
    disp('PT10_DOWN')
end
%%
ReN=ReN*1e6;
figure(1)
for i=1:11
    plot(-6:0.5:17, CL(:,i,4,11));
    hold on
    legend
end
E=CL./CD;

for i=1:21
    CL(:, :, :, i)=rInterp2_2(CL,i);
    CD(:, :, :, i)=rInterp2_2(CD,i);
end

CL=rInterp3_2(CL,rH,rP,rT,NN); %here they are becoming 101
profiles funziona
CD=rInterp3_2(CD,rH,rP,rT,NN); %here they are becoming 101
profiles

resolution=0.1;

CL=rInterp4_2(CL,minDeg,maxDeg,stepD,resolution,NN); %here data
are becoming every 0.1 degree instead of 0.5 degree
CD=rInterp4_2(CD,minDeg,maxDeg,stepD,resolution,NN); %here data
are becoming every 0.1 degree instead of 0.5 degree

E=CL./CD;
alphaD=minDeg:resolution:maxDeg;

filen='nrelXfoil_2.mat';
save(filen,'alphaD','CL','CD','NN','ReN','rH','rP','rT');
%%
close all
prof=75;

```

```
flap_angle=11;
Re_1=2;
for k=6:16:length(ReN)
    figure(1)
    plot(-6:resolution:17,CL(:,prof,2,k))    %, 'LineWidth',5)
    hold on
    legend
end
for k=6:16%1:length(ReN)
    figure(2)
    plot(-6:resolution:17,CD(:,prof,2,k))
    hold on
    legend
end
for k=6:16%1:length(ReN)
    figure(3)
    plot(-6:resolution:17,E(:,prof,2,k))
    hold on
end
for k=1:length(ReN)
    figure(4)
    plot(-6:resolution:17,CD(:,prof,k,flap_angle))
    hold on
    plot(-6:resolution:17,CL(:,prof,k,flap_angle))
    hold on
    plot(-6:resolution:17,E(:,prof,k,flap_angle)/100)
    hold on
    grid on
end
```

## 15 ANNEX [F1A]

---

```

function [res]=rInterp2_2(coeff, i)

[X,Y,Z,D]=size(coeff);
res=zeros(X,Y,Z,1);

for x=1:X
    for y=1:Y
        for z=1:Z
            if y<6
                %for each PT profile
                %for each Re
                %I don't interpolate in the HP
                profiles
                    res(x,y,z)=coeff(x,y,z,i);
                end
            if y>=6
                if i==1
                    res(x,y,z)=coeff(x,y,z,i);
                end
                if i>1 && i<11
                    dist=(coeff(x,y,z,11)-coeff(x,y,z,1))/10;
                    res(x,y,z)=coeff(x,y,z,1)+dist*(i-1);
                end
                if i==11
                    res(x,y,z)=coeff(x,y,z,i);
                end
                if i>11 && i<21
                    dist=(coeff(x,y,z,21)-coeff(x,y,z,11))/10;
                    res(x,y,z)=coeff(x,y,z,11)+dist*(i-11);
                end
                if i==21
                    res(x,y,z)=coeff(x,y,z,i);
                end
            end
        end
    end
end
end
end
end

```

## 16 ANNEX [F2A]

---

```
function [coeff_out]=rInterp3_2(coeff,rH,rP,rT,NN)
%sample cL=961x3x16 == alphas x sections x #Reynolds

[X,Y,Z,D]=size(coeff);           %[angles,number of Xfoil profile,Re#,
flap]
r=linspace(rH,rT,NN+1);         %Finer Re vector
r_old=linspace(rH,rT,Y);
coeff_out=zeros(X,NN+1,Z,D);

for i=1:X
    for k=1:Z                     %for each Re
        for p=1:D                 %for each angle

coeff_out(i,:,k,p)=interp1(r_old,coeff(i,:,k,p),r,'linear');
%could be linear too
            end
        end
    end
end
%
end
```

## 17 ANNEX [F3A]

---

```
function [res]=rInterp4_2(coeff,angle_in, angle_fin, OldStep,
NewStep,NN)
r_old=[angle_in:OldStep:angle_fin];
r=[angle_in:NewStep:angle_fin];
[X,Y,Z,D]=size(coeff);
res=zeros(length(r),NN+1,Z,D);

for p=1:D
    for k=1:Y                     %for each profile
        for i=1:Z                 %for each Re
            res(:,k,i,p)=interp1(r_old,coeff(:,k,i,p),
r,'spline');
                end
        end
    end
end

end
```

## 18 ANNEX [B]

```

%%Design Part
%%%%%%%%%%%%%%%%%%%%%%%%%%%%%%%%%%%%%%%%%%%%%%%%%%%%%%%%%%%%%%%%%%%%%%%%
%%%%%%%%%%%%%%%%%%%%%%%%%%%%%%%%%%%%%%%%%%%%%%%%%%%%%%%%%%%%%%%%%%%%%%%%
%% INPUT PARAMETERS AND GENERAL DATA

v0=8;   R=30/2;   lambda=7;   Nbl=3;
load('nrelXfoil.mat')           %'alphaD','CL','CD','NN','ReN'
rH=R*rH;
rP=R*rP;
rT=R*rT;

omega=lambda*v0/R;           ReMax=ReN(end);           ReMin=ReN(1);

ni20=1.5111e-5;

rho20=101325/(8314/28.9*293.15);

r=linspace(rH,rT,NN+1);           %number of delimiting radial
coordinates -->this radius must be dimensionless to interpolate
on profiles2
dr=abs(r(1)-r(2));           %radial step
dalpha=abs(alphaD(2)-alphaD(1));           %angle step
dRe=abs(ReN(2)-ReN(1));           %Reynolds step
rm=linspace(rH+dr/2,rT-dr/2,NN);

%%%%%%%%%%%%%%%%%%%%%%%%%%%%%%%%%%%%%%%%%%%%%%%%%%%%%%%%%%%%%%%%%%%%%%%%
%%%%%%%%%%%%%%%%%%%%%%%%%%%%%%%%%%%%%%%%%%%%%%%%%%%%%%%%%%%%%%%%%%%%%%%%
%% GLAUERT DISTRIBUTION

x=lambda*rm/R;           %lambda
local vector
a_gl=ones(1,NN);           %general
initialization
a_prime_gl=ones(1,NN);
a_glauert=ones(1,NN);
a_p_glauert=ones(1,NN);

for ii=1:NN           %system
solution
    funz=@(a) a*(1-a)-a*(1-3*a)/((4*a-1)^2)*x(ii).^2;
    a_gl=fzero(funz,0.3);
    a_prime_gl=(1-3*a_gl)./(4*a_gl-1);
    a_glauert(ii)=a_gl;           %output
row
    a_p_glauert(ii)=a_prime_gl;           %output
row
end

%%%%%%%%%%%%%%%%%%%%%%%%%%%%%%%%%%%%%%%%%%%%%%%%%%%%%%%%%%%%%%%%%%%%%%%%
%%%%%%%%%%%%%%%%%%%%%%%%%%%%%%%%%%%%%%%%%%%%%%%%%%%%%%%%%%%%%%%%%%%%%%%%
%% a Glauert - a' BEM

```

```

a_ii=a_glauert;
a_prime_ii=a_p_glauert;

Re_0=2000000; %Re first
guess
c_star_res = zeros(1,NN); %variables
initial
Beta_c = zeros(1,NN);
phi = zeros(1,NN);
Re = zeros(1,NN);
w_inf = zeros(1,NN);
F = zeros(1,NN);
cL = zeros(NN,length(alphaD));
cD = zeros(NN,length(alphaD));
E=zeros(NN,length(alphaD));
cLstar=zeros(1,NN);
cDstar=zeros(1,NN);
iemax = zeros(1,NN);

for ii=1
    vd = (1-a_ii(ii))*v0; %glauert > first
    guess
    u = (1+a_prime_ii(ii))*omega*rm(ii); %glauert >
    first guess
    phi(ii) = atand(vd./u);
    %atand(a_prime_ii(ii).*x(ii)./a_ii(ii));
    w_inf(ii) = (u.^2+vd.^2).^0.5;

    err=40000; toll=30000;
    while err>toll

[cL(ii,:),cD(ii,:),E(ii,:)]=profiles2(ii,Re_0,CL,CD,ReMin,ReMax,
dRe); %interpolating @given radius(ii) for the right Re
(Re0)
    [~,iemax(ii)]=max(E(ii,:)); %we select
incidence angle that maximize efficiency (better than CL since we
keep lower drag)
    %find
    give us the index corresponding to Emax not the value of efficiency

    alpha_E_max=alphaD(iemax(ii)); %we extract
incidence angle maximizing efficiency
    cLstar(ii)=cL(ii,iemax(ii)); %we
extract CL max E
    cDstar(ii)=cD(ii,iemax(ii)); %we
extract CD max E
    Beta_c(ii)=phi(ii)-alpha_E_max; %stagger angle

    f=0.5*Nbl*(1-rm(ii)/R)/(rm(ii)/R*sind(phi(ii)));
    F(ii)=2/pi*acos(exp(-f));

sigma=a_ii(ii)*4*v0*F(ii)./w_inf(ii)*1./(cLstar(ii)/tand(phi(ii)
)+cDstar(ii)); %compute solidity with a_glauert
    c_star_res(ii)=2*pi*rm(ii)*sigma/Nbl;
%compute new chord

```

```

a_prime_ii(ii)=(sigma*w_inf(ii))/(4*omega*rm(ii)*F(ii))*(cLstar(
ii)-cDstar(ii)/tand(phi(ii)));      %compute a' BEM using solidity

    vd = (1-a_ii(ii))*v0;
    u = (1+a_prime_ii(ii))*omega*rm(ii);
    phi(ii) = atand(vd./u);
%atand(a_prime_ii(ii).*x(ii)./a_ii(ii));
    w_inf(ii) = (u.^2+vd.^2).^0.5;

    Re(ii)=w_inf(ii)*c_star_res(ii)/ni20;
%new guess for Re
    err=abs(Re(ii)-Re_0);
    Re_0=Re(ii);
end
disp(Re(ii))
end

for ii=2:NN
    vd = (1-a_ii(ii))*v0;      %glauert >
first guess
    u = (1+a_prime_ii(ii))*omega*rm(ii);      %glauert >
first guess
    phi(ii) = atand(vd./u);
%atand(a_prime_ii(ii).*x(ii)./a_ii(ii));
    w_inf(ii) = (u.^2+vd.^2).^0.5;

    err=10e4; toll=5e4;
    niter=0;
    wid = 5;
    while err>toll || abs(Re(ii)-Re(ii-1))>50000 ||
c_star_res(ii)>c_star_res(ii-1) % || Beta_c(ii)>=Beta_c(ii-1)
        if niter >=1500
            wid=wid-1;
            if wid <0
                wid=0;
            end
            niter=1;
        end
end

[cL(ii,:),cD(ii,:),E(ii,:)]=profiles2(ii,Re_0,CL,CD,ReMin,ReMax,
dRe);      %interpolating @given radius(ii) for the right Re
(Re0)
    intorno = (E(ii,iemax(ii-1)-wid:iemax(ii-1)+wid)) ;

%we select incidence angle that maximize efficiency (better than
CL since we keep lower drag)
    [~,iemax(ii)]=max(intorno);
    iemax(ii)=iemax(ii)+iemax(ii-1)-wid-1;
%find give us the index corresponding to Emax not the value of
efficiency
%    [~,iemax(ii)]=max(E(ii,:));
    alpha_E_max=alphaD(iemax(ii));      %we extract
incidence angle maximizing efficiency

```



```

        cLstar(ii)=cL(ii,iemax(ii)); %we
extract CL max E
        cDstar(ii)=cD(ii,iemax(ii)); %we
extract CD max E
        Beta_c(ii)=phi(ii)-alpha_E_max; %stagger angle

        f=0.5*Nbl*(1-rm(ii)/R)/(rm(ii)/R*sind(phi(ii)));
        F(ii)=2/pi*acos(exp(-f));

sigma(ii)=a_ii(ii)*4*v0*F(ii)./w_inf(ii)*1./(cLstar(ii)/tand(phi
(ii))+cDstar(ii)); %compute solidity with a_glauert
        c_star_res(ii)=2*pi*rm(ii)*sigma(ii)/Nbl;
%compute new chord

a_prime_ii(ii)=(sigma(ii)*w_inf(ii))/(4*omega*rm(ii)*F(ii))*(cLs
tar(ii)-cDstar(ii)/tand(phi(ii)));
        vd = (1-a_ii(ii))*v0;
        u = (1+a_prime_ii(ii))*omega*rm(ii);
        phi(ii) = atand(vd./u);
%atand(a_prime_ii(ii).*x(ii)./a_ii(ii));
        w_inf(ii) = (u.^2+vd.^2).^0.5;

        Re(ii)=w_inf(ii)*c_star_res(ii)/ni20;
%new guess for Re
        err=abs(Re(ii)-Re_0);
        Re_0=Re(ii);
        niter=niter+1;

%         disp(Re(ii))
%         disp(niter)
        end
        disp(Re(ii))
        disp(ii)
end
%%
figure(1)
subplot(2,2,1)
plot(rm,c_star_res,'LineWidth',1)
grid on
title('Chord distribution')
subplot(2,2,2)
plot(rm,Beta_c,'LineWidth',1)
grid on
title('Stagger angle distribution')
subplot(2,2,3)
plot(rm,phi,'LineWidth',1)
grid on
title('\phi \infty distribution')
subplot(2,2,4)
plot(rm,Re,'LineWidth',1)
grid on
title('Reynolds distribution')
% subplot(2,3,5)
% plot(rm,F,'LineWidth',1)
% title('f')

```

```

%%%%%%%%%%%%%%%%%%%%%%%%%%%%%%%%%%%%%%%%%%%%%%%%%%%%%%%%%%%%%%%%%%%%%%%%
%%%%%%%%%%%%%%%%%%%%%%%%%%%%%%%%%%%%%%%%%%%%%%%%%%%%%%%%%%%%%%%%%%%%%%%%
%% a' Glauert - a BEM

a_ii_2 = a_glauert;
a_prime_ii_2 = a_p_glauert;

Re_0=1e6;
c_star_res_2 = zeros(1,NN);
Beta_c_2 = zeros(1,NN);
phi_2 = zeros(1,NN);
Re_2 = zeros(1,NN);
w_inf_2 = zeros(1,NN);
F_2 = zeros(1,NN);
cL_2 = zeros(NN,length(alphaD));
cD_2 = zeros(NN,length(alphaD));
sigma_2=zeros(1,NN);
cLstar_2=zeros(1,NN);
cDstar_2=zeros(1,NN);
alpha_E_max_2=zeros(1,NN);
iemax_2=zeros(1,NN);
E_2=zeros(NN,length(alphaD));

wid=5;

for ii=1
    vd = (1-a_ii_2(ii))*v0; %glauert >
    first guess
    u = (1+a_prime_ii_2(ii))*omega*rm(ii); %glauert >
    first guess
    phi_2(ii) = atand(vd./u);
    %atand(a_prime_ii(ii).*x(ii)./a_ii(ii));
    w_inf_2(ii) = (u.^2+vd.^2).^0.5;

    err=40000; toll=30000;
    while err>toll

[cL_2(ii,:),cD_2(ii,:),E_2(ii,:)]=profiles2(ii,Re_0,CL,CD,ReMin,
ReMax,dRe); %interpolating @given radius(ii) for the
right Re (Re0)
    [~,iemax_2(1)]=find(E_2(1,)==max(E_2(1,:)));
    %we select incidence angle that maximize efficiency (better than
    CL since we keep lower drag) %find give
    us the index corresponding to Emax not the value of efficiency

    alpha_E_max_2(ii)=alphaD(iemax_2(1)); %we
    extract incidence angle maximizing efficiency
    cLstar_2(ii)=cL_2(ii,iemax_2(1)); %we
    extract CL max E
    cDstar_2(ii)=cD_2(ii,iemax_2(1)); %we
    extract CD max E
    Beta_c_2(ii)=phi_2(ii)-alpha_E_max_2(ii);
    %stagger angle

```

```

f_2=0.5*Nbl*(1-rm(ii)/R)/(rm(ii)/R*sind(phi_2(ii)));
F_2(ii)=2/pi*acos(exp(-f_2));

sigma_2(ii)=(a_prime_ii_2(ii)*4*omega*rm(ii)*F_2(ii))/(w_inf_2(ii)
*(cLstar_2(ii)-cDstar_2(ii)/tand(phi_2(ii))));
c_star_res_2(ii)=(2*pi*rm(ii)*sigma_2(ii))/Nbl;

a_ii_2(ii)=(sigma_2(ii)*w_inf_2(ii))/(4*v0*F_2(ii)*(cLstar_2(ii)
)/tand(phi_2(ii))+cDstar_2(ii));

vd = (1-a_ii_2(ii))*v0;
u = (1+a_prime_ii_2(ii))*omega*rm(ii);
phi_2(ii) = atand(vd./u);
%atand(a_prime_ii(ii).*x(ii)./a_ii(ii));
w_inf_2(ii) = (u.^2+vd.^2).^0.5;

Re_2(ii)=w_inf_2(ii)*c_star_res_2(ii)/ni20;
%new guess for Re
err=abs(Re_2(ii)-Re_0);

Re_0=Re_2(ii);
%ci di; il
numero di iterazioni del ciclo while per ogni posizione radiale
(ii)
end
disp(Re_2(ii))
end

for ii=2:NN
%disp(ii/NN)
vd(ii)=(1-a_ii_2(ii))*v0;
u(ii)=(1+a_prime_ii_2(ii))*omega*rm(ii);
phi_2(ii)=atand(vd(ii)./u(ii));
%atand(a_prime_ii(ii).*x(ii)./a_ii(ii));
w_inf_2(ii)=(u(ii).^2+vd(ii).^2).^0.5;
err=10e4; toll=5e4;
niter=0;
wid = 5;
while err>toll || abs(Re_2(ii)-Re_2(ii-1))>50000 ||
c_star_res_2(ii)>c_star_res_2(ii-1)

if niter >=150
wid=wid-1;
if wid <0
wid=0;
end
end
end

[cL_2(ii,:),cD_2(ii,:),E_2(ii,:)] = profiles2(ii,Re_0,CL,CD,ReMin,
ReMax,dRe); %interpolating @given radius(ii) for the
right Re (Re0)
intorno = (E_2(ii,iemax_2(ii-1)-wid:iemax_2(ii-1)+wid));

```

```

        [~, iemax_2(ii)] = max(intorno); %we select
incidence angle that maximize efficiency (better than CL since we
keep lower drag)
        iemax_2(ii) = iemax_2(ii) + iemax_2(ii-1) - wid - 1;
%find give us the index corresponding to Emax not the value of
efficiency
%        [~, iemax(ii)] = max(E(ii, :));
        alpha_E_max_2(ii) = alphaD(iemax_2(ii)); %we
extract incidence angle maximizing efficiency
        cLstar_2(ii) = cL_2(ii, iemax_2(ii)); %we
extract CL max E
        cDstar_2(ii) = cD_2(ii, iemax_2(ii)); %we
extract CD max E
        Beta_c_2(ii) = phi_2(ii) - alpha_E_max_2(ii);

        f2 = 0.5 * Nbl * (1 - rm(ii) / R) / (rm(ii) / R * sind(phi_2(ii)));
        F_2(ii) = 2 / pi * acos(exp(-f2));

sigma_2(ii) = a_ii_2(ii) * 4 * v0 * F_2(ii) ./ w_inf_2(ii) * 1 ./ (cLstar_2(ii)
) / tand(phi_2(ii) + cDstar_2(ii)); %compute
solidity with a_glauert
        c_star_res_2(ii) = 2 * pi * rm(ii) * sigma_2(ii) / Nbl;
%compute new chord

a_ii_2(ii) = (sigma_2(ii) * w_inf_2(ii)) / (4 * v0 * F_2(ii)) * (cLstar_2(ii)
) / tand(phi_2(ii) + cDstar_2(ii)); %compute a' BEM using
solidity

        vd = (1 - a_ii_2(ii)) * v0;
        u = (1 + a_prime_ii_2(ii)) * omega * rm(ii);
        phi_2(ii) = atand(vd ./ u);
%atand(a_prime_ii(ii) .* x(ii) ./ a_ii(ii));
        w_inf_2(ii) = (u.^2 + vd.^2).^0.5;

        Re_2(ii) = w_inf_2(ii) * c_star_res_2(ii) / ni20;
%new guess for Re
        err = abs(Re_2(ii) - Re_0);
%        if niter > 1000 && err <= 10 * 10^5
%                Re(ii) = (Re_0 + Re_2(ii)) / 2;
%                break
%        end
        Re_0 = Re_2(ii);
        niter = niter + 1;
%        disp(Re_2(ii))
end
figure(3)
plot(ii, Re(ii), 'm+');
plot(ii, Re_2(ii), 'x');
hold on
figure(4)
plot(ii, c_star_res(ii), 'mo');
plot(ii, c_star_res_2(ii), 'o');
hold on
disp(Re_2(ii))

```

```

        disp(ii)
    end

    figure(2)
    subplot(2,2,1)
    plot(rm,c_star_res_2)
    grid on
    title('Chord distribution')
    subplot(2,2,2)
    plot(rm,Beta_c_2)
    grid on
    title('Stagger angle distribution')
    subplot(2,2,3)
    plot(rm,phi_2)
    grid on
    title('\phi \infty distribution')
    subplot(2,2,4)
    plot(rm,Re_2)
    grid on
    title('Reynolds distribution')

%DEBUG

% plot(alpha_E_max_2)
% plot(cL_star_2)
% plot(cLstar_2)
% plot(cLstar_2./cDstar_2)
% plot(F_2)
% plot(iemax_2)
% plot(sigma_2)
% plot(a_ii_2)

%%%%%%%%%%%%%%%%%%%%%%%%%%%%%%%%%%%%%%%%%%%%%%%%%%%%%%%%%%%%%%%%%%%%%%%%
%%%%%%%%%%%%%%%%%%%%%%%%%%%%%%%%%%%%%%%%%%%%%%%%%%%%%%%%%%%%%%%%%%%%%%%%
%% FINAL - AVERAGED - DISTRIBUTIONS
% c_star_res=c_star_res_2;
%a = (a_ii+a_ii_2)/2;
a=a_ii_2; %only take a_bem
and a'bem
%a_prime = (a_prime_ii+a_prime_ii_2)/2;
a_prime=a_prime_ii;
c = (c_star_res+c_star_res_2)/2;
Betac = (Beta_c+Beta_c_2)/2;
phin_f = (phi+phi_2)/2;
Re_f = (Re+Re_2)/2;
cLs=(cLstar+cLstar_2)/2;
cDs=(cDstar+cDstar_2)/2;
Fm=(F+F_2)/2;

    figure(3)
    subplot(2,2,1)
    plot(rm,c)
    title('Chord distribution')
    grid on
    subplot(2,2,2)
    plot(rm,Betac)

```

```

title('Stagger angle distribution')
grid on
subplot(2,2,3)
plot(rm,phinf)
title('\phi \infty distribution')
grid on
subplot(2,2,4)
plot(rm,Ref)
title('Reynolds distribution')
grid on

figure()
plot(rm,Fm, 'LineWidth',1)
grid on
title('F')
%%%%%%%%%%%%%%%%%%%%%%%%%%%%%%%%%%%%%%%%%%%%%%%%%%%%%%%%%%%%%%%%%%%%%%%%
%%%%%%%%%%%%%%%%%%%%%%%%%%%%%%%%%%%%%%%%%%%%%%%%%%%%%%%%%%%%%%%%%%%%%%%%
%% CHORD LINEARIZATION

clin = zeros(1,NN);
coeff = zeros(1,NN);
for k=1:NN-1
coeff(k) = (c(k+1)-c(k))/(rm(k+1)-rm(k)); %slope
end

index_m = find(rm>0.81*R,1);
m = coeff(index_m);

for j=1:NN
if j<=index_m
clin(j) = c(index_m)+m*(rm(j)-rm(index_m));
else
clin(j) = c(j);
end
end

clin=smooth(clin,10);
figure
plot(rm,clin, 'LineWidth',2);
hold on
plot(rm,c);
title('Chord distribution')
fprintf('maximum value\n of linearized chord is\n %s, so\n
%s/%i=%s <0.12\n',max(clin), max(clin), R, max(clin)/R);
%%%%%%%%%%%%%%%%%%%%%%%%%%%%%%%%%%%%%%%%%%%%%%%%%%%%%%%%%%%%%%%%%%%%%%%%
%%%%%%%%%%%%%%%%%%%%%%%%%%%%%%%%%%%%%%%%%%%%%%%%%%%%%%%%%%%%%%%%%%%%%%%%
%% CHORD CORRECTION

sigmalin=(Nbl/2/pi)*(clin)./(rm'); %200X1
sigmalin=sigmalin'; %1X200 as all other
vectors
a_0=a;
a_prime_0=a_prime;
phi_lin=zeros(1,NN);
Re_lin=zeros(1,NN);
f_lin=zeros(1,NN);

```

```

F_lin=zeros(1,NN);
cL_lin=zeros(NN,length(alphaD));
cD_lin=zeros(NN,length(alphaD));
cLstar_lin=zeros(1,NN);
cDstar_lin=zeros(1,NN);
Beta_c_lin=zeros(1,NN);
a_lin=zeros(1,NN);
a_prime_lin=zeros(1,NN);
w_inf_lin=zeros(1,NN);
alpha_E_max_lin=zeros(1,NN);
E_lin=zeros(NN,length(alphaD));
iemax_lin=zeros(1,NN);

toll=1e-3;

for ii=1

    err1=10;
    err2=10;
    toll=1e-3;
    niter=0;
    wid = 5;

    while err1>toll || err2 >toll

        phi_lin(ii)=atand(((1-
a_0(ii))*v0)/((1+a_prime_0(ii))*omega*rm(ii)));
        w_inf_lin(ii)=(((1+a_prime_0(ii))*omega*rm(ii)).^2+((1-
a_0(ii))*v0).^2).^0.5;
        Re_lin(ii)=w_inf_lin(ii)*clin(ii)/ni20;
        f_lin(ii)=0.5*Nbl*(1-
rm(ii)/R)/(rm(ii)/R*sind(phi_lin(ii)));
        F_lin(ii)=2/pi*acos(exp(-f_lin(ii)));

[cL_lin(ii,:),cD_lin(ii,:),E_lin(ii,:)]=profiles2(ii,Re_0,CL,CD,
ReMin,ReMax,dRe);
        iemax_lin(ii)=find(E_lin(ii,:)==max(E_lin(ii,:)));
%for ii=1 or if we don't use findpeaks (unconstrained max)
        alpha_E_max_lin(ii)=alphaD(iemax_lin(ii));
        cLstar_lin(ii)=cL_lin(ii,iemax_lin(ii));
        cDstar_lin(ii)=cD_lin(ii,iemax_lin(ii));
        Beta_c_lin(ii)=phi_lin(ii)-alpha_E_max_lin(ii);

a_lin(ii)=(sigmalin(ii)*w_inf_lin(ii))/(4*v0*F_lin(ii))*(cLstar_
lin(ii)/...
        tand(phi_lin(ii))+cDstar_lin(ii));

a_prime_lin(ii)=(sigmalin(ii)*w_inf_lin(ii))/(4*omega*rm(ii)*F_l
in(ii))*...
        (cLstar_lin(ii)-cDstar_lin(ii)/tand(phi_lin(ii)));

%update
err1=abs(a_lin(ii)-a_0(ii));

```

```

err2=abs(a_prime_lin(ii)-a_prime_0(ii));

a_0(ii)=a_lin(ii);
a_prime_0(ii)=a_prime_lin(ii);
Re_0=Re_lin(ii);
niter=niter+1;
end
end

for ii=2:NN

    err1=10;
    err2=10;
    toll=1e-3;
    niter=0;
    wid = 5;

    while err1>toll || err2 >toll %|| phi_lin(ii)>=phi_lin(ii-1)

        phi_lin(ii)=atand(((1-
a_0(ii))*v0)/((1+a_prime_0(ii))*omega*rm(ii)));
        w_inf_lin(ii)=(((1+a_prime_0(ii))*omega*rm(ii)).^2+((1-
a_0(ii))*v0).^2).^0.5;
        Re_lin(ii)=w_inf_lin(ii)*clin(ii)/ni20;
        f_lin(ii)=0.5*Nbl*(1-
rm(ii)/R)/(rm(ii)/R*sind(phi_lin(ii)));
        F_lin(ii)=2/pi*acos(exp(-f_lin(ii)));

        [cL_lin(ii,:),cD_lin(ii,:),E_lin(ii,:)] = profiles2(ii,Re_0,CL,CD,
ReMin,ReMax,dRe);
        intorno = (E_lin(ii,iemax_lin(ii-1)-wid:iemax_lin(ii-
1)+wid));
        iemax_lin(ii)=find(intorno==max(intorno));
%we select incidence angle that maximize efficiency (better than
CL since we keep lower drag)
        iemax_lin(ii)=iemax_lin(ii)+iemax_lin(ii-1)-wid-1;

        alpha_E_max_lin(ii)=alphaD(iemax_lin(ii));
        cLstar_lin(ii)=cL_lin(ii,iemax_lin(ii));
        cDstar_lin(ii)=cD_lin(ii,iemax_lin(ii));
        Beta_c_lin(ii)=phi_lin(ii)-alpha_E_max_lin(ii);

a_lin(ii)=(sigmalin(ii)*w_inf_lin(ii))/(4*v0*F_lin(ii))*(cLstar_
lin(ii)/...
        tand(phi_lin(ii))+cDstar_lin(ii));

a_prime_lin(ii)=(sigmalin(ii)*w_inf_lin(ii))/(4*omega*rm(ii)*F_l
in(ii))*...
        (cLstar_lin(ii)-cDstar_lin(ii)/tand(phi_lin(ii)));

        %update
        err1=abs(a_lin(ii)-a_0(ii));
        err2=abs(a_prime_lin(ii)-a_prime_0(ii));

```



```

        a_0(ii)=a_lin(ii);
        a_prime_0(ii)=a_prime_lin(ii);
        niter=niter+1;
        Re_0=Re_lin(ii);

    end
end

%%%%%%%%%%%%%%%%%%%%%%%%%%%%%%%%%%%%%%%%%%%%%%%%%%%%%%%%%%%%%%%%%%%%%%%%
%%%%%%%%%%%%%%%%%%%%%%%%%%%%%%%%%%%%%%%%%%%%%%%%%%%%%%%%%%%%%%%%%%%%%%%%
%% PLOTS

figure()
plot(phi_lin); title('phi lin');
figure()
plot(w_inf); title('w inf');
figure()
plot(Re_lin); title('Re lin');
figure()
plot(F_lin); title('F lin');
figure()
plot(alpha_E_max_lin); title('alpha E max');
figure()
plot(cLstar_lin, '-x'); title('cLstar lin');
figure()
plot(cDstar_lin); title('cDstar lin');
figure()
plot(Beta_c_lin, '-x'); title('Beta c lin');
grid on
figure()
plot(a_lin); title('a lin');
figure()
plot(a_prime_lin); title('a prime lin');

%%%%%%%%%%%%%%%%%%%%%%%%%%%%%%%%%%%%%%%%%%%%%%%%%%%%%%%%%%%%%%%%%%%%%%%%
%%%%%%%%%%%%%%%%%%%%%%%%%%%%%%%%%%%%%%%%%%%%%%%%%%%%%%%%%%%%%%%%%%%%%%%%
%% Cp, POWER EXTRACTION and FORCES

CP=zeros(2,NN);
CP_lin=zeros(2,NN);
Pw=zeros(2,NN);
Pw_lin=zeros(2,NN);
dFa1=zeros(NN,1);
dFt1=zeros(NN,1);
dFa2=zeros(NN,1);
dFt2=zeros(NN,1);

for ii=1:NN

    CP(1,ii)=Nbl*omega/(pi*R^2*v0^3)*(c(ii)*(w_inf(ii)).^2)*...
        (cLs(ii)*sind(phinf(ii))-
        cDs(ii)*cosd(phinf(ii)))*rm(ii);
    CP(2,ii)=8/(lambda.^2)*Fm(ii)*a_prime(ii)*(1-
    a(ii))*(lambda*rm(ii)/R).^3;

```

```

CP_lin(1,ii)=Nbl*omega/(pi*R^2*v0^3)*(clin(ii)*(w_inf_lin(ii)).^
2)*...
    (cLstar_lin(ii)*sind(phi_lin(ii))-
cDstar_lin(ii)*cosd(phi_lin(ii)))*rm(ii);
    CP_lin(2,ii)=8/(lambda.^2)*F_lin(ii)*a_prime_lin(ii)*(1-
a_lin(ii))*(lambda*rm(ii)/R).^3;

dFa1(ii)=Nbl*0.5*rho20*w_inf_lin(ii).^2*clin(ii)*(cLstar_lin(ii)
*cosd(phi_lin(ii))+cDstar_lin(ii)*sind(phi_lin(ii)));

dFt1(ii)=Nbl*0.5*rho20*w_inf_lin(ii).^2*clin(ii)*(cLstar_lin(ii)
*sind(phi_lin(ii))-cDstar_lin(ii)*cosd(phi_lin(ii)))*rm(ii);
    dFa2(ii)=F_lin(ii)*rho20*v0^2*4*a_lin(ii)*(1-
a_lin(ii))*pi*rm(ii);
    dFt2(ii)=F_lin(ii)*4*pi*rho20*omega*v0*(1-
a_lin(ii))*a_prime_lin(ii)*rm(ii)^3;
end

CPI1=sum(CP(1,:)).*dr;
CPI2=sum(CP(2,:))*(lambda/R).*dr;

figure()
plot(rm,smooth(dFa1,3));
hold on
plot(rm,smooth(dFa2,3));
title('Fa')
grid on
figure()
plot(rm,dFt1);
hold on
plot(rm,dFt2);
title('Ft')
grid on

fprintf('max Fa\n %d\n', max(dFa1));
fprintf('max Ft\n %d\n', max(dFt1));

CPI1_lin=sum(CP_lin(1,:)).*dr;
disp(CPI1_lin)
CPI2_lin=sum(CP_lin(2,:))*(lambda/R).*dr;
disp(CPI2_lin)
disp('T and M')
disp(sum(dFa1(:)))
disp(sum(dFt1(:)))

figure
subplot(2,2,1)
plot(rm,clin,'LineWidth',2);
hold on
plot(rm,c);
grid on
title('Chord distribution')
subplot(2,2,2)
plot(Re_lin); title('Re lin');

```

```
grid on
title('Re')
subplot(2,2,3)
plot(rm,dFt2);
title('Ft')
grid on
subplot(2,2,4)
plot(rm,smooth(dFa1,3));
hold on
plot(rm,smooth(dFa2,3));
title('axial force acting on the blade')
grid on

fprintf('CPI1=%s\n CPI2=%s\n', CPI1_lin, CPI2_lin)

filename='nominal_design.mat';
save(filename,'a_lin','a_prime_lin','clin','rH','rP','rT','r','d
r',...

'dalpha','dRe','rm','ReMax','ReMin','NN','rm','CPI1_lin','Beta_c
_lin','sigmalin');
```

## 19 ANNEX [F1B]

---

```

function [cL,cD,E]=profiles2(jj,Re,CL,CD,ReMin,ReMax,stepRe)

ind=round(ceil((Re-ReMin)/stepRe));           %ind=1 -> Re=ReMin
(1e6)
max=round(ceil((ReMax-ReMin)/stepRe));       %indice
corrispondente a Re=ReMax

CLav=zeros(size(CL,1),size(CL,3));           %#alphaD x #Re
CDav=zeros(size(CL,1),size(CL,3));

CLav(:,:)=0.5.*(CL(:,jj,:)+CL(:,jj+1,:));    %media fatta
perchè lavoriamo su rm
CDav(:,:)=0.5.*(CD(:,jj,:)+CD(:,jj+1,:));

if (ind>=1) && (ind<=max)                    %caso Re>1e6 , interp
lineare tra i CL e CD a due Re "vicini"
    Re_ref=ReMin+stepRe*(ind-1);
    cL=CLav(:,ind)+((CLav(:,ind+1)-CLav(:,ind))./stepRe).*(Re-
Re_ref);
    cD=CDav(:,ind)+((CDav(:,ind+1)-CDav(:,ind))./stepRe).*(Re-
Re_ref);
end

if ind<=0
    Re_ref=ReMin;
    mCL=(CLav(:,2)-CLav(:,1))./stepRe;
    mCD=(CDav(:,2)-CDav(:,1))./stepRe;
    cL=mCL.*(Re-Re_ref)+CLav(:,1);           %ottenuto dalla
retta tra i valori di CL e CD a Re=1e6 (ind=1)
    cD=mCD.*(Re-Re_ref)+CDav(:,1);
end

if ind>max
%     Re_ref=ReMax;
%     mCL=(CLav(:,10)-CLav(:,9))./stepRe;
%     mCD=(CDav(:,10)-CDav(:,9))./stepRe;
%     cL=mCL.*(Re-Re_ref)+CLav(:,10);
%     cD=mCD.*(Re-Re_ref)+CDav(:,10);
    cL=CLav(:,10);
    cD=CDav(:,10);
end

E=cL./cD;
E=E';
cL=cL';
cD=cD';

end

```

## 20 ANNEX [C]

---

```

%OFF DESIGN
clc
clear
close all

R=30/2;      lambda_des=7;      Nbl=3;      Ad=pi*R^2;      eta_el=0.96;
eta_m=0.97;
load('nrelXfoil.mat')          %'alphaD','CL','CD','NN','ReN'

%%
load('nominal_design.mat')     %BEM nominal design
for Vavg =8 m/s
ni20=1.5111e-5;
rho20=101325/(8314/28.9*293.15); %air density at 1 atm
and 20 degrees C
%%
%Velocity range
Vcut_in=3.5; Vcut_out=20; Vavg=8; Vr=11;
step=0.5;
%% Vcut_in - Vc

utip_max=70;
omega_c=utip_max/R;
omega_cut_in=lambda_des*Vcut_in/R;
Vc=omega_c/omega_cut_in*Vcut_in; %10 m/s (if
utip=70m/s)
V1=Vcut_in:step:Vc; % (1X141)
vector
omega1=lambda_des*V1./R;

a_0=ones(length(V1),1).*(a_lin); %mat(141x200)
with 1st guess axial induction factor (the one at Vavg)
a_prime_0=ones(length(V1),1).*(a_prime_lin); %mat(141x200)
with 1st guess tang induction factor (the one at Vavg)
a=zeros(length(V1),NN); %final one
(141x200)
a_prime=zeros(length(V1),NN); %final one
(141x200)
Beta_c=Beta_c_lin; % (1x200)
stagger angle @ nominal design (unchanged in the range Vcut_in-
Vc): same vector for all 141 velocities (no issues)
phi_inf=zeros(length(V1),NN); %mat(141x200)
beta_inf=zeros(length(V1),NN);
w_inf=zeros(length(V1),NN);
Re_0=zeros(length(V1),NN);
f=zeros(length(V1),NN);
F=zeros(length(V1),NN);
cL=zeros(NN,length(V1)); %mat(200x141)
1 beta inf for each radial position (200), for each velocity (141)

```

```

cD=zeros(NN,length(V1)); %cL and cD
defined reversely (rows=radial pos (200), columns= velocities
(141))
dFa_1=zeros(NN,length(V1));
dFt_1=zeros(NN,length(V1));
Fa_1=zeros(1,length(V1));
Ft_1=zeros(1,length(V1));
Fa_1_sum=zeros(1,length(V1));
dMyy_1=zeros(NN,length(V1)); %flap wise bending moment
dMxx_1=zeros(NN,length(V1)); %edge wise bending moment
Myy_1=zeros(1,length(V1));

for jj=1:length(V1)

    for ii=1:NN

        err1=10;
        err2=10;
        toll=1e-2;
        niter=0;

        while err1>toll || err2>toll %convergence on a,a'

            phi_inf(jj,ii)=atand(((1-
a_0(jj,ii))*V1(jj))/((1+a_prime_0(jj,ii))*omega1(jj)*rm(ii)));

w_inf(jj,ii)=(((1+a_prime_0(jj,ii))*omega1(jj)*rm(ii)).^2+((1-
a_0(jj,ii))*V1(jj)).^2).^0.5;
            Re_0(jj,ii)=w_inf(jj,ii)*clin(ii)/ni20;

            f(jj,ii)=0.5*Nbl*(1-
rm(ii)/R)/(rm(ii)/R*sind(phi_inf(jj,ii)));
            F(jj,ii)=2/pi*acos(exp(-f(jj,ii)));
            beta_inf(jj,ii)=phi_inf(jj,ii)-Beta_c(ii);
%incidence angle used to compute cL,cD

[cL(ii,jj),cD(ii,jj)]=profiles_off(ii,Re_0(jj,ii),CL,CD,ReMin,Re
Max,dRe,beta_inf(jj,ii),alphaD); %not sure

a(jj,ii)=sigmalin(ii).*w_inf(jj,ii)/(4*V1(jj)*F(jj,ii))*(cL(ii,j
j)./tand(phi_inf(jj,ii))+cD(ii,jj));

a_prime(jj,ii)=sigmalin(ii).*w_inf(jj,ii)/(4*omega1(jj)*rm(ii)*F
(jj,ii))*(cL(ii,jj)-cD(ii,jj)./tand(phi_inf(jj,ii)));
            err1=abs(a(jj,ii)-a_0(jj,ii));
            err2=abs(a_prime(jj,ii)-a_prime_0(jj,ii));
            a_0(jj,ii)=a(jj,ii);
            a_prime_0(jj,ii)=a_prime(jj,ii);
            disp(a_0(jj,ii))
        end

    end

end

```

```

%% CP CHECK

CP=zeros(2,NN,length(V1));           %3D matrix (2x200x141)
%Pw1=zeros(length(V1),1);
CPI1=zeros(length(V1),1);           %141x1
CPI2=zeros(length(V1),1);
P=zeros(NN,length(V1));
Pw1=zeros(length(V1),1);

for jj=1:length(V1)
    for ii=1:NN

CP(1,ii,jj)=Nbl*omegal(jj)/(pi*R^2*V1(jj)^3)*(clin(ii)*(w_inf(jj),ii).^2)*...
    (cL(ii,jj)*sind(phi_inf(jj,ii))-
cD(ii,jj)*cosd(phi_inf(jj,ii)))*rm(ii);

CP(2,ii,jj)=8/(lambda_des.^2)*F(jj,ii)*a_prime(jj,ii)*(1-
a(jj,ii))*(lambda_des*rm(ii)/R).^3;

dFa_1(ii,jj)=Nbl*0.5*rho20*w_inf(jj,ii).^2*clin(ii)*(cL(ii,jj)*c
osd(phi_inf(jj,ii))+cD(ii,jj)*sind(phi_inf(jj,ii)));

dFt_1(ii,jj)=Nbl*0.5*rho20*w_inf(jj,ii).^2*clin(ii)*(cL(ii,jj)*s
ind(phi_inf(jj,ii))-cD(ii,jj)*cosd(phi_inf(jj,ii)))*rm(ii);

P(jj,ii)=(4*rho20*pi*R^2*V1(jj).^3)/(lambda_des.^2)*F(jj,ii)*a_p
rime(jj,ii)*(1-a(jj,ii))*(lambda_des*rm(ii)/R).^3;
    dMyy_1(ii,jj)=0.5*rho20*((1-
a(jj,ii))^2*V1(jj)^2*cos(phi_inf(jj,ii)))/(sin(phi_inf(jj,ii)))^
2)*rm(ii)*clin(ii)*cL(ii,jj);

        end
        CPI1(jj)=sum(CP(1,:,jj)).*dr;           %blue curve
        CPI2(jj)=sum(CP(2,:,jj))*(lambda_des/R).*dr;           %orange
curve
        Fa_1(jj)=max(dFa_1(:,jj));
        Ft_1(jj)=max(dFt_1(:,jj));
        Fa_1_sum(jj)=sum(dFa_1(:,jj));
        Pw1(jj)=sum(P(jj,:))*(lambda_des/R).*dr;
        Myy_1(jj)=sum(dMyy_1(:,jj));

    end

% Pw1=0.5*rho20*Ad*V1.^3.*CPI2(jj)*eta_el*eta_m;           %electric
power output (W) including electric and mech efficiencies

figure()
plot(V1,CPI1,V1,CPI2);
title('CP in range Vcut in-Vc')

figure()
plot(V1,Pw1);

```

```

title('Electric Power Output: Vcut in-Vc');

figure()
plot(V1,Myy_1);
title('flap wise angle');
legend;

omega_c=utip_max/R;

V2=V1(end)+step:step:Vr; % 141 velocities
(for me 27 I guess)
a_02=ones(length(V2),1).*a_0(end,:); %mat(141xNN)
with 1st guess axial induction factor (the one at Vavg)
a_prime_02=ones(length(V2),1).*a_prime_0(end,:); %mat(141xNN)
with 1st guess tang induction factor (the one at Vavg)
a2=zeros(length(V2),NN); %final one
(141xNN)
a_prime2=zeros(length(V2),NN); %final one
(141xNN)
deltaBeta_c2=zeros(length(V2),1); %pitch angle
(141x1): 1 delta beta for each velocity V2
phi_inf2=zeros(length(V2),NN); %mat(141xNN)
beta_inf2=zeros(length(V2),NN); %mat(NNx141)
1 beta inf for each radial position (200), for each velocity (141)
w_inf2=zeros(length(V2),NN);
Re_02=zeros(length(V2),NN);
f2=zeros(length(V2),NN);
F2=zeros(length(V2),NN);
cL2=zeros(NN,length(V2));
cD2=zeros(NN,length(V2));
stallCheck=0; %mat(141x200) vector of stalled
radial position (1 column for each radial position, 1 row for each
V2)
Beta_c2=zeros(length(V2),NN); %mat(141x200)
stagger angle: 1 stagger angle for each radial position since
changes along the blade being twisted), for each velocity (since
is increased with Vc to avoid stall)
diffs=zeros(length(V2),NN);
E2=zeros(NN,length(V2)); %mat (200x141)
efficiency to check stall
tempE=zeros(NN,length(alphaD));
% Max_blade_eff=zeros(NN,1);
stalled_blade=zeros(length(V2),1);
stalled_percentage=101*ones(length(V2),1);

stall_limit=20; % 20% limit of the stall
betares=0.1;

for jj=1:length(V2)
    stallCheck=0;
    niterw=0;

    while stalled_percentage(jj)>=stall_limit
        niterw=niterw+1;

        for ii=1:NN

```



```

err1=10;
err2=10;
toll=1e-3;  %toll on a,a'
niter=0;

while err1>toll || err2>toll           %convergence on
a,a'

    phi_inf2(jj,ii)=atand(((1-
a_02(jj,ii))*V2(jj))/((1+a_prime_02(jj,ii))*omega_c*rm(ii)));

w_inf2(jj,ii)=(((1+a_prime_02(jj,ii))*omega_c*rm(ii)).^2+((1-
a_02(jj,ii))*V2(jj)).^2).^0.5;
    Re_02(jj,ii)=w_inf2(jj,ii)*clin(ii)/ni20;

    f2(jj,ii)=0.5*Nb1*(1-
rm(ii)/R)/(rm(ii)/R*sind(phi_inf2(jj,ii)));
    F2(jj,ii)=2/pi*acos(exp(-f2(jj,ii)));

Beta_c2(jj,ii)=round(Beta_c(ii)+deltaBeta_c2(jj),1);
%stagger + pitchAngle
    beta_inf2(jj,ii)=phi_inf2(jj,ii)-Beta_c2(jj,ii);
%incidence angle used to compute cL,cD

[cL2(ii,jj),cD2(ii,jj)]=profiles_off(ii,Re_02(jj,ii),CL,CD,ReMin
,ReMax,dRe,beta_inf2(jj,ii),alphaD);           %not sure

[~,~,tempE(ii,:)]=profiles2(ii,Re_02(jj,ii),CL,CD,ReMin,ReMax,dR
e);

    Max_blade_eff=max(tempE(ii,:));
    E2(ii,jj)=cL2(ii,jj)./cD2(ii,jj);

a2(jj,ii)=sigmalin(ii).*w_inf2(jj,ii)./(4*V2(jj)*F2(jj,ii))*(cL2
(ii,jj)./tand(phi_inf2(jj,ii))+cD2(ii,jj));

a_prime2(jj,ii)=sigmalin(ii).*w_inf2(jj,ii)./(4*omega_c*rm(ii)*F
2(jj,ii))*(cL2(ii,jj)-...
    cD2(ii,jj)./tand(phi_inf2(jj,ii)));
    err1=a2(jj,ii)-a_02(jj,ii);
    err2=a_prime2(jj,ii)-a_prime_02(jj,ii);
    re_factor=0.55;
    a_02(jj,ii)=(a2(jj,ii)+a_02(jj,ii))*re_factor;

a_prime_02(jj,ii)=(a_prime2(jj,ii)+a_prime_02(jj,ii))*re_factor;
end
    if E2(ii,jj) <= 0.94*Max_blade_eff           %0.94 with
Vr=11
        stallCheck=stallCheck+1;
    end
end
fprintf('stallCheck %d \n', stallCheck)
stalled_percentage_new=100*stallCheck/NN;

```

```

        stalled_percentage(jj)=stalled_percentage_new;
        deltaBeta_c2(jj)=deltaBeta_c2(jj)+betares;
        disp('Beta')
        disp(Beta_c2(jj,ii))
        disp('while iter :')
        disp(niterw)
        disp('speed number')
        disp(jj)
        disp('stalled percentage: ')
        disp(stalled_percentage(jj))
        stallCheck=0;
    end
end

Max_eff_matrix=Max_blade_eff(:).*ones(1,length(V2)); %200x8
Mat_eff_diff=E2(:,:)-Max_eff_matrix; %200x8
efficiency_differences_for_each_radia_position_for_each_velocity

plot(V2, deltaBeta_c2)
title('beta variations')

CP2=zeros(2,NN,length(V2)); %3D matrix (2x200x141)
CPI12=zeros(length(V2),1); %141x1
CPI22=zeros(length(V2),1);
CPI2=zeros(length(V2),1);
lambda2=(omega_c*R)./V2; %TSR variable with V2
P=zeros(length(V2),NN);
PI=zeros(length(V2),1);
dFa_2=zeros(NN,length(V2));
dFt_2=zeros(NN,length(V2));
Fa_2=zeros(1,length(V2));
Ft_2=zeros(1,length(V2));
Fa_2_sum=zeros(1,length(V2));
dMyy_2=zeros(NN,length(V2)); %flap wise bending moment
dMxx_2=zeros(NN,length(V2)); %edge wise bending moment
Myy_2=zeros(1,length(V2));

for jj=1:length(V2)
    for ii=1:NN

CP2(1,ii,jj)=Nbl*omega_c/(pi*R^2*V2(jj).^3)*(clin(ii)*(w_inf2(jj),ii).^2)*...
(cL2(ii,jj)*sind(phi_inf2(jj,ii))-
cD2(ii,jj)*cosd(phi_inf2(jj,ii)))*rm(ii);

CP2(2,ii,jj)=8/(lambda2(jj).^2)*F2(jj,ii)*a_prime_02(jj,ii)*(1-
a_02(jj,ii))*(lambda2(jj).*rm(ii)/R).^3;

P(jj,ii)=(4*rho20*pi*R^2*V2(jj).^3)/(lambda2(jj).^2)*F2(jj,ii)*a_
prime_02(jj,ii)*(1-a_02(jj,ii))*(lambda2(jj).*rm(ii)/R).^3;

```

```

dFa_2(ii,jj)=Nbl*0.5*rho20*w_inf2(jj,ii).^2*clin(ii)*(cL2(ii,jj)
*cosd(phi_inf2(jj,ii))+cD2(ii,jj)*sind(phi_inf2(jj,ii)));

dFt_2(ii,jj)=Nbl*0.5*rho20*w_inf2(jj,ii).^2*clin(ii)*(cL2(ii,jj)
*sind(phi_inf2(jj,ii))-cD2(ii,jj)*cosd(phi_inf2(jj,ii)))*rm(ii);
dMyy_2(ii,jj)=0.5*rho20*((1-
a_02(jj,ii))^2*V2(jj)^2*cos(phi_inf2(jj,ii)))/(sin(phi_inf2(jj,i
i))^2)*rm(ii)*clin(ii)*cL2(ii,jj);

    end
    CPI12(jj)=sum(CP2(1,:,jj)).*dr; %blue
curve
    CPI22(jj)=sum(CP2(2,:,jj))*(lambda2(jj)./R).*dr; %orange
curve
    CPI2(jj)=0.5*(CPI12(jj)+CPI22(jj));
    PI(jj)=sum(P(jj,:))*(lambda2(jj)/R).*dr;

    Fa_2(jj)=max(dFa_2(:,jj));
    Ft_2(jj)=max(dFt_2(:,jj));
    Fa_2_sum(jj)=sum(dFa_2(:,jj));
    Myy_2(jj)=sum(dMyy_2(:,jj));
end

figure()
plot(V2,CPI12,V2,CPI22);
title('CP in range Vc-Vrated')

V=Vcut_in:step:Vr;
%zeros(1,length(V1)+length(V2));
Pw=zeros(1,length(V));

for jj=1:length(V)
    if jj<=length(V1)
        Pw(jj)=Pw1(jj);
    else
        Pw(jj)=PI(jj-length(V1)); %+1 because Pw1(end) and Pw2(1)
        refers to same velocity Vc=10m/s
    end
end

figure()
plot(V,Pw);
title('Electric Power Output: Vcut in-Vrated');

V3=V2(end)+step:step:Vcut_out;
a_0=ones(length(V3),1).*(a_lin); % mat(8x200)
with 1st guess axial induction factor (the one at Vavg)
a_prime_0=ones(length(V3),1).*(a_prime_lin); % mat(8x200)
with 1st guess tang induction factor (the one at Vavg)
a=zeros(length(V3),NN); %final one
a_prime=zeros(length(V3),NN); %final one
phi_inf=zeros(length(V3),NN);
beta_inf3=zeros(length(V3),NN);
w_inf=zeros(length(V3),NN);

```

```

Re_0=zeros(length(V3),NN);
f=zeros(length(V3),NN);
F=zeros(length(V3),NN);
X=length(NN);
cL=zeros(NN,length(V3)); %l beta inf
for each radial velocity
cD=zeros(NN,length(V3));
CP=zeros(NN,length(V3));
CPI13=zeros(1,length(V3));
P=zeros(NN,length(V3));
PI=zeros(1,length(V3));
Prated=Pw(end);
toll_P=5000;
omega=omega_c;
Delta_beta=zeros(1,length(V3));

dFa_3=zeros(NN,length(V3));
dFt_3=zeros(NN,length(V3));
Fa_3=zeros(1,length(V3));
Ft_3=zeros(1,length(V3));
Fa_3_sum=zeros(1,length(V3));
dMyy_3=zeros(NN,length(V3)); %flap wise bending moment
dMxx_3=zeros(NN,length(V3)); %edge wise bending moment
Myy_3=zeros(1,length(V3));

for jj=1:length(V3)
    lambda=(omega*R)/V3(jj);
    err=1000000;
    Beta_c=Beta_c_lin;%stagger angle @ nominal design (not
changed in the range Vcut_in-Vc)
    disp(jj)
    while err>toll_P %convergence on abs(power)

        for ii=1:NN
            err1=10;
            err2=10;
            toll=10e-3;
            niter=0;
            %disp(ii)
            while err1>toll || err2>toll %convergence on
a,a'

                phi_inf(jj,ii)=atand(((1-
a_0(jj,ii))*V3(jj))/((1+a_prime_0(jj,ii))*omega*rm(ii)));

w_inf(jj,ii)=(((1+a_prime_0(jj,ii))*omega*rm(ii)).^2+((1-
a_0(jj,ii))*V3(jj)).^2).^0.5;
                Re_0(jj,ii)=w_inf(jj,ii)*clin(ii)/ni20;
                f(jj,ii)=0.5*Nbl*(1-
rm(ii)/R)/(rm(ii)/R*sind(phi_inf(jj,ii)));
                F(jj,ii)=2/pi*acos(exp(-f(jj,ii)));

                beta_inf3(jj,ii)=phi_inf(jj,ii)-Beta_c(ii)-
Delta_beta(jj); %incidence angle
used to compute cL,cD

```

```

[cL(ii,jj),cD(ii,jj)]=profiles_off(ii,Re_0(jj,ii),CL,CD,ReMin,Re
Max,dRe,beta_inf3(jj,ii),alphaD);

a(jj,ii)=sigmalin(ii).*w_inf(jj,ii)/(4*V3(jj)*F(jj,ii))*(cL(ii,j
j)./tand(phi_inf(jj,ii))+cD(ii,jj));

a_prime(jj,ii)=sigmalin(ii).*w_inf(jj,ii)/(4*omega*rm(ii)*F(jj,i
i))*(cL(ii,jj)-cD(ii,jj)./tand(phi_inf(jj,ii)));
err1=abs(a(jj,ii)-a_0(jj,ii));
err2=abs(a_prime(jj,ii)-a_prime_0(jj,ii));

CP(ii,jj)=8/(lambda.^2)*F(jj,ii)*a_prime(jj,ii)*(1-
a(jj,ii))*(lambda*rm(ii)/R).^3;

P(ii,jj)=(4*rho20*pi*R^2*V3(jj)^3)/(lambda^2)*F(jj,ii)*a_prime(j
j,ii)*(1-a(jj,ii))*(lambda*rm(ii)/R).^3;
a_0(jj,ii)=a(jj,ii);
a_prime_0(jj,ii)=a_prime(jj,ii);
%niter=niter+1;
%disp(niter)
% disp(jj)
% disp(err1)
% disp(err2)
end

%
dFa_3(ii,jj)=Nbl*0.5*rho20*w_inf(jj,ii).^2*clin(ii)*(cL(ii,jj)*c
osd(phi_inf(jj,ii))+cD(ii,jj)*sind(phi_inf(jj,ii)));

dFt_3(ii,jj)=Nbl*0.5*rho20*w_inf(jj,ii).^2*clin(ii)*(cL(ii,jj)*s
ind(phi_inf(jj,ii))-cD(ii,jj)*cosd(phi_inf(jj,ii)))*rm(ii);
dMyy_3(ii,jj)=0.5*rho20*((1-
a(jj,ii))^2*V3(jj)^2*cos(phi_inf(jj,ii)))/(sin(phi_inf(jj,ii)))^
2)*rm(ii)*clin(ii)*cL(ii,jj);

end

CPI13(jj)=sum(CP(:,jj))*(lambda/R).*dr;
PI(jj)=sum(P(:,jj))*(lambda/R).*dr;
Fa_3(jj)=max(dFa_3(:,jj));
Ft_3(jj)=max(dFt_3(:,jj));
Fa_3_sum(jj)=sum(dFa_3(:,jj));
Myy_3(jj)=sum(dMyy_3(:,jj));
%P_0=0.98*0.98^1/2*rho20*Cp/10^3; %kW/m^2
%P_0=Cp*0.5*(rho20*pi*R^5*omega^3)/lambda^3 %kW

Delta_beta(jj)=Delta_beta(jj)+0.1;
err=abs(PI(jj)-Prated);
end
end
%%
figure
plot(V3,CPI13)
title('CP range Vrated-Vcut_off')

```

```

figure
plot(V3,PI)
axis([V3(1) V3(end) 2.5e5 3.5e5])
title('power output Vrated-Vcut_off')

V23=Vc+step:step:Vcut_out;
beta=zeros(1, length(V23));
figure
j=1;
for i=1:length(V23)
    if i<=length(V2)
        beta(i)=deltaBeta_c2(i);
    else
        beta(i)=Delta_beta(j);
        j=j+1;
    end
end

plot(V23,beta)
% figure
% plot(V3, Delta_beta)
grid on
title ('pitch variation VS wind speed')
%%
v = Vcut_in:step:Vcut_out;
Pw_tot = [Pw PI];
CPI=zeros(1,length(v));
Fa=zeros(1,length(v));
Ft=zeros(1,length(v));
Fa_sum=zeros(1,length(v));
Myy=zeros(1,length(v));
Mxx=zeros(1,length(v));
figure
plot(v,Pw_tot,'LineWidth',2)
hold on
k=1;    j=1;
for i=1:length(v)
    if i<=length(V1)
        CPI(i)=CPI1(i);
        Fa(i)=Fa_1(i);
        Ft(i)=Ft_1(i);
        Fa_sum(i)=Fa_1_sum(i);
        Myy(i)=Myy_1(i);
        % Mxx(i)=Mxx_1(i);
    else if i>(length(V1)+length(V2))
        CPI(i)=CPI13(k);
        Fa(i)=Fa_3(k);
        Ft(i)=Ft_3(k);
        Fa_sum(i)=Fa_3_sum(k);
        Myy(i)=Myy_3(k);
        % Mxx(i)=Mxx_3(k);
        k=k+1;
    else
        CPI(i)=CPI22(j);
        Fa(i)=Fa_2(j);
    end
end

```

```

        Ft(i)=Ft_2(j);
        Fa_sum(i)=Fa_2_sum(j);
        Myy(i)=Myy_2(j);
    %       Mxx(i)=Mxx_2(j);
        j=j+1;
    end
end
end
plot(v,smooth(CPI*10^6,3),'LineWidth',2)
title ('Cp and power output of the turbine');
grid on

figure()
plot(v,Fa,'LineWidth',2)
title ('max axial force VS wind speed (1)');
grid on
figure()
plot(v,Fa_sum,'LineWidth',2)
title ('sum of axial forces VS wind speed (1)');
grid on
figure()
plot(v,Ft)
title ('Ft');
grid on
figure()
plot(v,Myy,'LineWidth',2)
title ('flap wise bending moment');
grid on
figure()
plot(v,Mxx,'LineWidth',2)
title ('edge wise bending moment');
grid on

%%
beta_temp=zeros(length(v),1);
j=1;
for i=1:length(beta_temp)
    beta_temp(i)=0;
    if i>length(beta_temp)-length(beta)
        beta_temp(i)=beta(j);
        j=j+1;
    end
end
end
beta_part_1=beta_temp;
figure()
plot(v,beta_part_1,'LineWidth',2)
title ('pitch control VS wind speed')
grid on
filename='beta_part_1.mat';
save(filename,'beta_part_1');

```

## 21 FIGURES

---

FIGURE 1: CONTROL REGULATION SYSTEM.....	5
FIGURE 2: TRAILING EDGE FLAP EXAMPLES .....	6
FIGURE 3: BLADE CONFIGURATION FOR THE PROJECT.....	6
FIGURE 4: AXIAL LOAD'S CHANGES DUE TO TRAILING EDGE FLAP.....	8
FIGURE 1: EFFICIENCY AT DIFFERENT CONSTANT WIND SPEEDS .....	20
FIGURE 2: USUAL POWER CURVE FOR STALL AND PITCH REGULATION .....	21
FIGURE 3: PITCH REGULATION .....	21
FIGURE 4: STALL REGULATION.....	22
FIGURE 5: 1=INITIAL CONDITION; 2= ADJUSTMENT WITH PITCH REGULATION; 2'=ADJUSTMENT WITH STALL REGULATION.....	23
FIGURE 6: DEGREES OF MOTION OF PITCH AND STALL REGULATIONS .....	24
FIGURE 7: SMA ACTUATION APPLICATION FOR THE ENTIRE BLADE AND SECTION OF THE ACTUATOR..	25
FIGURE 8: PART SPAN PITCH CONTROL [3] .....	25
FIGURE 9: TRAILING EDGE FLAPS [5].....	26
FIGURE 10: ACTUATIONS ON TRAILING EDGE FLAPS [6].....	27
FIGURE 11: MICRO TABS [8].....	27
FIGURE 12: AERODYNAMIC EFFECTS OF MICRO TABS [5].....	27
FIGURE 13: ACTIVE TWIST .....	28
FIGURE 14: CAMBER CONTROL.....	29
FIGURE 15: INTERNAL STRUCTURE FOR CAMBER CONTROL .....	29
FIGURE 16: INFLATABLE STRUCTURES [6] .....	30
FIGURE 17: SYNTHETIC JETS .....	31
FIGURE 18: THUNDER PIEZOELECTRIC ACTUATOR [17].....	35
FIGURE 19: ACTUATOR DISC MODEL FOR A WIND TURBINE [21] .....	38
FIGURE 20: OPERATING PARAMETER FOR A BETZ TURBINE.....	41
FIGURE 21: STREAM TUBE WITH WAKE ROTATION [22] .....	42
FIGURE 22: GEOMETRY FOR THE ROTOR ANALYSIS: STREAM TUBE.....	42
FIGURE 23: VECTORS OF THE CONSIDERED WIND SPEEDS.....	43
FIGURE 24: VARIATION OF THE POWER COEFFICIENT WITH THE TIP SPEED RATIO .....	44
FIGURE 25: VARIATION OF A AND A' WITH THE LOCAL SPEED RATIO X .....	45
FIGURE 26: SCHEMATICS OF THE BLADE ELEMENTS .....	46
FIGURE 27: AIRFOIL WITH LIFT AND DRAG VECTOR REPRESENTATION.....	46



FIGURE 28: TILT ANGLE AND CONING ANGLE .....47

FIGURE 29: CORRECTION OF A THEORIES.....50

FIGURE 30: NREL AIRFOIL FAMILIES [26].....53

FIGURE 31: REPRESENTATION OF THE BLADE .....54

FIGURE 32: PRIMARY AIRFOIL S809.....54

FIGURE 33: TIP AIRFOIL S810 .....55

FIGURE 34: HUB AIRFOIL S811 .....55

FIGURE 35: EXAMPLE OF XFLR5 INTERVIEW .....56

FIGURE 36: CL, CD, E VALUES AFTER INTERPOLATION, X-AXIS IS THE ANGLE OF ATTACK .....58

FIGURE 37: PARAMETERS ON AN AIRFOIL.....59

FIGURE 38: ITERATIVE COMPUTATION TO ACHIEVE THE BEST CHORD DISTRIBUTION .....60

FIGURE 39: MAIN RESULTS AFTER THE IMPLEMENTATION OF THE FIRST CODE .....60

FIGURE 40: MAIN RESULTS AFTER THE IMPLEMENTATION OF THE SECOND CODE.....61

FIGURE 41: PRANDTL COEFFICIENT F BEHAVIOUR TO INCLUDE THE TIP EFFECT.....61

FIGURE 42: FINAL AVERAGED VALUE .....62

FIGURE 43: CHORD LINEARIZATION PROCEDURE.....63

FIGURE 44: FINAL VALUES OF THE CORRECTED CHORD OF THE BLADE.....64

FIGURE 45: CONTROL STRATEGY.....65

FIGURE 46: FIRST PART OF THE OFF-DESIGN EVALUATION .....66

FIGURE 47: ITERATIVE PROCEDURE OF THE FIRST PART.....66

FIGURE 48: SECOND PART OF THE OFF-DESIGN EVALUATION .....67

FIGURE 49 :ITERATIVE PROCEDURE OF THE SECOND PART .....67

FIGURE 50: THIRD PART OF THE OFF-DESIGN EVALUATION .....68

FIGURE 51:ITERATIVE PROCEDURE OF THE THIRD PART .....68

FIGURE 52: CP AND POWER GRAPHICS IN THE LEFT PICTURE, PITCH VARIATION IN THE RIGHT PICTURE  
 VERTICAL AXIS FOR POWER OUTPUT IS IN kW, FOR PITCH REGULATION IN ° .....69

FIGURE 53: AXIAL FORCE, X-AXIS IS THE MEAN WIND SPEED [M/S], Y-AXIS IS IN N .....69

FIGURE 54: SCHEMATISATION OF THE FLAP [30]    FIGURE 55: FLAP LOCATION ON THE BLADE [30].....70

FIGURE 56: POWER AND CP OUTPUT IN CASE 1, WITH THE FLAP MOTION.....70

FIGURE 57: CP AND POWER OUTPUT .....71

FIGURE 58: FLAP VARIATION AND PITCH CONTROL ACTIVATION .....72

FIGURE 59: CP AND POWER OUTPUT .....73

FIGURE 60: FLAP VARIATION AND PITCH REGULATION .....73

FIGURE 61:POWER OUTPUT BETWEEN VCUT-IN AND VC .....74

FIGURE 62: SCHEMATISATION OF THE GUST ..... 75

FIGURE 63: WIND SPEED INCREMENT WITH THE PRESENCE OF THE GUST ..... 76

FIGURE 64: PITCH CONTROL ..... 77

FIGURE 65: ROTATIONAL SPEED OF THE TURBINE ..... 77

FIGURE 66: POWER OUTPUT AND  $C_p$  OF THE TURBINE ..... 78

FIGURE 67: AXIAL FORCE ACTING ON THE BLADE. .... 79

FIGURE 68: PITCH REGULATION AND ROTATIONAL SPEED ..... 80

FIGURE 69: FLAP VARIATION AT DIFFERENT WIND SPEED ..... 81

FIGURE 70: POWER OUTPUT AND  $C_p$  COMPARISON..... 82

FIGURE 71: PERCENTAGE VARIATION ON POWER PRODUCTION ..... 83

FIGURE 72: AXIAL FORCE ACTING ON THE TURBINE..... 84

FIGURE 73: AXIAL FORCES ..... 84

FIGURE 74: PERCENTAGE DIFFERENTIAL ON AXIAL FORCE ..... 85

FIGURE 75: MAP OF BARROW WIND FARM..... 92

FIGURE 76: UK WIND MEAN SPEED AT 100M ..... 92

FIGURE 77: POWER CURVE OF THE VESTAS V90 3MW..... 95

FIGURE 78: CUMULATIVE WEIBULL WIND DISTRIBUTION ..... 99

FIGURE 79: WEIBULL WIND DISTRIBUTION..... 99

FIGURE 80: RENEWABLE ENERGY GENERATION IN UK [46]..... 101

FIGURE 81: TYPICAL LCOE FOR DIFFERENT TECHNOLOGY [32]..... 105

FIGURE 82: AXIAL FORCES ACTING ON THE TWO TURBINES ..... 106

FIGURE 83: POWER OUTPUT OF THE TWO TURBINES ..... 107

FIGURE 84: DIFFERENCE IN POWER PRODUCTION ..... 107

FIGURE 85: FLAP ORIENTATION ..... 108

FIGURE 86: LINEARISED PERCENTAGE VALUE OF THE DIFFERENCE IN POWER OUTPUT OF THE TWO  
TURBINES ..... 109

FIGURE 87: WACC OF ORSTED COMPUTED FROM ANNUALS REPORTS 2007-2017 [52] ..... 114

## 22 TABLES

---

TABLE 1: COMPARISON BETWEEN TURBINES WITH SAME DIAMETER ..... 7

TABLE 2: BARROW ECONOMIC PARAMETERS ..... 9

TABLE 3: DATA OF THE TWO TURBINES..... 9

TABLE 4: RESULTS OF THE TWO ECONOMIC ANALYSIS ..... 10

TABLE 5: RESULTS.....	10
TABLE 6: TAX RATE IN UK .....	94
TABLE 7: WEIBULL WIND DISTRIBUTION .....	99
TABLE 8: FIRST PART OF COMPUTATIONS .....	103
TABLE 9: SECOND PART OF THE COMPUTATIONS .....	104
TABLE 10: FIRST PART OF COMPUTATIONS OF THE 3.6MW TURBINE.....	112
TABLE 11: SECOND PART OF COMPUTATIONS FOR THE 3.6MW TURBINE.....	113

## 23 LIST OF THE ACRONYMS

---

HAWT: Horizontal Axis Wind Turbine;

BEM: Blade Element Method;

DCF: Discounted Cash Flow;

NPV: Net Present Value;

IRR: Internal Rate of Return;

PT: Payback Time;

LCOE: Levelized Cost Of Electricity;

UK: United Kingdom;

CAPEX: Capital Expenditures;

OPEX: Operational Expenditures;

WACC: weighted average cost of capital

## 24 REFERENCES

---

- [1] A. M. A. L. J. Pujana-Arrese, « Design of Robust Controllers for Load Reduction in Wind Turbines,» 2014.
- [2] T. Buhl e C. Bak, «Load alleviation through adaptive trailing edge control surfaces: ADAPWING overview,» 2007.
- [3] A. Maheri, «Simulation of wind turbines utilising smart blades,» 2016.
- [4] F. K. Straub, «A feasibility study of using smart materials for rotor control,» 1996.
- [5] T. Barlas e G. van Kuik, «Review of state of the art in smart rotor control research for wind turbines,» 2010.
- [6] S. Daynes e P. M. Weaver, «Review of morphing concepts and materials for wind turbines blade applications,» *Wind Energy*, 2013.
- [7] C. Van Dam, D. Yen Nakafuji, C. Bauer, D. Chao e K. Dandish, «Computational Design and Analysis of a micro tab based aerodynamic loads control system for lifting surfaces,» 2003.
- [8] T. J. McCoy e D. A. Griffin, «Active Control of Rotor Aerodynamics and Geometry: Status, Methods, and preliminary results,» 2006.
- [9] R. Wu, C. Soutis, S. Zhong e A. Filippone, «A morphing aerofoil with highly controllable aerodynamic performance,» 2016.
- [10] D. Cadogan, T. Smith, F. Uhelsky e M. MacKusick, «Morphing Inflatable Wing Development for Compact package Unmanned Aerial Vehicles,» 2004.
- [11] Barlas e Thanasis, «Smart rotor blades and rotor control for wind turbines, state of the art,» 2007.

- [12] J. Sun, Q. Guan, Y. Liu e J. Leng, «Morphing aircraft based on smart materials and structures: A state-of-the-art review,» 2016.
- [13] T. Buhl, M. Gaunaa, C. Bak, P. Hansen e K. Clemmensen, «Measurements on the Thunder TH-6R actuator,» 2005.
- [14] G. Park, C. R. Farrar, A. C. Rutherford e A. N. Robertson, «Piezo-sensor self-diagnostic using electrical impedance measurements,» 2004.
- [15] T. Malysh e J. Erhart, «Electric Field Applicability Limits for PZT Ceramics,» 2011.
- [16] V. Gupta, M. Sharma e N. Thakur, «Optimization Criteria for Optimal Placement of Piezoelectric, Sensors and Actuators on a Smart Structure: A Technical Review,» 2010.
- [17] T. Barlas e G. van Kuik, «State of the art and perspectives of smart rotor control for wind turbines,» 2007.
- [18] P. B. Andersen, L. Henriksen, M. Gaunaa, C. Bak e T. Bulh, «Deformable trailing edge flaps for modern megawatt wind turbine controllers using strain gauge sensors,» 2009.
- [19] T. Verbruggen e L. Rademakers, «Fiber optic Blade Monitoring,» 2020.
- [20] R. Bos, A. Giyanani e W. Bierbooms, «Assessing the Severity of Wind Gusts with Lidar,» 2016.
- [21] J. Manwell, J. McGowan e A. Rogers, Wind Energy Explained, theory, design and application, Wiley, 2009.
- [22] E. Lysen, Introduction to wind energy, Consultancy services wind energy developing countries, 1983.
- [23] R. Wilson, P. Lissaman e S. Walker, «Aerodynamic performance of wind turbines. Final report,» 1976.

- [24] S. Miley, «Catalog of low-Reynolds-number airfoil data for wind-turbine applications,» 1982.
- [25] S. G. Voutsinas, K. G. Rados e A. Zervos, «Wake effects in wind parks: a newmodelling approach.,» 1993.
- [26] M. Buhl, «<https://wind.nrel.gov/airfoils/AirfoilFamilies.html>,» [Online].
- [27] J. Tangler e D. Somers, «NREL Airfoils Families for HAWTs,» 1995.
- [28] R. Reuss Ramsay, M. Hoffmann e G. Gregorek, «Effect of Grit Roughness and Pitch Oscillations on the S809 Airfoil,» 1995.
- [29] «<http://www.xflr5.tech/xflr5.htm>,» [Online].
- [30] B. Xu, J. Feng, T. Wang, Y. Yuan, Z. Zhao e W. Zhong, «Trailing-Edge Flap Control for Mitigating Rotor Power Fluctuations of a Large-Scale Offshore Floating Wind Turbine under the Turbulent Wind Condition,» 2018.
- [31] T. Maj, «Nozioni essenziali di calcolo finanziario di attualizzazione in relazione alla estimazione monetaria della dimensione ambientale,» 2020.
- [32] U.S. department of Eergy, «LCOE».
- [33] M. Mancini, R. Sala, D. Tedesco e A. Travaglini, «A real option investment model for the evaluation of wind and fotovoltaic plants,» 2016.
- [34] Y. Feng, H. Long e P. Tavner, «Early experiences with UK Round 1 offshore wind farms,» 2010.
- [35] «Global Wind Atlas,» 2021. [Online]. Available: <https://globalwindatlas.info/>.
- [36] Ismail, S. Kamal, Purnomo, Sarjiya e H. Budi, «Economic Feasibility of Wind Farm: a case study for coasta area in South Purworejo, Indonesia,» 2014.
- [37] G. D. Service, «<http://mrrcalculator.hmrc.gov.uk/MRR2.aspx>,» [Online].

- [38] G. D. Service, «<https://www.gov.uk/government/publications/rates-and-allowances-corporation-tax/rates-and-allowances-corporation-tax>,» [Online].
- [39] T. Freyman e T. Tran, «Renewable energy discount rate survey results - 2018,» 2018.
- [40] Vestas, *General Specification - V90 - 3.0 MW VCRS*, 2006.
- [41] L. Fingersh, M. Fend e A. Laxson, *Wind turbine design cose and scaling model - NREL Technical report*, 2006.
- [42] E. Takle e J. Brown, «Note on the use of Weibull Statistics to Characterize Wind-Speed Data,» 1977.
- [43] R. J. Barthelmie, F. Murray e S. Pryor, «The economic benefit of short-term forecasting for wind energy in the UK electricity market,» 2008.
- [44] P.-E. Morthorst e S. Awerbuch, «The Economics of Wind Energy,» 2009.
- [45] D. Toke, «Community wind power in Europe and in the UK,» 2005.
- [46] Department for Business, Energy & Industrial Strategy, «Energy Trends, UK,» 2021.
- [47] Orsted, «OFFSHORE WIND FARMS1 - Asset Book updated as of 31 March 2021,» 31 March 2021. [Online].
- [48] J. Bosch, I. Staffell e A. D. Hawkes, «Global levelised cost of electricity from offshore wind».
- [49] M. Meissner, «Offshore wind turbine cost scaling - A critical assessment and the theoretical investigation,» 2020.
- [50] A. Ioannou, A. Angus e F. Brennan, «Parametric CAPEX, OPEX, and LCOE expressions for offshore wind farms based on global deployment parameters,» 2018.
- [51] Dong Energy, «financial statements for 2006 of the parent company,» 2006.

- [52] A. Edemann, R. Lang Pedersen e T. D., «Valuation of Orsted - determining the fair price of orsted,» 2019.
- [53] The Government of the United Kingdom, «New plans to make UK world leader in green energy,» 6 Ottobre 2020. [Online]. Available: <https://www.gov.uk/government/news/new-plans-to-make-uk-world-leader-in-green-energy>.
- [54] HM Government, «The Ten Point Plan for a Green Industrial Revolution,» 2020.
- [55] Department for Business, Energy & Industrial Strategy - UK Government, «Contracts for Difference,» 2 March 2020. [Online]. Available: <https://www.gov.uk/government/publications/contracts-for-difference/contract-for-difference>.
- [56] P. Morthorst, H. Auer, A. Garrad e I. Blanco, «Wind Energy - The facts. Part III: The Economics of wind power.».
- [57] A. Hulskamp e H. E. Bersee, «Implementation of the "smart" control concept,» 2010.
- [58] D. E. Berg, D. G. Wilson, B. R. Resor, M. F. Barone e J. C. Berg, «Active aerodynamic blade load control impacts on utility-scale wind turbines,» 2009.
- [59] Vehicle Certification Agency - Government of the UK, «Fuel Consumption and CO<sub>2</sub>,» 2021. [Online]. Available: <https://www.vehicle-certification-agency.gov.uk/fuel-consumption-co2/>.